



# NSTX-U FY2019 Year End Report

J. Galayda, S. Kaye, S. Gerhardt, L. Hill, and the NSTX-U Team

Report editor: S. Horst

October 16, 2019 – Version 1

<b>EXECUTIVE SUMMARY OF FY2019 NSTX-U YEAR-END REPORT</b>	<b>4</b>
Executive Summary for FY2019 Notable Outcomes	4
Executive Summary for the NSTX-U Recovery Project	5
Executive Summary of Research Results - FY2019 Milestones	7
Executive Summary for Additional Research Highlights	9
<b>Performance of FY2019 Notable Outcomes</b>	<b>14</b>
<b>NSTX-U Recovery Project - Project Management Accomplishments</b>	<b>15</b>
September 2018 Director's Review	15
Response to Recommendations from the September 2018 Director's Review	16
March 2019 Basis of Estimate Review	17
Response to Recommendations from the Basis of Estimate Review	18
Recovery Project Management Changes	18
July 2019 Director's Review	19
Response to Recommendations from the July 2019 Director's Review	20
August 2019 CDE-2/3A Integrated Project Review	21
ESAAB Approval	22
<b>NSTX-U Recovery Project - Technical Accomplishments</b>	<b>22</b>
Plasma Facing Components (WBS 1.01.01)	22
Vacuum Vessel and Internal Hardware (WBS 1.01.02)	22
Magnets	24
Vacuum and Fueling	26
Plasma Diagnostics / NSTX-U Diagnostics	26
Power Systems / AC & DC Power Systems	27
Test Cell Improvements / Test Cell (WBS 1.08.01)	27
Site Preparation & Assembly / Accelerator Safety Order	28
NSTX-U Reassembly	28
NSTX-U Commissioning and KPPs	29
NSTX-U Personnel Safety System	29
Real Time Protection and Control	29

---

<b>NSTX-U Maintenance and Run Preparation</b>	<b>29</b>
Neutral Beams	30
High Harmonic Fast Wave Systems	30
Motor Generator Systems	31
Field Coil Power Conversion	31
Central Instrumentation and Control	32
Vacuum and Fuelling	33
<b>NSTX-U Research Program</b>	<b>33</b>
H-mode Pedestal Fueling With Conventional And Supersonic Gas Injections	33
Neutral Density Studies In NSTX-U: Validation Of Midplane Neutral Density Measurements	36
Experimental Analysis Of Radial Neutral Density And Ionization Rate Profiles	37
<b>Research Milestones</b>	<b>38</b>
R19-1: Validate Transport Models For High-beta ST H-mode Plasmas And Assessing The Importance Of Multi-scale Effects In NSTX/NSTX-U Turbulent Transport	38
Validate Transport Models For High-beta ST H-mode Plasmas	39
Assessing The Importance Of Multi-Scale Effects	40
R19-2: Develop Optimized Ramp-up Scenarios In Spherical Tokamaks	42
R19-3: Validate Tearing Mode Physics For Tearing Avoidance In High-performance Scenarios	44
Validation Of Tearing Mode Predictions In DIII-D	45
Applications Of Resistive DCON To NSTX-U	46
R19-4: Assess energetic particle transport by sub-TAE instabilities and develop reduced EP transport modeling tools	47
EP Transport By Sawteeth	47
EP Transport By Fishbones	48
EP Transport By NTMs.	49
<b>Additional Research Highlights</b>	<b>51</b>
Boundary Science	51
Divertor and Scrape-Off-Layer	53
Materials and PFCs	54
<b>Core Science</b>	<b>61</b>
Transport and Turbulence Physics Research	61
Energetic Particles	65
Macroscopic Stability	73
<b>Integrated Scenarios</b>	<b>78</b>
Solenoid-Free Startup and Ramp-Up	78

---

---

<b>Wave Heating and Current Drive</b>	<b>82</b>
Modeling Of High Harmonic Fast Wave Scenarios For NSTX Upgrade [WCD-1]	82
Effect Of Wall Boundary On The Scrape-Off Layer Losses Of High Harmonic Fast Wave In NSTX And NSTX-U [WCD-3]	84
3D Full Wave Fast Wave Modeling With Realistic Antenna Geometry And SOL Plasma For NSTX-U [WCD-7]	84
Modeling Of 2nd Harmonic Electron Cyclotron Heating And Current Drive Solenoid-free Start-up Experiment In QUEST [WCD-10, WCD-11]	85
<b>Advanced Scenarios and Control</b>	<b>88</b>
Reduced Model For Direct Induction Startup Scenario Development On MAST-U And NSTX-U	88
Reduced Model For Current Profile, Density, Temperature, And Fast Ion Pressure On NSTX-U	89
References:	93
<b>NSTX-U Publications</b>	<b>94</b>
Papers Published by NSTX-U Researchers (Oct. 2018 - Sept. 2019)	94
<b>NSTX-U Presentations</b>	<b>98</b>
Invited / Oral Talks at Scientific Conferences (Oct. 2018 - Sept. 2019)	98
<b>Seminars and Colloquia by NSTX-U Researchers</b>	<b>104</b>
<b>NSTX-U Awards and Leadership</b>	<b>107</b>
Major Awards by NSTX-U Researchers	107
Invention Disclosures and Patents	107
Hosted / Organized Meetings and Workshops	107
NSTX-U PPPL Employee FY19 Leadership in Venues Outside of PPPL	108
NSTX-U PPPL Employee Membership and Participation in Scientific Groups and Meetings Outside of PPPL	110
<b>NSTX-U Collaborator Institutions</b>	<b>112</b>

## EXECUTIVE SUMMARY OF FY2019 NSTX-U YEAR-END REPORT

### Executive Summary for FY2019 Notable Outcomes

The status of the Recovery Project FY2019 Notable Outcomes is given in the table below. The NSTX-U Recovery Project completed four of the five PEMP Notable Outcomes during FY2019. One Notable Outcome was not achieved in FY19 due to the delay in ESAAB approval relative to expectations at the start of the fiscal year.

	<b>FY2019 NSTX-U Recovery Project PEMP Notable</b>	<b>Defined Finish By Date</b>	<b>Status as of September 30, 2019</b>
A	Complete Basis of Estimate documentation for baseline review	3/31/2019	<b>Completed</b> 3/20/2019
B	Complete Center Stack Casing (CSC) FDR	12/31/2018	<b>Completed</b> 12/28/2018
C	CSC Procurement Award Sub-Contract(s)	3/31/2019	<b>Completed</b> 3/29/2019
D	Fabricate and test a production PF1 coil via electrical testing and dimensional inspection	9/30/2019	This coil fabrication and testing will occur in FY20 due to the delay in ESAAB approval.
E	Develop ASO Implementation Plan and obtain DOE concurrence	9/30/2019	<b>Completed</b> 3/24/2019. A revision to the ASO Implementation Plan was signed and submitted to the DOE Princeton Site Office (PSO). PSO accepted the plan as meeting this Noteable.

## Executive Summary for the NSTX-U Recovery Project

The Project's primary management focus for FY2019 was to obtain approval of Critical Decision Equivalent 2 (acceptance of the overall project scope, cost and schedule) and Critical Decision 3a (authorizing acquisition of plasma-facing components, machine core structures and other needed for installation during 2020 as well as other key items). The project's readiness for these activities was reviewed by DOE in August, following standard methodology for DOE-SC projects. Preparations for DOE review included a Basis of Estimate Review (BoER) and a Director's Review, in addition to verification of the design at a TF Bundle review. These reviews confirmed readiness for the Independent Project Review (IPR). Each of these activities, along with supplemental efforts and tasks, played a pivotal role in defining and verifying the Project to baseline.

The Project also completed a large number of technical reviews of subsystems, the results of which were communicated to the CDE-2/3a review as evidence of readiness to proceed. The Project is moving ahead with the CDE-3A activities that support the early finish of May, 2021.

The project cost, schedule and technical baseline as well as planned procurements and preparedness for the 2020 installation were subjected to, and endorsed by an ESAAB-equivalent process convened by Steve Binkley, leading to his approval of CDE2/3a on September 30.

### Recovery Project Management Highlights

The Recovery Project had a number of Project-level reviews in FY2019. These reviews included:

- The Basis of Estimate Review (March 18-March 20, 2019). This review evaluated the basis of estimate of the NSTX-U Recovery Project. This involved examination of detailed cost books prepared by the Project of the P6 schedule file, the Cobra cost file, and the documentation associated with risk (risk and uncertainty matrices). This review validated the basis of estimate as "well-documented, comprehensive, accurate, and credible" as per the criteria of GAO-09-3SP and DOE Order 413.3B.
- A second Director's Review was held in July 2019 that covered the same charge questions as the previous Director's Review and subsequent IPR. The committee found that the Project was ready for the CDE-2/3A review following the completion of some modest recommendations. Those recommendations were completed.

- The CDE-2/3A IPR was held August 27-29, 2019. This review found that the Project was ready for CDE-2/3A ESAAB approval following modest corrections for the cost and schedule.
- The Preliminary Project Execution Plan (PPEP) was fully signed on October 22, 2018. The draft Project Execution Plan was signed by all PPPL, PSO, and FES stakeholders on July 1, 2019.

### **Recovery Project Organization Updates**

- In the fall of 2018, the Project was reorganized with the addition of four Associate Project Managers. These individuals act as control account managers (CAMs) for the control accounts assigned to them, which allows the Cognizant Engineers (COGs) to focus on the technical aspects of the Project.
- Rich Hawryluk was named interim Project Director in March 2019, while Les Hill was named interim Project Manager at that same time. John Galayda became Project Director for NSTX-U Recovery on August 1, 2019, and Les Hill became the permanent Project Manager on September 4, 2019.

### **Recovery Technical Highlights**

The NSTX-U Recovery Project held a total of thirty-two conceptual design reviews (CDRs), preliminary design reviews (PDRs), and final design reviews (FDRs). Key final design reviews facilitating the CDE-3A scope include:

- Heat Transfer Plate and Heat Transfer Tubing (November 1, 18) - [link](#)
- CS Casing Final Design Review (December 28, 2018) - [link](#)
- Test Cell Shielding (January 14, 2019) - [link](#)
- Passive Plates (August 21, 2019) - [link](#)
- Machine Core Structures (August 5 - 6 2019) - [link](#)
- Radiation Annunciation (February 12, 2019) - [link](#)
- Plasma Facing Component Diagnostics (March 28, 2019) - [link](#)
- PF-4/5 Realignment Clamps (August 9, 2019) - [link](#)
- 13.8 kV Breaker Refurbishment and Upgrade (July 12, 2019) - [link](#)

Additionally, key PDRs were held that supported the CDE-2 baselining and maintaining momentum towards the CDE-3B review:

- Personnel Safety System PDR (June 26, 2019) - [link](#)
- CS Casing PDR (October 16, 2018) - [link](#)
- Inner-PF Bus Work (February 28, 2018) - [link](#)

### **Recovery Procurement Highlights**

Key procurements launched in FY19 under DOE pre-authorization were critical in maintaining the early finish schedule. These included:

- The purchase of Graphite material to support PF manufacturing.
- Copper conductor for the inner-PF coils was purchased from Luvata (Finland), followed by grit blasting and priming at ICAS (Italy). G10 spacers and filler material were also procured.
- A contract was placed with Sigma Phi for the construction of six inner-PF coils. The work before ESAAB will allow tooling to be developed, the winding lines to be set up, and the procedures and test plans to be developed. Actual winding will be done following ESAAB CDE-2/3A approval.
- A contract was placed for the Center Stack casing.
- A contract was placed for the heat transfer plate.
- Work was initiated at PPPL for the PF-1b power loop and the shielding improvements.

## **Executive Summary of Research Results - FY2019 Milestones**

**Summary of R(19-1): Validate transport models for high-beta ST H-mode plasmas and assessing the importance of multi-scale effects in NSTX/NSTX-U turbulent transport**

- Linear CGYRO analysis has identified unstable MTM & TEM outside  $r/a \geq 0.6$ , with missing transport in central region. Central profiles predicted to be very near or above threshold for energetic particle mode (EPM), whose threshold depends on the total pressure (thermal + fast ion) gradient. Furthermore, global, low-n ballooning modes also predicted unstable (M3D-C1). These results lead to a developing hypothesis that the central  $T_e$  ultimately clamped by pressure limit.

- A comprehensive validation effort suggests electron-scale (ETG) alone can account for anomalous electron losses in certain discharges. The effort utilized high-k turbulence measurements + novel synthetic diagnostic to constrain simulation results using numerous sensitivity scans. It was found that variation in  $\nabla n$  and  $\nabla T$  improve heat flux agreement, but small variation in geometry (s and q) required to best match high-k fluctuation spectra.
- Single-scale conditions identified in an NSTX H-mode at intermediate  $\beta$  (between L-mode and high- $\beta_{pol}$  H-mode) with strong ETG drive + near-marginal ion-scale stability, which indicates that multiscale effects may be important for understanding the transport in these plasmas.

### **Summary of R(19-2): Develop optimized ramp-up scenarios in spherical tokamaks**

- A reduced model for the plasma breakdown phase, where the plasma transitions from partially to fully ionized along open field lines, was developed in conjunction with the NSTX-U/MAST-U collaboration. This predictive model gives the ability to predict the timing of the initial rise in the plasma current based on the prefill gas pressure and the evolution of the axisymmetric magnetic and electric fields.
- The TOKSYS simulation platform was advanced with the addition of reduced models for the evolution of the q-profile and fast ion pressure using a fast solver for the magnetic diffusion equation along with neural network models for geometric parameters, plasma resistivity, bootstrap current, and current drive. These tools support the development and testing of control solutions that increase the resiliency of current ramp-up scenarios.

### **Summary of R(19-3): Validate tearing mode physics for tearing avoidance in high-performance scenarios**

- Predictive capabilities of tearing modes have been tested with resistive DCON and M3D-C1 simulations against an experiment on DIII-D ITER Baseline (IBS) scenarios. The tearing mode index  $\Delta'$  in resistive DCON is shown to be a convenient measure of qualitative trends, and M3D-C1 demonstrated its ability to predict the stability boundary of tearing modes.
- Resistive DCON have been used to predict ideal and resistive MHD instabilities for NSTX-U, showing both 2/1 and 3/1 tearing modes can be unstable in high-performance target scenarios without rotation stabilization.

### **Summary of R(19-4): Assess energetic particle transport by sub-TAE instabilities and develop reduced EP transport modeling tools**

- The effect of sawteeth on fast ion transport has been studied in reproducible, 2 sec-long sawtoothing NSTX-U L-mode discharges. The study indicated that standard partial and full reconnection models could not fully reproduce the changes in the fast ion distribution induced by sawtooth crashes. The “kick model,” which takes into account both the energy and pitch angle of the fast ions, achieves better agreement.
- The kick model was used to model the evolution of the fast ion population during fishbones, showing a slightly different localization of the depletion of the distribution when mode amplitude and frequency variations are taken into account. The model has been extended to MAST, and results indicate that fishbones can efficiently redistribute NB-driven current, leading to changes in the q-profile.
- TRANSP/kick model simulations have been carried out to study the effect of NTMs in DIII-D discharges. The results, which are based on experimentally inferred NTM island widths, show good agreement with measured neutron rates and the fast ion distribution as measured by the FIDA and NPA diagnostics. The model, along with algorithms to identify NTM properties from SXR and Mirnov coil data, is being extended for use on NSTX-U.

## **Executive Summary for Additional Research Highlights**

### **Boundary Science**

#### **Summary of Research Highlights for Pedestal Structure and Control**

- Lithium granule injection, as part of the collaboration on EAST, has identified a granule size threshold of  $>500 \mu\text{m}$  for triggering ELMs. With injection of granules below this threshold size, a higher ELM frequency, and reduced peak heat flux, was observed.
- Gas Puff Imaging data reveal the existence of “blob wakes,” transient small structures seen in the wakes of blobs moving poloidally through the scrape-off layer in high-power H-mode discharges. The wakes share features of drift waves and/or drift Alfvén waves.

#### **Summary of Research Highlights for Divertor and Scrape-Off Layer**

- Studies of blob disconnection from the divertor have been carried out within the framework of an electrostatic, two regime model. The normalized blob size and its radial velocity both increase with radius outside the separatrix, the latter following the theoretical scaling in the “connected ideal-interchange” regime except for the farthest distances from the separatrix.

## Summary of Research Highlights for Materials and PFC

- Collaborative experiments on EAST with lithium microsphere injection using the new W upper divertor led to an improvement in edge stability that resulted in the elimination of ELMs and the achievement of 100 s pulse lengths. Analysis using SOLPS suggested that the powder injection reduced the divertor recycling coefficient by ~25% from near unity, consistent with the observed 10% reduction in stored energy.
- A new Impurity Powder Dropper (IPD), capable of injecting a wide range of impurity species including boron-based compounds, was deployed on ASDEX-Upgrade, DIII-D, EAST, and KSTAR. Boron-nitride (BN) injection into ELM-suppressed ASDEX-Upgrade discharges resulted in 10-20% increased stored energy, and the conditioning lifetime was found to be approximately four discharges. BN injection into KSTAR resulted in ELM mitigation.
- A second-generation flowing lithium liquid limiter (FLiLi) was designed and installed on EAST. Operation with this FLiLi limiter resulted in progressive conditioning and ELM mitigation.
- A third-generation FLiLi, entirely constructed out of TZM, was also built and tested on EAST. The limiter performed well in reducing recycling and suppressing ELMs, but upon removal, damage to the electron-drift side was evident.

## Core Science

### Summary of Research Highlights for Transport and Turbulence

- Large-scale  $m=2/n=1$  modes were observed to affect high-k turbulence, with a jump in frequency and a broadening of the spectral width of the high-k turbulence with the presence of the 2/1 mode. Bi-spectral analysis indicates a non-linear coupling between the 2/1 mode and high-k turbulence over a broad frequency range.
- First-of-a-kind non-linear global GTS simulations were carried out to study low-k turbulence and associated transport in an L-mode discharge. The simulations indicated significant ITG and DTEM modes for  $\rho > 0.65$ . The turbulence from these modes produced large energy transport for ions (but not for electrons) in this region.
- A reduced model that takes into account the effect of ion orbit excursions, which can modulate the effects of transport sources and losses and (indirectly) the radial electric field, is under development. The formulation will be applied to NSTX and NSTX-U data to investigate the dominant processes determining the edge electric field at low aspect ratio.

### Summary of Research Highlights for Macroscopic Stability

- The resonant and non-resonant error field effects over various combinations of possible PF4U/L, PF5U/L, and Inner-TF misalignments were investigated using the Monte-Carlo analyses based on IPEC, NTV, and M3D-C1 calculations. A set of engineering requirements was successfully identified to meet physics and engineering requirements for coil tolerances in NSTX-U.
- The error field effects on the field-pitch and footprint near the divertors have also been investigated by M3D-C1, indicating the importance of multi-modal error field corrections.
- The machine learning approaches of neural networks and random forests have been used to improve the estimation of the ideal MHD no-wall beta limit in NSTX for use in the DECAF disruption forecasting code.
- CORSICA code has been adapted for NSTX-U in order to improve accuracy of equilibria for resistive stability analyses such as resistive DCON, MARS, and M3D-C1 simulations.
- CORSICA and DCON codes have been applied to a compact toroid device to identify the variations of the tearing mode stability boundaries for validation purpose through collaboration between NSTX-U and General Fusion. The applications give a theoretical foundation for designing a future compact toroid to optimize dynamic path to remain MHD-stable to full compression.
- The EPI prototype systems have been successfully tested by demonstrating their rapid response time and capability to attain the required high projected speeds on this fast time scale, e.g., a 3.2 g sabot to over 150 m/s within 1.5 ms, consistent with the calculations, giving confidence that larger ITER-scale injector can be developed.

### Summary of Research Highlights for Energetic Particles

- Magnetic fluctuations in the ion cyclotron range of frequencies are commonly observed on NSTX(-U). While similar to ICE, as observed on conventional aspect ratio tokamaks in terms of frequency relative to the magnetic field, the emission in NSTX(-U) corresponds to a source region deeper in the plasma near the location of an internal transport barrier. Measurements from a toroidal array of fast probes indicate that the emission is long wavelength and coherent spatially.
- 3D non-linear simulations of GAEs in NSTX-U have been carried out, and results show excellent agreement with experimentally measured toroidal mode numbers and frequencies. The simulation predictions also show agreement with the experimentally

observed suppression of GAEs with tangential beam injection, indicating complete suppression of these modes with just a small fraction (7%) of the beam ion population being tangential.

- An analytic expression for non-linear wave evolution in the presence of scattering of EP from background turbulence was derived, and solutions recover trends in saturation amplitudes and characteristic evolution time scales of TAE/RSAE modes.
- Chirping of Alfvén waves has been reproduced by the guiding center ORBIT code, which indicates the chirping occurs when small changes in the equilibrium bring a saturated Alfvén mode in contact with the Alfvén continuum, thus experiencing strong damping.
- A machine learning algorithm has been applied to interpret NSTX(-U) magnetics data and characterize the unstable regimes in phase space. The work is being done in collaboration with MAST-U and York University, and it will have possible application for real-time AE control, mitigation and suppression.

### **Summary of Research Highlights for Solenoid-Free Start-Up and Ramp-Up**

- Calculations have been carried out using the TSC code in support of a design using localized biased electrodes, rather than vessel wall, biasing for transient co-axial helicity injection. The results show that substantial current, up to 1 MA, and closed flux can be generated. A double-biased electrode configuration is being designed for testing on the URANIA spherical tokamak.
- The physics of 3-D plasmoid-mediated magnetic reconnection during transient CHI in a spherical tokamak has been investigated with non-linear MHD simulations. It was found that even in the presence of 3-D fluctuations during the injection phase, a large volume of closed flux surfaces is possible as the fluctuations subside during the decay phase. Complete stabilization of the fluctuations is found for higher TF, showing promise for future, high- $B_T$  spherical tokamaks.
- A collaboration on CHI on the QUEST tokamak in Japan has employed a new power supply-PF coil configuration with more elongated and inside-shifted plasmas to reduce the injector flux footprint and result in easier plasma detachment from the CHI electrodes and more effective flux closure. The plasma was generated in a higher TF region, which holds the promise for higher current amplification and potentially higher toroidal current.

### **Summary of Research Highlights for Wave Heating and Current Drive**

- The AORSA code was used to explore HHFW absorption for two different frequencies, and with and without NB heating. The electron and ion (both fast and thermal)

absorption was found to be a sensitive function of the electron to ion temperature ratio. The presence of fractional amounts of hydrogen could open up new HHFW heating scenarios in NSTX-U, particularly without NBI.

- HHFW propagation and power losses in the scrape-off layer have been studied using a new 2-D full wave code that contains realistic boundaries. Lower SOL power losses occur when the SOL volume is smaller and the distance between the last closed flux surface and the antenna is smaller.
- The PPPL team, in collaboration with the RF SciDAC team, examined the full 3-D device geometry including realistic antenna geometry to capture 3-D effects, the antenna-plasma interaction in the SOL, and core wave propagation. Using PETRA-M, a stronger interaction between HHFW and the SOL plasma is found for lower antenna phasing consistent with NSTX observations. PETRA-M and the SPIRAL full orbit following code will be used in conjunction to study the 3-D wave field effects on NB-generated fast ions.
- Modeling of a high frequency, high TF scenario is being performed in support of the ECH-assisted, solenoid-free startup component of the NSTX-U/QUEST collaboration. First results of the calculations indicate that the startup process is a self-amplifying non-linear process that can result in a rapid plasma current rise.

### **Summary of Research Highlights for Advanced Scenarios and Control**

- A large database of direct-inductively-started ST discharges was used to develop the reduced semi-empirical model to yield prefill and feed-forward coil current targets for reliable startup on NSTX-U and MAST-U. The predictions are constrained by operational limits unique to each device, including coil heating and mechanical stress limits, as well as by semi-empirical models for current drive, equilibrium, and stability.
- A control-oriented modeling approach for magnetic and kinetic profiles, using a fast solver for the magnetic diffusion equation and neural networks for geometry, plasma resistivity, bootstrap current and current drive, has been developed.
- This modeling approach has been extended to include neural network modeling of density and temperature profile shapes based on constraints given by the Greenwald fraction, 0-D power balance, and assumptions on  $Z_{\text{eff}}$ , impurity species, and  $T_e/T_i$ . These models have been tested and shown to enable faster-than-real-time predictions.
- A prototype fault detection algorithm that makes use of the TOKSYS model of NSTX-U has been implemented in Simulink and is being tested for implementation on the

---

NSTX-U real-time computer. This development improves upon previously developed algorithms to prevent operation beyond coil current or mechanical stress limits.

## Performance of FY2019 Notable Outcomes

**FES:** Prepare an NSTX-U Recovery Project cost estimate that is deemed by external review to be well documented, comprehensive, accurate, and credible, as defined by GAO-09-3SP and DOE Order 413.3B, by March 31, 2019.

- **Completed.** A Basis of Estimate Review (BoER) was held at PPPL on March 18-20, 2019. The BoER team affirmed that the NSTX-U Recovery Project cost estimate is well documented, comprehensive, accurate, and credible as defined by GAO-09-3SP and DOE Order 413.3B. The NSTX-U Recovery team has reviewed the BoER debrief slides and will implement the panel's recommendations in the near-term including those items recommended to be completed prior to EVMS certification refresh, Director's Review, and/or the CDE-2/3A review.

**FES:** For the NSTX-U Recovery Project, complete a final design review(s) for the integrated casing assembly, including the heat-transfer tubing and plates and associated attachment hardware, the vertical and angled sections of the Center Stack casing, and the horizontal divertor end-flanges, bellows, collars, and organ pipes by December 31, 2018 (Objective 2.1).

- **Completed.** The Center Stack casing final design review (FDR) was held on December 28, 2018. The FDR was held to review the Center Stack Casing design, ensure all casing requirements are met, and to ensure all casing interfaces have been identified and accounted for - all in support of the procurement and manufacturing of a new Center Stack Casing. The FDR was deemed successful pending resolution of chits.

**FES:** For the NSTX-U Recovery Project, award a sub-contract(s) for the procurement of the integrated casing assembly, including the heat-transfer tubing and plates and associated attachment hardware, the vertical and angled sections of the Center Stack Casing, and the horizontal divertor end-flanges, bellows, collars, and organ pipes by March 31, 2019 (Objective 2.2).

- **Completed.** Center Stack Casing bid proposals arrived on March 15. The SPEB met March 16 to review bids for the fabrication of the CSC. A phased subcontract was issued for the casing, and additional subcontracts were issued on March 29, 2019 to meet the FES Notable deadline of March 31, 2019.

**FES:** For the NSTX-U Recovery Project, fabricate at least one production inner-poloidal magnetic field coil. Verify the quality of the coil through electrical testing and dimensional inspection by September 30, 2019 (Objective 2.2).

- **Missed** The achievement of this Notable Outcome was not possible because permission to wind a coil either at a vendor or at PPPL required ESAAB approval which required a

CDE-2/3A IPR, and the IPR dates were later than previously planned due to the addition of the Basis of Estimate Review, the TF bundle analysis and sample testing, and a second Director's Review as prerequisites for the IPR. The winding of the coil will take place in FY20 after ESAAB approval.

### **Goal 5.0 - Environment, Safety, and Health**

**PSO:** Establish an effective and appropriately tailored Accelerator Safety Order Implementation Plan for the NSTX-U Recovery Project and obtain DOE's concurrence. (Due September 30, 2019.)

- **Completed.** Internal approval was obtained for Rev. 0 of the Accelerator Safety Order Implementation Plan (ASOIP) on May 23, 19. Comments on Rev. 0 of this plan were received from DOE. A revision to the ASO implementation plan was signed and submitted to the DOE Princeton Site Office (PSO). PSO subsequently accepted the plan as satisfying the PEMP Notable for Goal 5 related to the development of the implementation plan on May 24, 19.

## **NSTX-U Recovery Project - Project Management Accomplishments**

The project management focus for the NSTX-U Recovery Project has been to accomplish the CDE-2/3A baseline review. The progress towards this baseline review is marked by the project actions described below.

### **September 2018 Director's Review**

The September 2018 Director's review, held at the end of FY18 (September 5-7, 2018), was envisioned to proceed baselining (CDE-2) and initial fabrication approval (CDE-3A) for the Recovery Project, and as such was a complete review of the Project. The committee members for this review were as follows:

**Table 1: Membership of the September 2018 Director’s Review**

<b>DIRECTOR’S REVIEW PANEL CHAIR</b>	
John Post	
<b>COST AND SCHEDULE COMMITTEE</b>	
John Bielecki	Karl Flick
Doug Gray	Diane Hatton
<b>TECHNICAL COMMITTEE</b>	
Ken Fouts	Steve Renfro
Greg Tietbohl	Tom Todd
<b>ES&amp;H, ASO, &amp; OPS</b>	
Mike Bebon	Stefan Bosch
Ian Evans	Peter Grivins
<b>MANAGEMENT COMMITTEE</b>	
Ronald Lutha	John Post
George Srajer	

Key findings from the review include:

- The technical scope designated for CDE-3A approval was found to be appropriate.
- The cost estimate was found to not be appropriately documented.
- Risk mitigation strategies were found to be not fully documented.
- It was strongly cautioned not to re-use the legacy access control system.

These outcomes set the stage for many project management actions taken in FY19. For more information on this review, see the Annual Report for FY2018.

The Preliminary Project Execution Plan (PPEP) was fully signed on October 22, 2018.

## **Response to Recommendations from the September 2018 Director’s Review**

The findings from the September 2018 Director’s review were addressed in FY19 in the following fashion:

- The Personnel Safety System was added to the Project.
- The risk registry was revisited, with mitigation steps more clearly documented.
- A set of 50 comprehensive cost books were developed by the Cognizant Engineers and Associate Project Managers. These cost books included comprehensive backup information. These cost books were reviewed by the Project Management team as well as the PPPL Project Management Office and consultants from Tecolote Research, Inc.

### March 2019 Basis of Estimate Review

The FY19 PEMP Notable Outcome was met by the successful completion of the Basis of Estimate Review. This committee met at PPPL March 18-20, 2019 for a three day review. The web site for the review is here:

<https://sites.google.com/pppl.gov/20190121-nstx-u-basis-of-estim/home>

The committee members are listed in Table 2.

**Table 2: Membership of the March 2019 Basis of Estimate Review (\* Review Chairperson)**

BASIS OF ESTIMATE REVIEW	
Diane Hatton*	
Kathy Bailey	Mike Barry
Rejean Boivin	Brian Bozarth
Doug Gray	Khianne Jackson
David Jansen	Joseph Milines

The committee was provided plenary talks by R. Hawryluk (Interim PD), L. Hill (Interim PM) and G. Swider (Risk Manager at that time). The committee then broke into smaller groups, where it conducted interviews with APMs and Project Cognizant Engineers.

The committee ultimately answered the charge questions as follows:

1. Is there sufficient detailed information available and documented to support the cost estimates? **Met**
2. Are the estimates accurate, credible, comprehensive, and do they follow the GAO 12 Steps for Cost Estimating Best Practices? **Met**

3. Are the project risks identified reasonable and included in the project cost?  
*Substantially Met*
4. Is the schedule resource loaded, identify a critical path, and include sufficient details to successfully achieve CD-4 on time? *Met*
5. Can you positively affirm the NSTX-U Recovery Project cost estimate is well documented, comprehensive, accurate and credible as defined by GAO-09-3SP and DOE Order 413.3B?

***Basis of Estimate Review Committee response: The BoER Team affirms that the NSTX-U Recovery Project cost is well-documented, comprehensive, accurate, and credible.***

A link to the final report of the BoER committee is [here](#). The committee made a number of recommendations, which were addressed in advance of the July 2019 Director's Review.

## **Response to Recommendations from the Basis of Estimate Review**

Actions taken in response to the BoER recommendations include:

- Out-year escalation was removed from the cost books and included in Cobra and P6 rate sets.
- The P6 schedules for Recovery and Maintenance and Run Preparation were electronically linked.
- Project CAMs were given access to P6 via a stand-alone viewer program.

## **Recovery Project Management Changes**

A number of management changes occurred in FY19 to support the efficient execution of the project.

A new layer of management was added between the Project Manager and the Cognizant Engineers. These four Associate Project Managers have extensive experience in project management, both within DOE and, in some cases, commercial nuclear and other non-government organizations. These individuals function as CAMs for the control accounts assigned to them.

Rich Hawryluk was named interim Project Director in March of 2019, and Les Hill was named interim Project Manager at the same time. Les was named permanent Project Manager on September 4, 2019. Les has significant experience in managing large, complex projects in the

commercial nuclear power industry and has worked in the DOE system managing projects for almost 20 years, first at Brookhaven National Laboratory, and at PPPL since April 2016.

A search was conducted for a permanent Project Director. John Galayda was selected and started work at PPPL August 1st. John has extensive experience with large DOE projects, including work at Brookhaven (NSLS), Argonne (APS), and SLAC (LCLS and LCLS-II)

## July 2019 Director’s Review

With the success of the BoER, the Recovery Project turned to preparations for the CDE-2/3A IPR. This involved calling a Director’s review in order to evaluate readiness for the IPR. The web site for the review is at:

<https://sites.google.com/pppl.gov/nstx-u-recovery-cde23a-dr2/home>

The Director’s Review team is indicated in Table 3.

**Table 3: Membership of the July 2019 Director’s Review (\*Subcommittee Chairperson)**

<b>DIRECTOR’S REVIEW PANEL CHAIR</b>	
Kem Robinson, LBNL	
<b>COST AND SCHEDULE COMMITTEE</b>	
Tanya Boysen	Diane Hatton*
David Jansen	Wayne Steffey
<b>ES&amp;H, ASO, &amp; OPS COMMITTEE</b>	
Ian Evans	Bob Lee
Jim Tarpinian*	
<b>MANAGEMENT COMMITTEE</b>	
Angus Bampton	Allison Lung*
George Srajer	
<b>TECHNICAL COMMITTEE</b>	
Kevin Freudenberg	Steve Renfro*
Greg Tietbohl	Tom Todd

The review committee addressed a set of charge questions that addressed the full spectrum of Project considerations (technical, cost, schedule, risk, ES&H, management). The committee was provided specific technical presentations on the CDE-3A scope, provided in Table 4.

**Table 4: Recovery Project CDE-3A Scope<sup>1</sup>**

<b>Description</b>
Plasma Facing Components
Machine Core Structures
Passive Plates
Center Stack Casing Fabrication and Delivery
PF-4/5 Realignment
PF Coil Winding, Fabrication, and Delivery
Interspace Pumping System
PFC Diagnostics
Ip Rogowski
PF1B Bipolar Circuit
NSTX-U Camera Surveillance
Rad Mon Compliance
NTC Shielding
PSS Circuit Breakers

The committee was also provided a version of the draft Project Execution Plan (PEP) signed by all PPPL, PSO, and FES stakeholders.

The committee determined that the Project was ready for the CDE-2/3A IPR following the completion of a small number of recommendations (final report [link](#)). These recommendations were closed in advance of the CDE-2/3A Independent Project Review.

## **Response to Recommendations from the July 2019 Director's Review**

Key findings from the July 2019 Director's review were addressed in the following fashion:

- Documentation was provided to the CDE-2/3A IPR team showing the detailed status of the CDE-3A scope.
- The list of ES&H elements included in the ARR scope was refined to include only those relevant to NSTX-U operations.
- Drill-down training was held with the CAMs

<sup>1</sup> The Cooling Tube/Plate scope was separately authorized by DOE in its entirety in April 2019.

- An advanced/critical procurement planning program was defined.
- The project tailoring was clearly defined in a set of detailed matrices, as well as a summary table in a revised draft of the PEP.

## August 2019 CDE-2/3A Integrated Project Review

The CDE-2/3A Independent Project Review was called August 27-29, 2019. The web site for the review is:

<https://sites.google.com/pppl.gov/nstx-urecoverycde-23areview/home>

The committee for the IPR is given in Table 5.

**Table 5: Membership of the August 2019 Independent Project Review**  
 (\*Subcommittee Chairperson)

<b>IPR CHAIR</b>	
Hanley Lee	
<b>COST AND SCHEDULE COMMITTEE</b>	
Jerry Kao	Cathy Lavelle*
Pam Utley	
<b>ES&amp;H, QA, &amp; ASO</b>	
Mike Epps*	Dave Freeman
Bob May	
<b>MAGNETS COMMITTEE</b>	
Renuka Rajput-Ghoshal	Soren Prestemon*
<b>MANAGEMENT COMMITTEE</b>	
David Arakawa	Bill Cahill*
Joe Eng	Bill Matisiak
<b>NON-MAGNET, TECHNICAL SYSTEMS, ENGINEERING, &amp; COMMISSIONING COMMITTEE</b>	
Arnie Kellman*	Brad Nelson
Will Oren	

This committee found that the Project was ready for CDE-2 baseline and CDE-3A approval for the scope noted above following the completion of a small number of recommendations.

## **ESAAB Approval**

CDE-2 baseline and CDE-3a procurement (for specific components) approval was granted on September 30th, 2019.

## **NSTX-U Recovery Project - Technical Accomplishments**

Key technical progress on the NSTX-U Recovery Project is highlighted in the following sections.

### **Plasma Facing Components (WBS 1.01.01)**

The PFC tiles underwent a successful FDR (final design review) in late September 2018, and 2019 has been spent preparing for fabrication that is scheduled to start after ESAAB approval. As a key step, graphite material for the tiles has been ordered as part of the DOE pre-authorized work. This includes ET-10 for the CSFW tiles, Sigraphine 6510 for the CSA/IBDH/IBDV/OBD12 tiles, T933 for the OBD345 tiles, and 6/6/6 3DCFC for the OBD345 unique diagnostics and gap tiles. All of this material has been delivered and is ready for use in fabrication.

Additionally, an activity was launched to identify key manufacturers via a prototype manufacturing assessment; numerous potential vendors are fabricating one of each tile type. This will enable PPPL to identify which vendors are best able to produce the tiles, while giving the vendor that is ultimately selected a head start by having already programmed the manufacturing.

Finally, all chits from the September 2018 FDR were resolved.

### **Vacuum Vessel and Internal Hardware (WBS 1.01.02)**

#### **1.01.02.01 Machine Core Structures (6010)**

In FY18, the full set of vacuum interfaces and coil supports were brought to preliminary design review (PDR). FY19 saw the design finalized and the fabrication commence.

A preliminary design review for the CS Casing was held on October 16, 2018. Information presented at that review, as well as information gained from consultation with experts from Edison Welding Institute, resulted in a decision in December 2018 to fabricate a new casing. This enabled all interfaces with the new PFCs and cooling features to be accommodated, while allowing full penetration welds which can easily handle all static and transient load cases. This design was validated at the Casing FDR on December 28, 2019, and all chits were resolved for

that FDR. The vendor for the CSC design HOLTEC. This FDR satisfied a PPPL Notable Outcome.

The remainder of the machine core structures (MCS) scope underwent an FDR August 5-6, 2019. This review validated the design of the PF-1a & -1b coil slings, the PF-1c reentrant flanges, the double O-ring vacuum seals, the upper ceramic break, the outer skirt, the lateral supports, and the pedestal.

The MCS was reviewed at the July Director's Review and the CDE-2/3A IPR and found to be ready for CDE-3A approval.

#### **1.01.02.02 Passive Plates (6000)**

The passive plate repair design was completed in August 2019; the combination of plate-back stiffeners, bracket reinforcements, electric straps and He-tube supports was found to be sufficient to support the passive plates against disruption loads. This was confirmed at the FDR held August 21, 2019. The passive plate scope was reviewed at the July Director's Review and the CDE-2/3A IPR, and found to be ready for CDE-3A approval.

#### **1.01.02.04 Cooling Tube/Plate (6005)**

The FDR for the Heat Transfer Tubing (HTT) and Heat Transfer Plate (HTP) was successfully completed on November 1, 2018.

Based on pre-authorization letters, the contract for the HTP was placed with Hollis on March 31, 2019. The manufacturing, inspection, and testing plan and the machining readiness review at the vendor's site have been successfully completed. The HTP sub-components are in the process of being fabricated. The HTT will be bent into shape at PPPL, and contracts for tooling for that operation have been released. These contracts were part of satisfying a 2019 Notable Outcome.

Though fully authorized under pre-authorization, the HTT and HTP were reviewed at the July Director's Review and the CDE-2/3A IPR, and found to be appropriate.

#### **1.01.02.06 & .07 Center Stack Casing Fabrication (6035, 6040)**

This WBS element is responsible for the fabrication of the Center Stack (CS) casing. A source selection process was held from January to March 2019. This resulted in Oak Ridge Technology (ORT) / Holtec International as a small business protege joint venture being selected to fabricate the components. The contract was awarded, all material is on order, and fabrication is ongoing. Weekly meetings are held to monitor progress and address any design or fabrication issues.

The placing of this contract was part of satisfying a 2019 Notable Outcome.

### **1.01.02.08 PF-4 / 5 Alignment and Vessel Metrology (6030)**

A vendor came to PPPL in winter of 2019 to set up a “global” metrology coordinate system, with metrology monuments that allow precise locating of components both inside and outside the NSTX-U vacuum vessel. This metrology system was used to make an assessment of the PF-4 and PF-5 coil tilts and shifts. A peer review covering the PF-4/5 realignment process was held on May 31, 2019, while a PDR and FDR for “pancake clamps” was held on July 10, 2019 and August 9, 2019, respectively. These reviews were successful. The pancake clamps were reviewed at the July Director’s Review and the CDE-2/3A IPR, and found to be ready for CDE-3A approval.

## **Magnets**

### **1.01.03.01 & .01A Inner PF Coil Replacement (4010, 4011)**

Work in FY19 completed the final design elements of the Inner-PF coils, completed the prototyping program, and resulted in the contracting of the coils to Sigma Phi in France.

The prototype program, initiated in FY18, was designed to assess the ability of potential manufacturers to fabricate the coils on schedule with appropriate quality. Four coils were manufactured as part of this program. The assessment was completed on October 10, 2018, with the submission of the final report.

A modest improvement to the design was vetted in an FDR on January 4, 2019. This review assessed an improved design to the water fitting and was successful.

The source selection process was conducted between December and March 2019, which assessed three outside vendors and PPPL for the optimal fabricator of the PF Coils. After a several week evaluation process, a recommendation to have all coils fabricated at Sigma Phi was approved by the Source Selection Official and PSO. The contract was let on June 13, 2019. The terms of the contract allowed all work on the winding line and tooling to be done before ESAAB CDE-2/3A approval, but the winding itself is contingent upon that approval.

Once Sigma Phi was selected, a building was leased by Sigma Phi to house the two winding lines, and building preparations began. Additionally, Sigma Phi placed contracts to purchase winding line materials which will be pre-assembled prior final assembly in the leased building. Tooling designs are in process, and the draft Manufacturing, Inspection, and Testing plan is in review at PPPL.

The Inner-PF coil scope was reviewed at the July Director's Review and the CDE-2/3A IPR, and found to be ready for CDE-3A approval.

#### **1.01.03.02 Coil and Bakeout Bus Support (4020)**

A successful PDR for the Inner-PF bus work was held on February 28, 2019.

#### **1.01.03.05 TF Torsional and Tensile Effects (4030)**

A task force was assembled as a result of outstanding concerns related to the ability of the Inner-TF Bundle to achieve the GRD shot spectrum. The design verification and validation review (DVVR) process identified a number of potential concerns with the bundle, largely related to the shear capability of the insulation system and the ability of the bundle to accommodate thermal conditions resulting in tensile stress. In consultation with FES, this study was identified as a prerequisite to baselining.

A focused working group was formed to address this critical issue starting in March 2018, and developed a plan which involved the following elements:

- Assessment of the stress and strain in the bundle and surrounding structures with advanced FEA models.
- Assessment of delamination with various numerical models.
- Collection of new test data on the tensile, shear, and fracture strength of the bundle.

Two reviews were held to resolve this issue. A Stage 1 review was held April 9, 2019 to receive feedback from subject matter experts to determine if proposed analysis and test plans would allow the project to address issues previously identified at the DVVR and ECO reviews. The committee validated PPPL's plans, with some additional suggestions.

The second review, held August 7- 8 2019, presented the final conclusions of the study. It was found that limited delamination of the bundle would likely occur, but would be limited in spatial extent. It would not deleteriously impact the overall structural behavior of the machine. The committee agreed with PPPL's conclusion that this degree of delamination would not pose a problem in achieving the target spectrum. The committee recommended a small number of follow-up items to further solidify this conclusion.

## **Vacuum and Fueling**

### **1.03.03.03 Interspace Vacuum Pumping System (3010)**

An FDR for the Interspace Vacuum Pumping system was held on February 20, 2019. This review was successful. The system was reviewed at the July Director's Review and the CDE-2/3A IPR, and found to be ready for CDE-3A approval.

## **Plasma Diagnostics / NSTX-U Diagnostics**

### **1.04.01.01 Instrumentation (8000)**

A laser-based TF twist measurement was added to the instrumentation scope as part of the inner-TF review; this scope was briefly reviewed at the second inner-TF bundle review. Design work on the instrumentation job resumed in April 2019. The layout of the fiber routing, from the DARM to the patch panel and then to the torus, was completed. Additional small cable trays have been designed, and installation layouts for 90% of the sensors has been completed.

### **1.04.01.02 PFC Diagnostics (8035)**

An FDR for the PFC Diagnostics was held on March 28, 2019. This review was successful. The system was reviewed at the July Director's Review and the CDE-2/3A IPR, and found to be ready for CDE-3A approval.

### **1.04.01.03 Aerodag Replacement (8010)**

A successful CDR for the Aerodag replacement was held on August 22, 2019.

### **1.04.01.04 Plasma Current Rogowski Replacement (8015)**

An FDR for the Plasma Current Rogowski Replacement was held as part of the PFC diagnostics review on March 28, 2019. This review was successful. The system was reviewed at the July Director's Review and the CDE-2/3A IPR, and found to be ready for CDE-3A approval.

## **Power Systems / AC & DC Power Systems**

### **1.05.01.03 PF1B Bipolar Circuit (P105)**

The FDR for the PF-1B power loop was held on September 20, 2018; this review was successful. Work was initiated on this scope under terms of the pre-authorization letter of May 16, 2018. The pre-authorized work completed includes the fabrication, bench testing, and installation of two firing generators for the repurposed power converters for the PF1BU circuit, and installation and testing of PLC racks and components (opto-isolators, I/O and communication modules) for remote control and converter monitoring. Additionally, DC CTs (DC current transducers) were installed for power circuit closed loop current control and protection. This consisted of the installation of four measuring heads and metering units in the cable spread room with associated wiring back to the junction area and central PLC. The system was reviewed at the July Director's Review, and the CDE-2/3A IP and found to be ready for CDE-3A approval.

## **Test Cell Improvements / Test Cell (WBS 1.08.01)**

### **1.08.01.01 Radiation Annunciation (5005)**

The PDR for the Radiation Annunciation scope was held on August 14, 2018, while the FDR was held on February 12, 2019; both reviews were successful. The system was reviewed at the July Director's Review and the CDE-2/3A IPR, and found to be ready for CDE-3A approval.

### **1.08.01.02 Oxygen Monitor (5010)**

A successful PDR for the test cell ODH monitors was held on August 14, 2018.

### **1.08.01.03 NTC Shielding (5000)**

The PDR for the test cell shielding scope was held on August 6, 2018, and an FDR was held on January 14, 2019. The following work was initiated for this scope under the terms of the pre-authorization letter on May 16, 2018:

- Subcontract awarded for test cell door replacement on July 11, 2019.
- Subcontract awarded for the labyrinth roof blocks on August 1, 2019.
- Interference removal for test cell labyrinth construction commenced on August 21, 2019.

The system was reviewed at the July Director's Review and the CDE-2/3A IPR, and found to be ready for CDE-3A approval.

## **Site Preparation & Assembly / Accelerator Safety Order**

### **1.09.01.01 Accelerator Safety Order (ASO) Implementation (\*ASO)**

FY2019 saw the completion of plans for the implementation of the Accelerator Safety Order on NSTX-U, and the beginning of implementation. The following project plans were approved:

- NSTX-U Accelerator Safety Order Implementation Plan (Rev. 1): May 23, 2019
- NSTX-U ACC Plan: May 29, 2019
- NSTX-U ARR Plan: August 11, 2019
- NSTX-U Commissioning Plan: February 21, 2019
- NSTX-U Training and Qualification Plan: May 25, 2019
- Hazard Analysis Report (Rev. 3): August 10, 2019

Note that the ASO Implementation Plan (Rev. 1) was accepted by DoE-PSO as completing a Notable Outcome.

With these complete, work has started on the Safety Assessment Document (SAD), which is a key deliverable of the ASO Implementation WBS. Frank Kornegay (ORNL, retired) was retained as a consultant to support the ASO implementation. The consulting relationship with Scott Davis (DOE, retired) has been maintained.

Jessica Malo, hired as the Accelerator Safety Specialist, observed ARRs at Argonne National Labs April 29 - May 1, 2019 and Thomas Jefferson National Lab June 26-28, 2019. She also served on the organizing committee for the 2019 Accelerator Safety Workshop.

Progress toward the ASO Implementation was presented at both the July Director's Review and the CDE-2/3A IPR, and extremely helpful advice was received from both committees.

## **NSTX-U Reassembly**

A comprehensive cost estimate was developed for the reassembly of NSTX-U. This estimate was reviewed at the March Basis of Estimate Review.

## **NSTX-U Commissioning and KPPs**

A comprehensive cost estimate was developed for the commissioning of NSTX-U. This estimate was reviewed at the March Basis of Estimate Review.

## **NSTX-U Personnel Safety System**

The personnel safety system (PSS) scope was added to the NSTX-U Recovery Project in October 2018 following the September 2018 Director's Review.

The scope development started with a thorough review of the requirements from other SC accelerator facilities and the familiarization of Project Staff with the requirements of IEC 61508/511. A hazard analysis was developed in order to determine the hazards that needed mitigation by the system, and a Layer Of Protection Analysis was performed to determine the required level of risk reduction.

The system that has been developed includes three components. A system of configuration managed safeguards is used to prevent electrical and thermal contact hazards. A trapped key system is used to maintain the configuration of the safeguards, as well as maintain the configuration of doors, RF switches, etc. A PLC-based safety instrumented system is used to mitigate direct ionizing radiation and magnetic hazards by sensing door violations, inconsistent states of actuators, and the activation of emergency stop buttons.

As part of this effort, the need to upgrade select 13.8 kV fixed and variable frequency breakers to have a failsafe trip mechanism was identified; that breaker upgrade is part of a breaker refurbishment that is not included in the Project.

This evolution of the PSS design was vetted at a CDR on December 13, 2019, and a PDR on June 26, 2019. External reviewers participated in both reviews. The system was also reviewed at the July Director's Review and the CDE-2/3A IPR.

## **Real Time Protection and Control**

### **1.10.01.01 Shorted Turn Protection**

Work continued on the shorted turn protection system, with a successful CDR held on May 9, 2019. The PDR is scheduled for September 12, 2019.

## **NSTX-U Maintenance and Run Preparation**

In addition to the Recovery Project, NSTX-U operations funding supports facility maintenance and targeted modernizations in a scope of work known as "Maintenance and Run Preparation"

---

(M&RP). The distinguishing characteristics of this work are described in the Recovery Project WBS Dictionary.

Key progress in the M&RP scope in FY19 is described in this section.

## Neutral Beams

Work on Neutral beams in FY 2019 included:

*Replacement of the obsolete fiber optic telemetry systems:* This work scope includes replacement of the fiber optic cable connectors (completed), replacement of the photodiodes on the receiver cards (completed), and replacement of the LED transmitters (35% complete).

*Replacement of the Neutral Beam armor backing plate:* The backing plate has been fully machined, the cooling tube has been bent to shape and brazied into the plate, and the plate reinforcement and attachment brackets have been welded to the backing plate.

*Calorimeter Repairs:* Repairs to both calorimeters were completed and the calorimeters were re-installed in the beamlines.

*Ion sources:* Two failed ion sources were removed due to internal and external water leaks. One replacement ion source was refurbished and tested, and a second ion source was refurbished and is awaiting testing. Fabrication of replacement ion source parts this fiscal year include new langmuir probe tips, probe Vespel blocks, and grid module parts, including the fabrication of new Mod/Reg control boards to replace obsolete electronic components.

The NSTX-U Neutral Beam staff also provided support for other NSTX-U subsystems and other PPPL projects (LTX, FLARE) during this fiscal year.

## High Harmonic Fast Wave Systems

The primary goal of work on the High Harmonic Fast Wave (HHFW) system in FY19 was maintenance of operations personnel and equipment following a long shutdown. Following suspension of NSTX-U Research Operations, all RF systems were accessed and secured in FY17 and maintained in safe shutdown mode since then. In 2QFY19, a preservation effort was launched so the equipment and staff would be available to support future RF science on NSTX-U. Significant attrition occurred due to the retirement of most of the RF Group. Cross-training and refreshing of operators began in order to capture and develop core knowledge.

Re-commissioning and dummy load testing of HHFW Systems 3, 4, 5, and 6 was successfully completed in FY19. All four systems operated into dummy load at 0.5 MW for 0.5 sec. Re-commissioning of HHFW Systems 1 and 2 is expected to be completed in FY20.

A number of repairs and maintenance activities were completed in order to successfully re-commission and dummy load test HHFW Systems 3, 4, 5, and 6. Electronics and control cabinet repairs were completed. A HHFW System #4 cooling water leak was repaired. A leaking dummy load recirculation pump was repaired and tested. All deionized cooling water pumps have been placed on a preventative maintenance schedule, and are run periodically. Procedure and training material updates are ongoing.

## **Motor Generator Systems**

Work on the motor generator in 2019 included test runs of the set, analysis, upgrades, and preventive/mothball maintenance. Motor Generator bi-monthly test runs were accomplished in 2019 in November, February, April, June, and September. These test runs consisted of successful demonstration of transitioning into doubly fed mode, with applied excitation to a generating speed of 65 Hz. Preventive maintenance procedures were scheduled and carried out as per monthly and annually predetermined regiment. Mothball maintenance has been performed on motor generator no. 2 and its associated systems. This includes a 6 month rotation of the motor generator no. 2, completed February and Sept 2019, and overfilling of the upper and lower bearing housing with oil.

In FY 2019, we completed an extensive repair on the motor generator brake cylinders. Due to a water hammer effect, a repair was also made on the emergency water system valve in January 2019 where we changed out the main valve with a one-to-one replacement. Because of a fluctuation of the readout with regards to shaft speed, there was a repair made in Feb 2019 to the speed signal conditioner. Rust was found on a MG No.1 lower journal and subsequent scoring on the surface of the associated bearing segments. The repair of the damaged segments is under way, as a statement of work is in progress for the repair to be completed by a vendor. The CO2 main valve for MG set no. 1 had a faulty limit switch which was replaced and calibrated in July 2019. Modernization upgrades to the MG system include the thrust bearing temperature controller completed in June 2019, shaft speed recorder in August 2019 and shaft vibration monitor system in September 2019.

## **Field Coil Power Conversion**

Work on the Field Coil Power Conversion (FCPC) systems in 2019 included completion of the power converter double pole double throw switch maintenance for all of the thirty nine power converters (activity commenced last fiscal year). Additionally, complete grounding switch maintenance was performed on all of the coil power circuit's safety disconnect switches (SDS).

This maintenance activity consisted of a complete teardown, inspection, and restoration of all the high current carrying components of the grounding switch circuitry. Following this activity, the SPA circuits' DC link SDS and output RWM (resistive wall mode) SDS received complete maintenance, including inspection of contact surfaces and operating linkages, contact resistance, lubrication, and switch travel checks.

Maintenance on the FCPC power converter transformers began this fiscal year. This includes insulation resistance, winding resistance, and TTR (transformer turns ratio) testing as well as inspection and testing of the associated components of the converter transformers (potential transformers, lightning arresters, and line disconnect switches). In the converter units, resistors in all of the master gate driver power supply boards were replaced with those of higher wattage to address a known issue. In the FCPC PF ground fault detection circuitry, non-functioning ground fault relays were successfully troubleshooted and repaired.

## **Central Instrumentation and Control**

Considerable work occurred in the instrumentation and control area during 2019 as part of the M&RP scope. A successful test and FDR was held for the expansion of Ethernet connectivity in the NSTX-U Test cell. The application of Course Wave Division Multiplexing technology will ensure adequate networking resources will be available for the foreseeable future. This effort will support the NSTX-U Test Cell Surveillance (Recovery project) cameras slated to be installed in FY20.

There was significant documentation and cross training in the area of data acquisition system support in FY19. Progress was made in the area of CAMAC replacement with work done in the Control I/O area to facilitate the removal of equipment in the D-Site pumphouse, replacing it with a modern Programmable Logic Controller.

A significant effort was undertaken to replace computing equipment that uses the Windows 7 operating system due to support for it being discontinued in Q2 of FY20. This far-reaching effort mainly included areas of Central Instrumentation & Control, Diagnostic systems and Real-time Control and Protection. In some cases control software had to be rewritten and hardware had to be replaced to maintain functionality.

In the area of Real-Time Control and Protection, the review and production of the Stand Alone Digitizer 2 (SAD2) was completed and the production units were tested. A final design for the Digital Input and Time Stamp 2 (DITS2) module was generated and reviewed, with a prototype effort providing the new boards capabilities prior to production runs. The final design for the Front Panel Data Port (FPDP) clock boards were completed with a similarly successful prototype leading production. A Preliminary design was created for the FPDP Input Multiplexing Module 2 (FIMM2) which will eliminate the requirement of using a no longer obtainable transceiver board (Systran) for future expansion.

During this period, the Central Timing and Clock, Plasma Control, Digital Coil Protection, Plant Control, and Monitoring and Data Archiving Systems were all maintained at 99% availability and were used to train new staff in their operation and support development and testing efforts for the project.

## Vacuum and Fuelling

In the area of vacuum and fueling, work was done on the replacement NSTX-U vacuum vessel backing pump, a repair to the GDC electrodes, and adding a burst disc to the expansion tank of gas delivery system (GDS).

For the vacuum vessel backing pump job, the new backing pump and its dedicated vacuum roughing line have been fully installed in the NSTX-U test cell. The chiller used for pump cooling has also been installed. Power supply installation for both the pump and the chiller has been completed. For the GDC electrodes work, GDCs at both Bay B and Bay G have been successfully installed inside NSTX-U vacuum vessel. They are also electrically tested to be OK. The burst disc for the expansion tank of the NSTX-U GDS has been installed in the test cell. Leak check for the burst disc seal was a success.

## NSTX-U Research Program

**JRT19: Conduct research to understand the role of neutral fueling and transport in determining the pedestal structure**

### *H-mode Pedestal Fueling With Conventional And Supersonic Gas Injections*

Present-day magnetically confined fusion (MCF) devices, e.g., tokamaks, use gas injection at the plasma edge for fueling of high-temperature plasmas. In future high-temperature MCF devices, the main fueling techniques are cryogenic pellet injection, energetic neutral beam injection (NBI), and compact toroid injection. Potential applications of gas puffing include plasma fueling during start-up, local density control (for example, in front of radio-frequency antennas or diagnostic mirrors), and even general discharge fueling. An improved version of conventional gas injection technique - a supersonic gas jet (also referred to as a supersonic molecular beam) - was proposed nearly fifty years ago and implemented on a number of MCF devices, including NSTX. The gas jet is a highly-collimated high-pressure high-velocity stream of gas that could provide higher fueling efficiency and less gas spread over the vacuum chamber.

Present analysis of NSTX H-mode fueling experiments aims to clarify the following research questions:

- Supersonic gas injection fueling efficiency and ionization source distribution
- Comparison between conventional gas injection, and low-field-side supersonic gas injection w.r.t. effect on fueling efficiency and pedestal structure (pedestal height, width, foot)

Figure JRT-1 shows an example of multi-pulse SGI fueling of a 6 MW NBI-heated H-mode plasmas. During the SGI pulses, an averaged line density does not always increase, however, the pedestal density increases by up to 10-15 %.

The SGI provides a higher fueling efficiency. In the experiment, two H-mode plasmas were obtained with fully matched average density, but different fueling scenarios. One scenario used a much-reduced HFS fueling, mostly for plasma stability, and several SGI pulses. The other scenario used the same amount of reduced HFS fueling and a few fueling pulses from a

conventional gas injector. Time traces of relevant quantities are shown in Figure JRT-2. After the experiment, the amount of injected gas was compared by measuring gas pressure in a closed NSTX vacuum vessel by reproducing the two-gas injection scenario. The pressure time histories are shown in Figure JRT-2 (b). Both gas injectors operated at their highest injection rate of about 200 Torr l/s. The SGI injected nearly twice as little gas as the LFS gas injector in order to obtain the same plasma density. This result is understood as the SGI provided a higher efficiency ionization source in the SOL (however, not necessarily a better penetration inside the separatrix), due to high collimation and higher density of the gas stream. The conventional gas injection results in large quantities of gas molecules scattered around the vacuum vessel that do not participate in directed fueling.

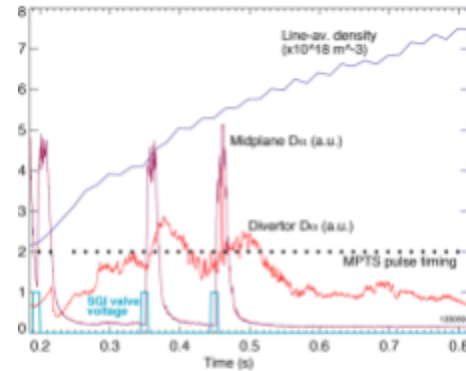


**Figure JRT-1:** Time traces of line-averaged density, MPTS points, SGI valve voltage, and divertor and midplane  $D_{\alpha}$  intensity.

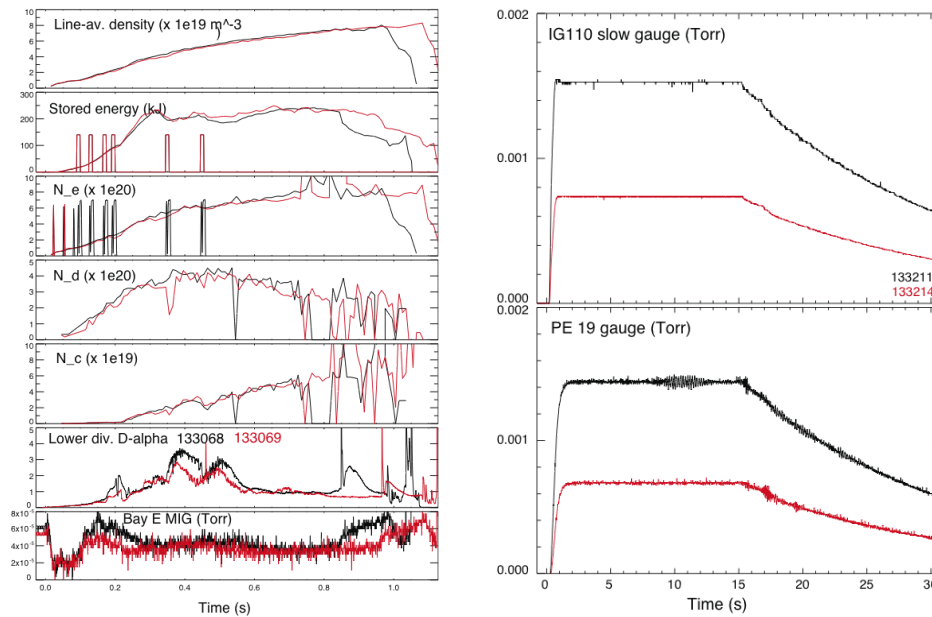


**Figure JRT-2:** Time histories of two H-mode discharges fueled by the SGI (red) and LFS conventional gas injector. While the plasma densities are matched, the amount of injected gas from the SGI is much less (right figures).

Pedestal structure parameters have been analyzed using Multi-pulse Thomson Scattering (MPTS) electron density profiles from 4-6 MW NBI-heated mostly ELM-free H-mode plasmas obtained in a highly shaped lower single null configuration with B-gradB ion drift toward the lower divertor. Obtained were the electron density pedestal heights  $(5-8) \times 10^{19} \text{ m}^{-3}$ , and pedestal widths 1-4 cm. The analysis was aimed to test the hypothesis that the pedestal width is determined by the neutral penetration depths, which in turn is connected to the ionization mean free path. Three NSTX gas injectors can be compared – the supersonic gas injector (SGI), the high-field side (HFS) gas injector, and the low field side (LFS, top) gas injector. The hypothesis is that the supersonic gas jet penetrates deeper into the SOL and pedestal and this would be reflected on the pedestal width. The present analysis uses Thomson scattering electron density profiles. Shown in Figure JRT-3 is an example of edge density profiles. The MPTS diagnostic provides  $n_e$  profiles, whereas the CHERS diagnostic provides C VI density profiles, and the ion density profile is obtained by subtracting (six) electrons due to each carbon ion from the electron density profile. However, NSTX H-mode plasmas were known for high edge concentration of carbon. Because of this, subtle  $n_e$  pedestal width changes due to the SGI fueling may not be apparent. If, however, we assume that carbon contribution to electron density profiles does not change on a fueling time scale, we obtain pedestal parameters using modified hyperbolic tangent fits. Shown in Figure 3 are pedestal operating spaces ( $n_e$  pedestal width and height) with the three gas injectors. Since the SGI and the LFS injectors are pulsed, the profiles are analyzed over some time during and immediately following the gas pulse (i.e. on a faster time scale than impurity transport). The HFS gas injector is continuous, hence the profiles are analyzed over a time period with densities similar to the other two cases. The data are

scattered, and it is not possible to distinguish the SGI from other injectors based on the present analysis. This result may imply that the supersonic gas jet penetration (ionization profile) was similar to conventional HFS and LFS gas injection. This could be possible if the supersonic jet is fully penetrated by the ambient plasma leading to molecular dissociation and atom ionization in a single particle approximation rather than acting as a self-shielding fluid jet.

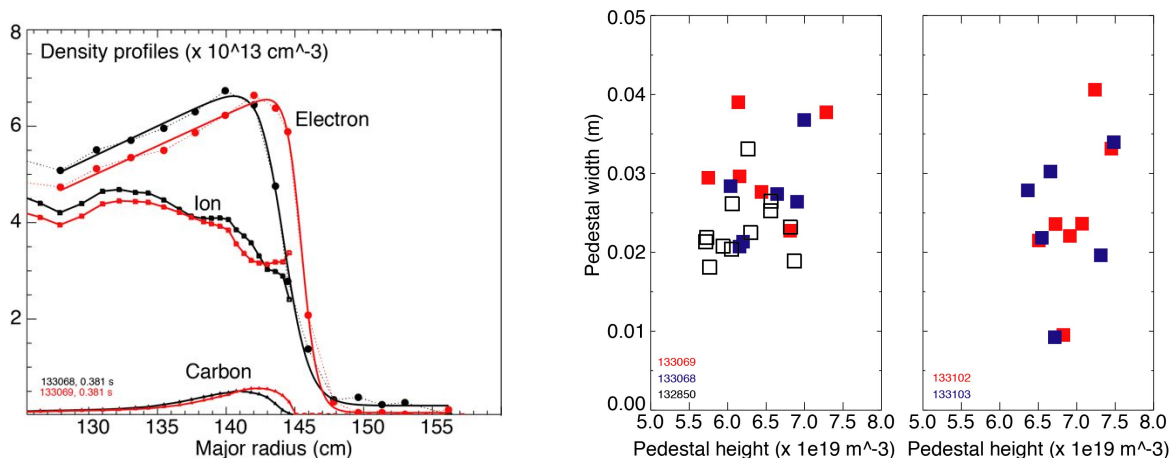


**Figure JRT-3:** (left) An example of NSTX kinetic profile fitting:  $n_e$  experimental data – circle symbols, thick line – modified tanh fits of  $n_e$  profiles, other symbols and lines –  $n_i$  and  $n_C$  profiles. Red – SGI, black – conventional gas injection. (right) Comparison between pedestal widths obtained at similar pedestal heights using three gas injectors on NSTX: red - SGI (plus reduced HFS), black - HFS, blue - LFS (plus reduced HFS)

### Neutral Density Studies In NSTX-U: Validation Of Midplane Neutral Density Measurements

Midplane neutral density and ionization rate profiles were derived in NSTX-U from the outboard midplane  $D_\alpha$  emissivity obtained from the inversion of the brightness measured by the Edge Neutral Density Diagnostic (ENDD) diagnostic. Validation of the new ENDD measurements was performed via the Monte Carlo neutral transport code DEGAS 2 to enable the direct use of ENDD ionization rate profiles for pedestal fueling studies. Neutral densities derived from ENDD using photon emission coefficients from electron impact excitation were compared with those obtained constraining DEGAS 2 with ENDD measurements. An automated workflow enabled a large set of comparisons in both L-mode and H-mode discharges. The  $D_\alpha$  emissivity calculated in the DEGAS 2 simulations was normalized to the peak of the ENDD emissivity. Peak emissivity location, emissivity profile shape, neutral deuterium density inside the separatrix (1 cm) and integrated ionization rate were compared between ENDD measurements and DEGAS 2 simulations.

Good agreement was generally observed between the measured and simulated profiles (Figure JRT-4). The main deviations observed were an overestimation of the radius of peak emissivity (by 3-4 mm on average) and an underestimation of the  $D_\alpha$  in the far SOL. Despite these deviations, DEGAS 2 simulations indicated that the majority of the  $D_\alpha$  emissivity inside the separatrix was due to electron impact excitation of neutral deuterium atoms, thereby confirming assumptions used in the ENDD neutral density derivation. Neutral densities inferred from ENDD

one cm inside the separatrix were on average ~10-15% higher than those determined by DEGAS 2 (due to  $D_\alpha$  emission from atoms excited by molecular processes which is not accounted in the ENDD derivation). Total ionization rates inferred from ENDD were consistent with those determined from DEGAS 2 simulations.

Observed deviations in the peak emissivity location and SOL profile shape are thought to be related to uncertainties in the molecular model in DEGAS 2 and the possible role of intermittent transport. DEGAS 2 simulations are based on  $T_e$ ,  $n_e$  from a single Thomson scattering profile, assumed to

be representative of the steady state profiles. In the presence of intermittent SOL transport, due to the non-linearity of atomic physics coefficients with respect to  $T_e$  and  $n_e$ , the use of profiles from a single time point might not result in an accurate representation of the experimental emissivity. A scan in the far SOL  $T_e$ ,  $n_e$  input profiles was performed in DEGAS 2 simulations. Minor changes in the far SOL  $T_e$ ,  $n_e$  from the experimental values resulted in an improved agreement between the simulations and measurements in both peak emissivity location and far SOL emissivity. In particular, the increase in far SOL  $T_e$ ,  $n_e$  resulted in an increase molecular dissociation in the far SOL, thereby increasing far SOL emissivity and reducing the molecular contribution to  $D_\alpha$  emissivity around the peak location which was responsible for the observed outward shift. Only minor changes in the inferred neutral density and total ionization source inside the separatrix were observed while scanning far SOL parameters. This further justified the use of single-time Thomson profiles and the normalization of DEGAS 2 simulations by the peak ENDD emissivity.

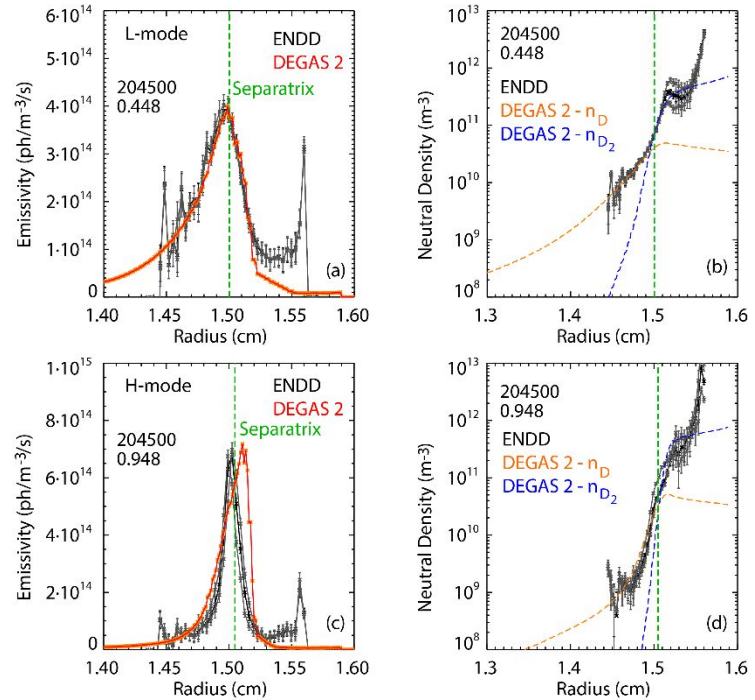


**Figure JRT-4:** Comparison of  $D_\alpha$  emissivity (a,c) and inferred neutral densities (b,d) between ENDD and DEGAS 2 for an L-mode profile (a,b) and an H-mode profile (c,d) during discharge 204500. In the emissivity plots, ENDD measurements are shown in black and DEGAS 2 results are shown in red. In the neutral density plots, ENDD measurements are shown in black and DEGAS 2 results are shown with an orange dashed line for atomic deuterium densities a blue dashed line for molecular deuterium density.

### Experimental Analysis Of Radial Neutral Density And Ionization Rate Profiles

Based on the validation work for the ENDD measurements, neutral (atomic and molecular) density profiles can now be obtained from the coupled ENDD/DEGAS2 analysis while radial ionization profiles inside the separatrix can be directly inferred from the ENDD data. An example of neutral density profiles and their time evolution through an L-H transition is shown below in

Figure JRT-5 based on DEGAS 2 simulations at each Thomson time normalized by ENDD peak emissivity at each time. Unchanged SOL neutral densities and a shorter neutral density scale length inside the separatrix can be observed transitioning from L- to H- mode. The evolution of the radial profiles of the ionization rate for the same discharge is shown in Figure JRT-6 (below).

Radial profiles of the ionization rate are now being evaluated for H-mode discharges in different conditions. The inferred profiles will be related to pedestal width/height.

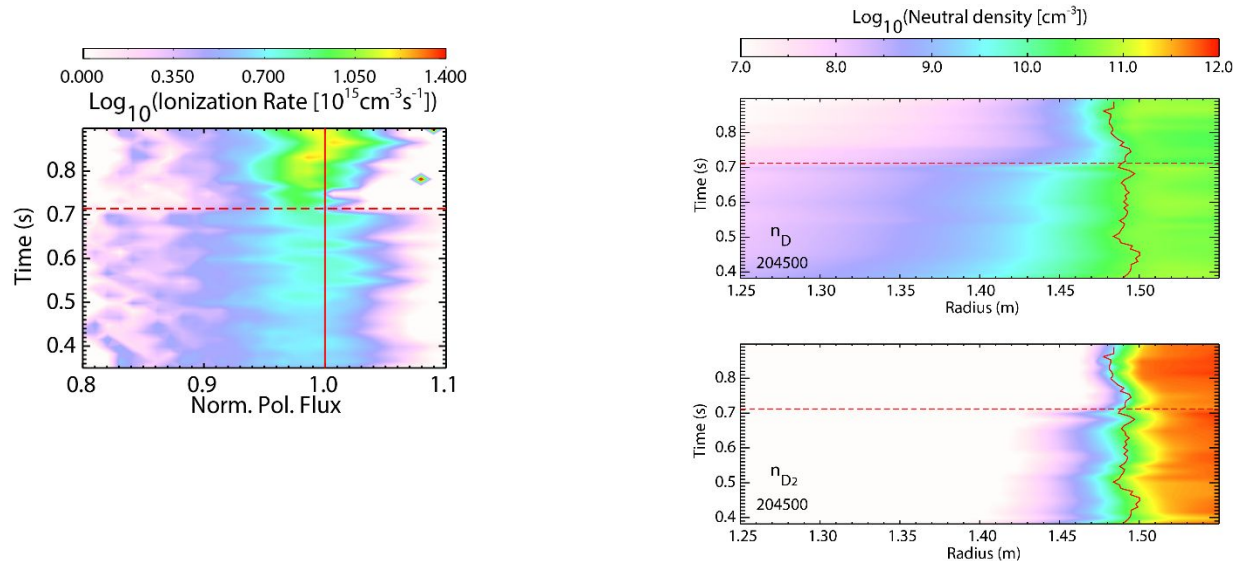


*Figure JRT-5: Time evolution of radial profiles of atomic and molecular deuterium density across an L-H transition (indicated with red dashed line) from the coupled ENDD/DEGAS 2 analysis.*

*Figure JRT-6: Ionization rate profile inferred from the ENDD emissivity as a function of normalized poloidal flux and time. Separatrix location from EFIT02 is shown with a solid red line. A dashed red line indicates the L-H transition.*

## Research Milestones

### R19-1: Validate Transport Models For High-beta ST H-mode Plasmas And Assessing The Importance Of Multi-scale Effects In NSTX/NSTX-U Turbulent Transport

The R19-1 milestone made progress in two primary areas. First, the core profile in high- $\beta_{\text{pol}}$  discharges was found to be near or above the threshold of kinetic ballooning modes (KBM) and energetic particle modes (EPM), suggesting they may provide the ultimate limit of near-axis  $T_e$ . Second, as part of an MIT Ph.D. thesis, an additional gyrokinetic validation study was completed for a low-beta NSTX H-mode. Using both transport and high-k turbulence measurements, the study illustrates that electron-scale ETG turbulence alone can account for the anomalous electron thermal losses. This occurs even though the conditions (strong ETG drive, near marginal ion-scale drive) are very similar to conditions in other tokamaks where

multi-scale effects have been found to be important. This illustrates that multi-scale effects may not always be needed under these conditions.

### Validate Transport Models For High-beta ST H-mode Plasmas

Previous milestone work (R18-3) illustrated that the recently developed Lehigh microtearing mode (MTM) transport model [R19-1] is capable of predicting  $T_e$  profiles in high beta, high-collisionality NSTX H-mode discharges. This unified fluid/kinetic model was shown to reproduce many of the gyrokinetic linear stability results and scaling trends [R19-2]. However, the collisionality scaling of the transport model could not reproduce non-linear gyrokinetic scaling trends and consequently underpredicts  $T_e$  profiles at low- $v_{*i}$ . As part of R19-1, the Lehigh MTM transport model was updated with a more accurate collisionality dependence, specifically in the magnetic correlation length,  $L_c$ , used in the stochastic electron thermal transport model,  $\chi_e = v_{Te} |\delta B/B|^2 L_c$ . Recent tests show the updated model provides a small improvement in predicted  $T_e$  for previously analyzed discharges, however it still overpredicts transport as collisionality is reduced. Possible additional refinements in the saturation model for magnetic fluctuation amplitude  $|\delta B/B|$  have been identified and ways to implement this are being discussed with T. Rafiq.

The ability of the MTM model to predict  $T_e$  profiles was also tested in high- $\beta_{pol}$  discharges that form the basis for high bootstrap fraction, 100% non-inductive scenarios envisioned for NSTX-U operation [R19-3]. An example of this is shown in Fig. R19-1-1 (top) for discharge 133964 that exhibited the lowest achieved surface voltage in NSTX [R19-4]. While MTM alone predicts the  $T_e$  profile in the far outer region of the plasma ( $r/a > 0.6$ ), it is incapable of reproducing the flat  $T_e$  as the magnetic axis is approached. This is consistent with linear CGYRO analysis illustrating MTM modes are strongly unstable outside  $r/a \geq 0.6$ , while inside this radius the  $E \times B$  shearing rates are large enough to suppress MTM.

While previous analysis in high-power NSTX H-modes suggests GAE/CAE-KAW modes may play a role in flattening the central  $T_e$  profile [R19-5,6,7], another set of mechanisms is investigated here based on additional gyrokinetic analysis. As the magnetic axis is approached, linear CGYRO simulations find that the profiles are very close to the threshold for kinetic ballooning modes (KBM) or energetic particle modes (EPM) when including the drive from NBI

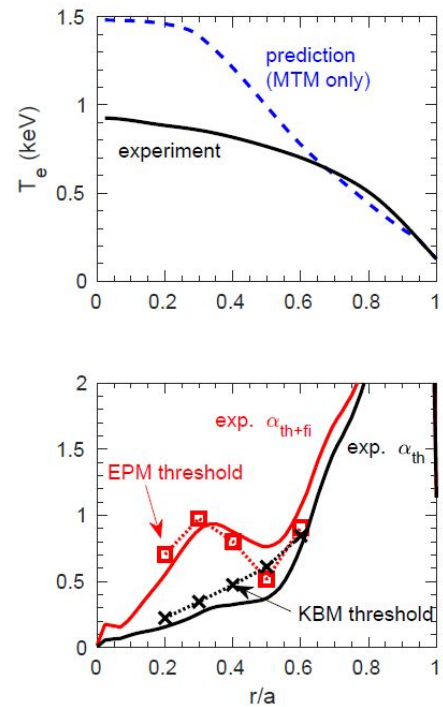


**Fig. R19-1-1:** (top)  $T_e$  profile measured in high- $\beta_{pol}$  discharge 133964 ( $t=0.8$  sec) and predicted by the Lehigh MTM model. (bottom) Profiles of the normalized pressure gradient parameter alpha. Solid lines represent the measured values using only thermal pressure or thermal + fast ion pressure. Squares connected by dotted lines illustrate the linearly thresholds calculated by CGYRO for KBM (using thermal pressure only) or EPM (using thermal + fast ion pressure).

fast ions. Transport from these pressure gradient driven MHD-like modes is expected to be very stiff so that profiles would be held close to the threshold. Fig. R19-1-1 (bottom) shows that the experimental pressure gradient ( $\alpha = -2\mu_0 q^2 R \nabla p / B^2 \sim \beta_{\text{pol}} / L_p$ ) is very near or even above the KBM or EPM thresholds determined from numerous linear CGYRO simulations when using thermal-only or thermal + fast-ion kinetic species, respectively. The proximity of the core profiles to KBM/EPM pressure limits is reminiscent of the KBM constraint used to model the maximum achievable pedestal pressure gradient e.g. in the EPED model [R19-8].

The above KBM/EPM analysis was performed in the local (low- $\rho_s$ ) limit. However, the relevant normalized wavenumbers ( $k_\theta \rho_s \sim 0.1$ ) correspond to low toroidal mode numbers ( $n=2-3$ ) in these particular conditions bringing into question the local approximation. M3D-c1 was used to calculate global stability of ballooning modes in the MHD limit. The resulting simulations predict for the base equilibrium that low- $n$  modes ( $n=2,4,6$ ) are indeed linearly unstable with eigenmode amplitudes spanning half the minor radius ( $r/a \leq 0.5$ ), consistent with the proximity to local linear thresholds shown above. Previous nonlinear M3D-c1 simulations for a different high- $\beta$  NSTX H-mode predict a “soft” beta limit [R19-9], i.e. the low- $n$  modes saturate and limit the peak pressure profile regardless of increasing source strength, supporting the notion of a stiff transport effect.

The emerging hypothesis based on the above local gyrokinetic and global MHD analysis is that the central profiles may be limited by pressure gradient constraints set by low- $n$  KBM/EPM instabilities. However, to test this hypothesis more rigorously requires a model that accounts for multi-channel transport to understand how energy fluxes and profiles evolve independently for all species. For instance, thermal ion energy transport is neoclassical in this discharge and evidence suggests that fast ion transport is governed by classical processes (e.g., no anomalous fast ion diffusivity was required to match neutron rates or reconstructed current profiles in TRANSP/NUBEAM analysis [R19-4]). It is yet to be understood if the KBM/EPM turbulence can effectively limit the  $T_e$  profile as the overall pressure evolves towards these instability thresholds. Recently, the TGLF linear gyrofluid model (using modified settings) has been used to predict EPM stability and thresholds [R19-10], and has similarly been used to predict KBM stability and transport in DIII-D high- $\beta_{\text{pol}}$  discharges with some success [R19-11]. Future work will test whether TGLF is capable of reproducing the linear threshold behavior of KBM and EPM modes at low aspect ratio, although nonlinear gyrokinetic simulations are required to have confidence in the partitioning of predicted energy transport.

### Assessing The Importance Of Multi-Scale Effects

Analysis in Alcator C-Mod L-mode plasmas [R19-12,13,14] found that multiscale gyrokinetic simulations (simultaneously spanning ion-scale to electron-scale) were required to accurately predict electron thermal transport when certain criteria were met: (i) electron-scale (ETG) turbulence is strongly driven and (ii) ion-scale turbulence (ITG in the C-Mod L-mode) is near-marginal. These similar conditions have been identified to occur in some regions of NSTX L-mode [R19-15; R18-3 milestone] and NSTX-U L-mode [R19-16] plasmas. In these cases, single-scale gyrokinetic simulations alone have not been able to recover the resulting electron thermal transport, suggesting that multiscale simulations may also be required.

Recently, an additional gyrokinetic validation study was completed for a low- $\beta$  NSTX H-mode plasma to further investigate the possible role of ETG turbulence and transport. The study utilized not only experimentally inferred energy fluxes but also high-k microwave scattering measurements to constrain the nonlinear gyrokinetic simulations. Critical to the analysis was the application of a newly developed synthetic diagnostic to mimic the response function of the high-k measurements [R19-17,18]. The analysis found that electron-scale ETG turbulence predictions could account for the experimentally inferred electron thermal losses for weak and strong density gradient profiles (achieved before and after a current ramp-down) at the location of the high-k measurement,  $r/a \sim 0.7$  [R19-19]. Additional confidence in the simulations is given by the simultaneous match in predicted and measured transport, high-k scattering frequency spectra, wavenumber spectra shape, and change in relative fluctuation amplitude for the two density-gradient cases. The simultaneous agreement was possible only after significant sensitivity analysis was performed by varying input gradient ( $a/L_n$ ,  $a/L_{Te}$ ) and equilibrium parameters. Fig. R19-1-2 (top) illustrates how a small change in safety factor ( $\Delta q/q=10\%$ ) and magnetic shear ( $\Delta s/s=20\%$ ) improves agreement in the high-k scattering wavenumber spectra and electron thermal transport [R19-20].

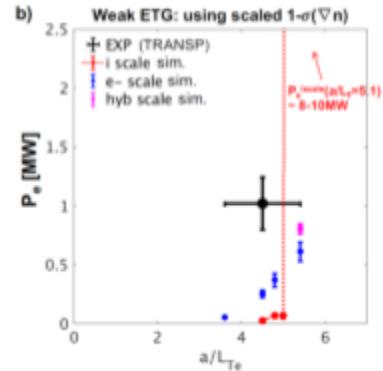
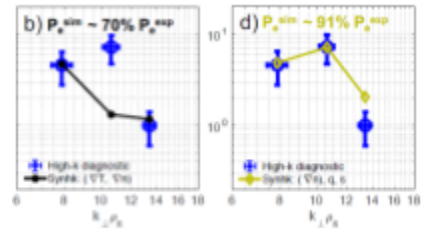


**Fig. R19-1-2:** (top) Power spectra from high-k microwave scattering (open symbols) measurements and (lines) predictions from nonlinear ETG simulations + synthetic diagnostic. The two cases correspond to (left) base case equilibrium parameters and (right) modified safety factor and magnetic shear. (bottom) Electron thermal flux vs. normalized electron temperature gradient from (black symbol + error bars) experimental analysis, (blue and magenta symbols) single-scale ETG simulations, and (red symbols and line) single-scale ion-scale simulations.

What is additionally notable, in particular for the high-density gradient case, is that it appears to satisfy the same criteria where multiscale effects were found to be important in the C-Mod analysis. This is illustrated by single-scale nonlinear simulation results in Fig. R19-1.2 (bottom) where the ETG transport increases to match the experimental value with slightly increased temperature gradient (and increased numerical resolution), while the ion-scale simulations show an extremely stiff response at a temperature gradient just above the experimental value, indicative of near-marginal conditions. While the onset of ion-scale transport occurs within the uncertainty of the experimental gradient, the predicted transport jumps abruptly to a magnitude far larger than the experimental value. The analysis suggests that transport from the ion-scale modes cannot realistically play a role unless nonlinear multi-scale interactions reduce their role leading to a more gradual increase in transport with increasing gradient.

**References:**

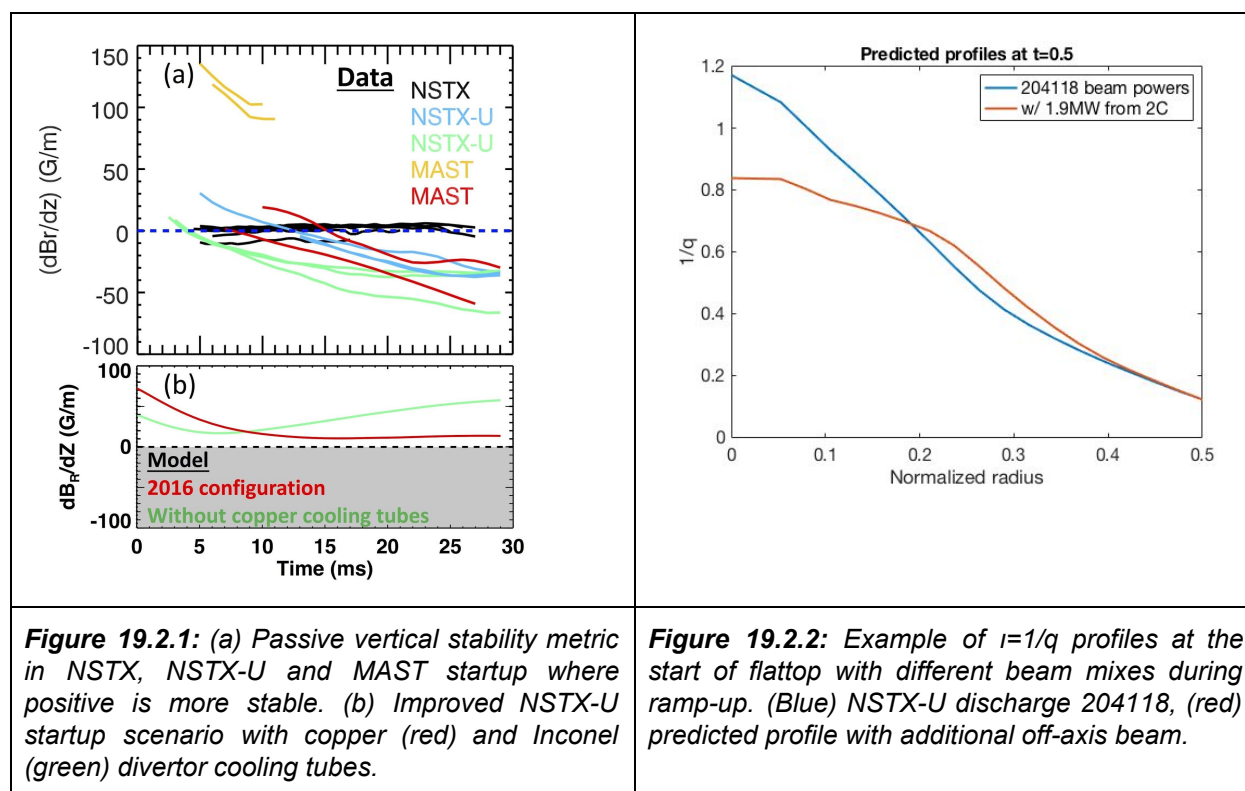
- [R19-1] T. Rafiq, et al., Phys. Plasmas **23**, 062507 (2016).  
[R19-2] T. Rafiq, et al., IAEA-FEC, Ahmedabad, India (2018).  
[R19-3] S.P. Gerhardt, et al., Nucl. Fusion **52**, 083020 (2012).  
[R19-4] S.P. Gerhardt, et al., Nucl. Fusion **51**, 073031 (2011).  
[R19-5] D. Stutman, et al., Phys. Rev. Lett **102**, 115002 (2009).  
[R19-6] N. Gorelenkov, et al., Nucl. Fusion **50**, 084012 (2010).  
[R19-7] E. Belova, et al., Phys. Rev. Lett **115**, 015001 (2015).  
[R19-8] P.B. Snyder, et al., Nucl. Fusion **51**, 103016 (2011).  
[R19-9] J. Breslau, et al., 40<sup>th</sup> EPS-DPP, P5.150 (2013).  
[R19-10] H. Sheng, et al., Phys. Plasmas **24**, 072305 (2017).  
[R19-11] G.M. Staebler, et al., Phys. Plasmas **25**, 056113 (2018).  
[R19-12] N.T. Howard, et al., Phys. Plasmas **21**, 112510 (2014).  
[R19-13] N.T. Howard, et al., Nucl. Fusion **56**, 014004 (2016).  
[R19-14] N.T. Howard, et al., Phys. Plasmas **23**, 056109 (2016).  
[R19-15] S.M. Kaye, et al., Nucl. Fusion **59**, 112007 (2019).  
[R19-16] W. Guttenfelder, et al., Nucl. Fusion **59**, 056027 (2019).  
[R19-17] J. Ruiz-Ruiz, MIT Ph.D. Thesis (2019).  
[R19-18] J. Ruiz-Ruiz, to be submitted (J. Plasma Physics).  
[R19-19] J. Ruiz-Ruiz, et al., Phys. Plasmas **22** 122501 (2015).  
[R19-20] J. Ruiz-Ruiz, Plasma Phys. Control Fusion (in press).

## **R19-2: Develop Optimized Ramp-up Scenarios In Spherical Tokamaks**

This research milestone builds on results from the FY18 NSTX-U milestone R18-2 that produced a simulation framework for breakdown and ramp-up modeling on NSTX-U. The capabilities of this simulation framework were expanded in FY19 in order to produce predictive calculations with fewer fixed assumptions on the plasma evolution in the breakdown and ramp-up phase. The improved capabilities accelerate the realization of the control and scenario solutions required for reliable operations with low internal inductance and high shaping.

One advance completed in FY19 was the development of a reduced model for the plasma breakdown phase where the plasma transitions from partially ionized to fully ionized along open magnetic field lines. Previously, the predictive model fixed the timing of the plasma breakdown independent of the field evolution. The important advance is the ability to predict the timing of the initial rise in plasma current ( $I_p$ ) based on the prefill gas pressure and the evolution of the axisymmetric magnetic and electric fields. Additional details of the reduced breakdown model are provided in the ASC section.

Operations on NSTX-U in 2016 did not achieve reliable vertical stability concurrently with the target  $I_p$  ramp rate (10 MA/s) in the current ramp-up phase. This issue was due to destabilizing field curvature resulting from large induced currents in copper cooling tubes installed behind the divertor tiles. Figure R19-2-1 quantifies this issue where more negative values indicate destabilizing curvature of the vacuum magnetic fields that increase the risk for a vertical disruption. Scenarios on NSTX-U (blue and green) and MAST (red) did not operate with sufficient margin (positive values) for reliable operation (Figure R19-2-1a). The simulation framework was used in FY19 to optimize the feed-forward coil current evolution for the early ramp-up phase on NSTX-U to achieve the target  $I_p$  ramp rate with suitable field curvature (red trace in Figure R19-2-1b). The redesign of NSTX-U will use Inconel cooling tubes, reducing the required  $V_{loop}$  for breakdown and meeting the target  $I_p$  ramp rate with sufficient stability margin to explore larger  $I_p$  ramp rates (green trace).



Another challenge during the first operation of NSTX-U in 2016 was achieving a reproducible timing of the evolution from a limited to diverted plasma boundary. The TOKSYS simulation platform developed in FY18 supports the design and testing of control solutions that increase the resiliency of the ramp-up scenarios. This simulation framework was advanced in FY19 with the addition of reduced models for the evolution of the  $q$ -profile and fast-ion pressure using a fast solver for the magnetic diffusion equation with neural network models for geometric parameters, plasma resistivity, bootstrap current, and current drive. The neural network models build on the successful development of an accelerated neutral beam calculation based on a neural network trained on a database of NUBEAM calculations. This modeling approach was

extended to include a reduced model for density and temperature evolution where a neural network has been trained to predict the profile shapes, while the magnitudes are constrained based on a prescribed Greenwald fraction, a zero-dimensional power balance, and assumptions on  $Z_{\text{eff}}$ , impurity species, and the ratio of  $T_e/T_i$ . Additional details on the reduced model development are provided in the ASC section.

These added capabilities have been used for initial studies of optimizing the current profile evolution in the ramp-up phase. In Figure R19-2-2, the  $r=1/q$  profile near the start of the flattop phase using the beam mix from NSTX-U H-mode discharge 204118 (blue) is compared with the profile predicted with the addition of 1.9MW of power from the new beam source 2C. The additional off-axis current drive results in a profile with higher  $q_{\text{min}}$ , avoiding the values below 1 predicted to drive MHD activity that enhances transport. In FY20, the modeling tools will be combined with optimization algorithms to provide a fast, automated scenario design tool.

A higher-fidelity approach to modeling the evolution of the plasma parameters in the simulation platform is to utilize a connection between the TOKSYS and TRANSP calculations completed in FY18. Work undertaken in FY19 found that predictive simulations using TRANSP, which are based on core turbulence transport models, do not reproduce the observed behavior of the plasma evolution on NSTX in the ramp-up phase, particularly with regards to the density evolution. This effort identified avenues for improvement in FY20 toward developing a model for the pedestal width and height that is valid for low-aspect tokamaks in addition to a self-consistent core-edge physics-based transport model.

The completion of the R19-2 milestone advances the simulation capabilities for optimizing the control and scenario solutions for the ramp-up phase on NSTX-U. The improved simulation framework was used to understand the challenges in the 2016 operation of NSTX-U and develop solutions. These results will accelerate the pace of progress in realizing high-performance discharges on NSTX-U when operations resume.

### **R19-3: Validate Tearing Mode Physics For Tearing Avoidance In High-performance Scenarios**

The CORSICA code [R19-3-1] and resistive DCON code [R19-3-2] are applied to predict the stability boundary of ideal and resistive MHD instabilities in NSTX-U experiments. The Corsica code was previously installed on the PPPL cluster to solve NSTX equilibrium. In this year, a collaborative effort between NSTX-U and the theory department was made to update the code for NSTX-U experiments successfully. With the unique feature of varying  $q$  profile and pressure profile, the Corsica code is capable of performing the equilibrium scan and solving the NSTX-U equilibria with high numerical accuracy (low Grad-Shafranov error), which is important to the computation of resistive DCON to get the well converged ideal kink energy and the outer region corresponding to the resistive MHD instabilities.

### Validation Of Tearing Mode Predictions In DIII-D

The prediction of tearing instability depends on the reliable simulation of resistive MHD modelling. The DIII-D ITER Baseline (IBS) experiments, which is sensitive to tearing instability, is an ideal target for testing the codes such as resistive DCON and M3D-C1 codes (MARS will be included later). In the IBS discharge 160161 with  $N=2.12$ ,  $q_{95}=3.29$ , an unstable  $n=1$  is observed and finally disrupts the plasma in DIII-D experiment. Fig. R19-3-1a presents the evolution of perturbed fields,  $B_p$ , which is measured by the poloidal sensor located at LFS midplane and shows a big amplification of  $B_p$  due to the quick growth of tearing mode. To perform resistive DCON and M3D-C1 simulations, the equilibrium is reconstructed by OMFIT, where the constraint  $q_{\min} > 1$  is imposed in order to avoid the presence of an ideal 1/1 internal kink. In Fig. R19-3-1b, resistive DCON finds  $\Delta'$  at  $q=2$  surface has the positive value and is significantly amplified due to the change of equilibrium at 3.2s where the tearing mode develops quickly. This  $\Delta'$  variation is consistent with the experimental observation. On the other hand, M3D-C1 is also applied to calculate the linear stability of MHD mode by using resistive single-fluid MHD model. M3D-C1 calculates stability by evolving the linearized fluid equations in time starting from random initial perturbations, and it is thus able to calculate the fastest growing eigenmode of the equilibrium.

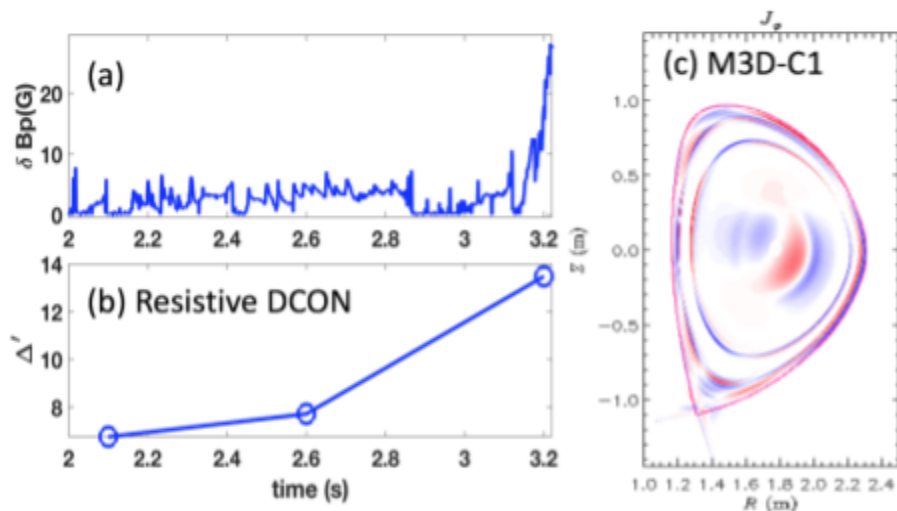


**Fig. R19-3-1:** In DIII-D IBS discharge 160161, (a) presents the time evolution of  $n=1$  perturbed poloidal fields measured at LFS midplane and (b) reports' value at  $q=2$  surface calculated by resistive DCON at 2.1s, 2.6s and 3.2s respectively. (c) Toroidal current density associated with a tearing mode at  $t=3.1$ s as calculated using M3D-C1 with a single-fluid resistive model.

M3D-C1 finds the equilibrium at  $t=2.2$ ms to be stable and  $n=1$  tearing mode to be unstable at 3.1s, which is in qualitative agreement with the experiment observation. Fig. R19-3-1c presents the perturbation of current density when  $n=1$  tearing mode is unstable at 3.1s. It is different from the conventional understanding that classical tearing mode is stable and NTM is responsible for

the plasma disruption in high beta tokamak experiments. Both resistive DCON and M3D-C1 codes indicates the classical tearing mode actually can be unstable in DIII-D IBS plasmas.

It is noted  $\Delta'$  at  $q=2$  surface, solved by resistive DCON, is positive. It indicates the outer region has free energy tending to release at the resistive layer. However, to finally determine the growth rate of tearing mode in resistive DCON, a new generalized inner layer code is being developed to provide the reliable outer-inner layer matching condition and a more flexible framework to include more non-ideal MHD physics in the resistive inner layer.

### Applications Of Resistive DCON To NSTX-U

The resistive DCON has been used to predict the tearing mode instabilities of high performance NSTX-U equilibrium with 2 MA plasma current, over various  $q_{95}$  and  $\beta_N$ , as shown in Fig. R19-3-2. The  $q_{95}$  scan in Fig. R19-3-2a shows NSTX-U plasma is unstable to the  $n=1$  ideal kink when  $q_{95} < 5$  as well as  $q_{95} > 9$ . It implies an appropriate choice of  $q_{95}$  is necessary since the high  $q_{95}$  can not ensure the stabilization of ideal kink. On the other hand,  $\Delta'$  at  $q=2$  and  $q=3$  surfaces is also solved by resistive DCON when the plasma is stable to the  $n=1$  kink mode. It is noted that  $\Delta'$  at  $q=2$ , with small variation, is positive and indicates a tearing instability may exist in NSTX-U plasma.  $\Delta'$  at  $q=3$  is negative and can be stable to tearing instabilities, but the value is more sensitive to the change of  $q_{95}$ . In Fig. R19-3-2b, the  $N$  scan suggests the lower  $\beta_N$  value can significantly decrease  $\Delta'$  at  $q=2$  and 3 surfaces which will help to avoid tearing instabilities in NSTX-U plasmas. Particularly, while approaching to the no wall  $\beta_N$  limit, the island at  $q=3$  surface may also be unstable.

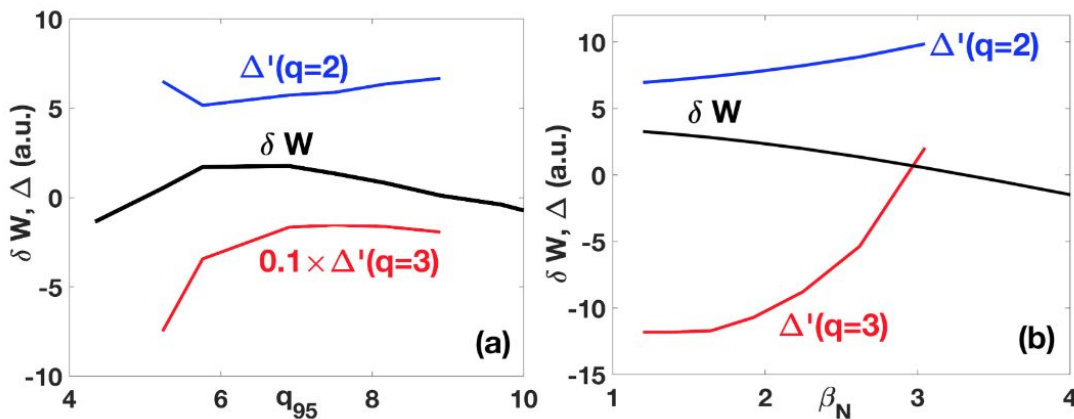


**Fig. R19-3-2:** Resistive DCON prediction for tearing stability index for NSTX-U target plasmas as a function of  $q_{95}$  and  $\beta_N$

### References:

- [R19-3-1] J. A. Crotinger, et al., LLNL Report UCRL-ID-126284 (1997).
- [R19-3-2] A. H. Glasser, et al., Phys. Plasmas **23**, 112506 (2016).

---

## **R19-4: Assess energetic particle transport by sub-TAE instabilities and develop reduced EP transport modeling tools**

Milestone R19-4 has been fulfilled by conducting an assessment of the effects of instabilities with frequency below the Toroidal Alfvén Eigenmode (TAE) gap on energetic particle (EP) transport. In collaboration with DIII-D and MAST-U, experimental research has been complemented by the development and testing of a common framework to include the effects of enhanced EP transport by both AEs and low-frequency instabilities in TRANSP.

Data from NSTX/NSTX-U, DIII-D, MAST and other tokamaks indicate that low-frequency modes such as kink, fishbones, sawteeth and tearing modes (TMs) can indeed result in greatly enhanced energetic particle transport. Compared to Alfvénic modes, low-frequency instabilities present specific features that require a thorough re-examination and validation of the transport models previously used for Alfvénic modes. For instance, low-f MHD modes typically feature a reduced number of resonances with fast ions. Conversely, the strength of each resonance tends to be larger for low-f modes than for AEs. This can cause a further departure of EP transport from a “diffusive-like” character, introducing convective terms that - at present - cannot be correctly handled by theories and models based on a quasi-linear approach. Also, the low frequency (near the rest frequency in the plasma frame) can introduce “non-resonant” transport mechanisms that are closer to the effects of ripple or static 3D perturbations.

The “kick model” implemented in the NUBEAM module of TRANSP has been used in this work. Within the kick model, the primary input for TRANSP to represent enhanced EP transport is a set of transport probability matrices that condense the effects of instabilities on EP dynamic.

Matrices are defined over the phase-space constant of motion variables  $E$ ,  $P_\zeta$  and  $\mu$ , which represent the EP energy, canonical toroidal angular momentum, and magnetic moment. Transport matrices are computed via particle following codes such as the Hamiltonian guiding-center code ORBIT. For Alfvénic modes, which can feature a complex radial mode structure, mode structures are computed through MHD codes such as NOVA/NOVA-K. Low-frequency modes such as TMs and kink/fishbones are usually characterized by simpler mode structures that can be approximated by analytical expressions.

The following paragraphs summarize the main results of activities related to the R19-4 Milestone goals on EP transport by sawteeth, fishbones and Neoclassical TMs (NTMs).

### *EP Transport By Sawteeth*

The effect of sawteeth on fast ion transport has been studied in reproducible, 2s-long sawtooth L-mode discharges during the 2016 NSTX-U campaign. Initial analysis of the discharges [R19-4-1] has demonstrated that standard sawtooth models, namely the full & partial

reconnection models implemented in TRANSP, were not capable to fully reproduce the changes in the fast ion redistribution induced by sawtooth crashes. Although some global parameters such as neutron rate can be recovered, detailed features of the EP distribution show differences with respect to the available experimental data from FIDA and ssNPA [R19-4-2]. Inconsistencies are attributed to the fact that the sawtooth models in TRANSP do not include the different response of fast ions with different orbits (co-passing, counter-passing, or trapped) to sawteeth. To overcome these limitations, the kick model has been applied to replace the standard sawtooth models. Previous work [R19-4-2] had focused on preparatory work using the ORBIT code to infer the kick model inputs, and to compare the resulting fast ion redistribution for different orbit types, resulting in satisfactory agreement with existing theories [R19-4-3]. For the R19-4 milestone, work has been extended to a more comprehensive assessment of TRANSP/kick model simulations. Results using the kick model, thus taking into account the characteristics of fast ion such as energy and pitch angle, achieve a better agreement with the experimental neutron rate with an average difference of less than 10%. An initial comparison of the measurements and synthetic diagnostics of FIDA and ssNPA using the TRANSP/kick model results also shows improved agreement with respect to previous models [R19-4-4], see Fig. R19-4-1.

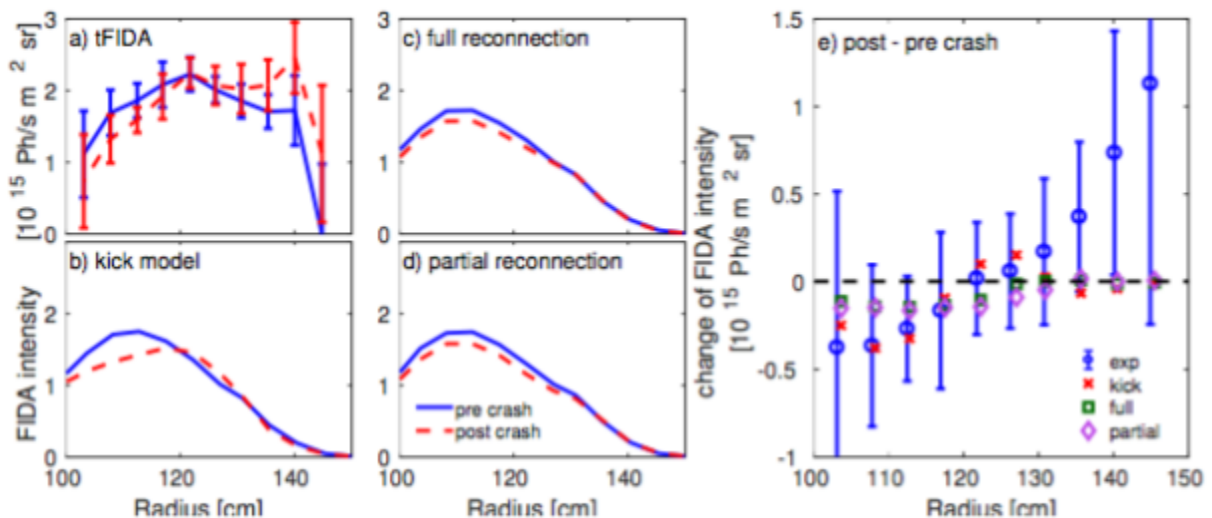


**Fig. R19-4-1:** (a) Experimental FIDA data before and after a sawtooth crash, compared to simulated t-FIDA spatial profiles using (b) kick model, (c) full reconnection and (d) partial reconnection. (e) Change of profiles after a crash for the experimental and simulation results. Using kick model, qualitative trends of the fast ion distribution modification due to a sawtooth crash are reproduced. (From [R19-4-4]).

### EP Transport By Fishbones

Fishbones share with sawteeth a similar radial mode structure, which can be approximated with a hat-like radial displacement for the fundamental  $(n,m)=(1,1)$  harmonic. Contrary to the sudden

sawtooth crash events occurring in less than  $\sim 1$ ms (typically shorter than the TRANSP simulation time-step), fishbones feature a measurable temporal evolution of both amplitude and frequency over time-scales of 1-5 ms. The characterization of fast ion transport by fishbones has a long history [R19-4-5], and work in FY-19 has focused on importing previous results (e.g. from the ORBIT code [R19-4-6, R19-4-7]) into TRANSP simulations through the kick model [R19-4-8]. Results from the kick model indicate that the rapid amplitude and frequency changes are probably a second-order effect for TRANSP simulations, for which the main fast ion redistribution is already captured by a single, fixed-frequency mode.

However, more detailed analysis on the modifications of the fast ion distribution (e.g. as a function of energy and pitch) indicates slightly different localization of the depletion of the distribution caused by the instability if amplitude and frequency variations are taken into account.

TRANSP/kick model simulation of fishbone-unstable scenarios have been recently extended to MAST [R19-4-9] to investigate scenarios with both unstable fishbones and TAEs [R19-4-10]. Preliminary results confirm that fishbones are efficiently redistributing NB-driven current, leading to modifications of the  $q$ -profile, cf. Fig. R19-4-2. Future work will further explore the role of fishbones in *predictive* simulations, in which the current profiles is evolved in TRANSP including the effects of instabilities.

### EP Transport By NTMs.

In collaboration with DIII-D, previous work on fast ion transport induced by NTMs [R19-4-11] has been extended to several scenarios on DIII-D [R19-4-12, R19-4-13]. To assess the results from TRANSP/kick model, simulations are performed using values of the NTM island width inferred from the experiment. TRANSP results are in good agreement with the experiment in terms of both global quantities, such as neutron rate [R19-4-12], and measurements of the fast ion distribution function from FIDA and NPA [R19-4-14, R19-4-8].

The successful application of the TRANSP/kick model approach to DIII-D scenarios has motivated its extension to NSTX/NSTX-U discharges. Work is in progress to develop analysis software to infer

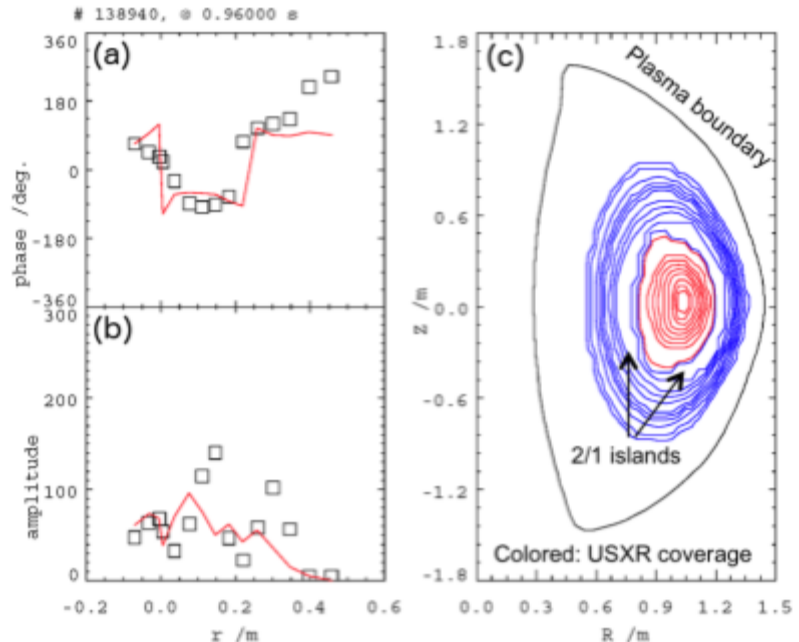


**Fig. R19-4-2:** Fit of experimental SXR data from NSTX to infer the NTM island properties. (a-b) Measured (symbol) and simulated (red line) radial profile of perturbation phase and amplitude. (c) Reconstructed NTM perturbation in the poloidal cross-section. (From [R19-4-15]).

the NTM properties (frequency, helicity, island width) from Soft X-Ray and Mirnov coils data, see Fig. R19-4-2 [R19-4-15]. Once the mode properties are known, ORBIT simulations will provide the required input for TRANSP. This will enable a comprehensive study of the effects of NTMs on fast ion transport in NSTX/NSTX-U, including their impact on redistribution of NB driven current and on NB current drive efficiency and controllability.

### Future Work

Initial results from TRANSP/kick model simulations of scenarios featuring low-frequency instabilities are promising and indicate a path forward for further improvements. One limitation of the present analysis is that input for TRANSP/kick model is computed in ORBIT at a single time (or at a few given times), assuming that plasma profiles and equilibrium do not change “substantially” as time evolves with respect to the reference time-slice(s). However, in some cases - e.g. during the current ramp-up - profiles can vary rapidly. To improve the simulations, two steps are required: (i) develop a version of ORBIT that is fast enough to be implemented in TRANSP simulations, and (ii) implement a framework in TRANSP to update the kick model input as the profiles vary. Progress has been made on (i), with a test version of ORBIT that runs on GPUs in seconds, as opposed to several minutes (or hours) required by the standard version of the code. For (ii), work has begun with the TRANSP group to define requirements common to different codes (not just the kick model). The plan is to make TRANSP results for profiles and equilibrium available during a run to codes for MHD stability analysis and additional tasks such as computing and updating the kick model input.

Overall, the improved tools to model fast ion transport by low-frequency instabilities complement previous work on AE-induced transport. The expanded set of tools will enable more thorough physics analysis of complex scenarios, in which the effects of multiple types of instabilities can lead to enhanced EP losses and redistribution.

### **References:**

- [R19-4-1] D. Kim, et al., Nucl. Fusion **58** (2018) 082029.
- [R19-4-2] D. Liu, et al., Nucl. Fusion **58** (2018) 082028.
- [R19-4-3] Ya. I. Kolesnichenko, et al., Phys. Plasmas **4** (1997) 2544.
- [R19-4-4] D. Kim, et al., Nucl. Fusion **59** (2019) 086007.
- [R19-4-5] R. B. White, et al., Phys. Fluids **26** (1983) 2958.
- [R19-4-6] E. M. Carolipio, et al., Nucl. Fusion **42** (2002) 853.
- [R19-4-7] M. Gobbin, et al., Nucl. Fusion **49** (2009) 095021.
- [R19-4-8] M. Podestà, et al., Nucl. Fusion (in press, 2019)  
<https://doi.org/10.1088/1741-4326/ab3112>.
- [R19-4-9] M. Cecconello, et al., “Analysis of TAEs and FBs induced fast ion redistribution and losses in MAST using a reduced fast ion transport model”, to be presented at the 16th IAEA-TCM on Energetic Particles in Magnetic Confinement Systems, Shizuoka City - Japan (September 3-6, 2019).
- [R19-4-10] M. Cecconello, et al., Plasma Phys. Control. Fusion **57** (2015) 014006.
- [R19-4-11] W. W. Heidbrink, et al., Nucl. Fusion **58** (2018) 082027.
- [R19-4-12] L. Bardóczi, et al., Plasma Phys. Control. Fusion **61** (2019) 055012.

[R19-4-13] D. Liu, et al., “Fast Ion Instabilities In DIII-D hybrid discharges,” to be presented at the 16th IAEA-TCM on Energetic Particles in Magnetic Confinement Systems, Shizuoka City - Japan (September 3-6, 2019).

[R19-4-14] C. C. Petty and the DIII-D Team, Nucl. Fusion **59** (2019) 112002.

[R19-4-15] J.-H. Yang, et al., “Characterization Of Tearing Modes On NSTX,” to be presented at the 61<sup>st</sup> APS-DPP Meeting, Fort Lauderdale FL (October 21-25, 2019).

## Additional Research Highlights

### Boundary Science

### Pedestal Structure and Control

#### ELM Mitigation Via ELM Pacing With Impurity Pellets In EAST

The ability to trigger ELMs with pellet injection depends on predicting and identifying a pellet size threshold necessary to create a sufficiently large pressure perturbation to destabilize 3D ballooning modes. Experimentally this requires the ability to inject multiple pellet sized and velocities to identify an ELM triggering threshold. The lithium granule injector on EAST was equipped with four reservoirs for independent selection of granule sizes: 300  $\mu\text{m}$ , 500  $\mu\text{m}$ , 700  $\mu\text{m}$ , and 900  $\mu\text{m}$ , with nominal variability of 100  $\mu\text{m}$  each. The maximum granule injection frequency through the LGI decreases rapidly with increasing granule size. Dedicated experiments have identified a size threshold of  $\geq 500$   $\mu\text{m}$  Li granules for ELM triggering on EAST [PED-1] (Fig. PED-1), in agreement with complementary experiments on DIII-D [PED-2]. However, the natural ELM frequency of the available discharges was  $\sim 200$ -250 Hz, i.e. well above the maximum injection capability of LGI granules at 700  $\mu\text{m}$  and 900  $\mu\text{m}$ . Thus, it was not possible to assess whether the peak heat flux was affected with ELM triggering. It was however observed that use of 300  $\mu\text{m}$  at 800 Hz injection frequency increased the overall ELM frequency to 600 Hz, despite the fact that each granule did not trigger an ELM [PED-3]. Rather, the edge stability was changed via granule injection to a smaller, more rapid ELM regime with reduced peak heat flux. The extrapolability of such a technique (ELM frequency enhancement without 1:1 pellet-ELM pacing) to future devices merits further investigation.

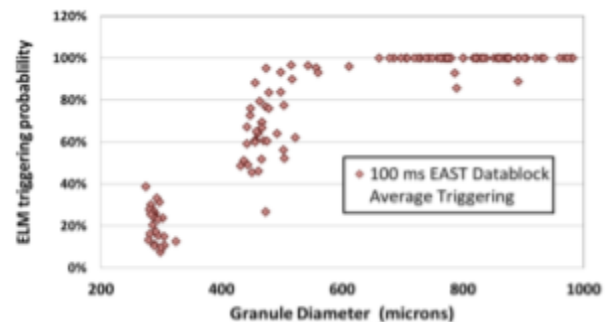


**Fig. PED-1:** ELM triggering probability vs. Li granule size for midplane injected granules at  $\sim 100$  m/s in EAST, indicating a size threshold.

### Blob Wakes

A new phenomenon called “blob wakes” was discussed in a recently published paper [PED-4]. These are transient small-scale structures seen in the wake of blobs moving poloidally through the scrape-off layer of high-powered H-mode plasmas in NSTX, using data from the gas puff imaging (GPI) diagnostic taken in 2010 (see Fig. PED-2). These blob wakes had a poloidal wavelength in the range of  $\lambda_{pol} = 3.5 \pm 0.7$  cm, which is significantly smaller than the average blob scale of  $L_{pol} \sim 12$  cm, and a poloidal velocity of  $V_{pol} = 1.5 \pm 1.0$  km/s in the electron diamagnetic direction, which is opposite the blob poloidal direction in these shots. The wakes were radially localized 0–4 cm outside the separatrix and occurred within  $\sim 50$   $\mu$ s after the passage of a blob through the GPI field of view. The clearest wakes were seen when the GPI viewing angle was well aligned with the local B field line, as expected for such small-scale structures given the diagnostic geometry. A plausible theoretical interpretation of the wakes was discussed: the observed wakes share some features of drift waves and/or drift-Alfven waves which could be excited by the blobs.

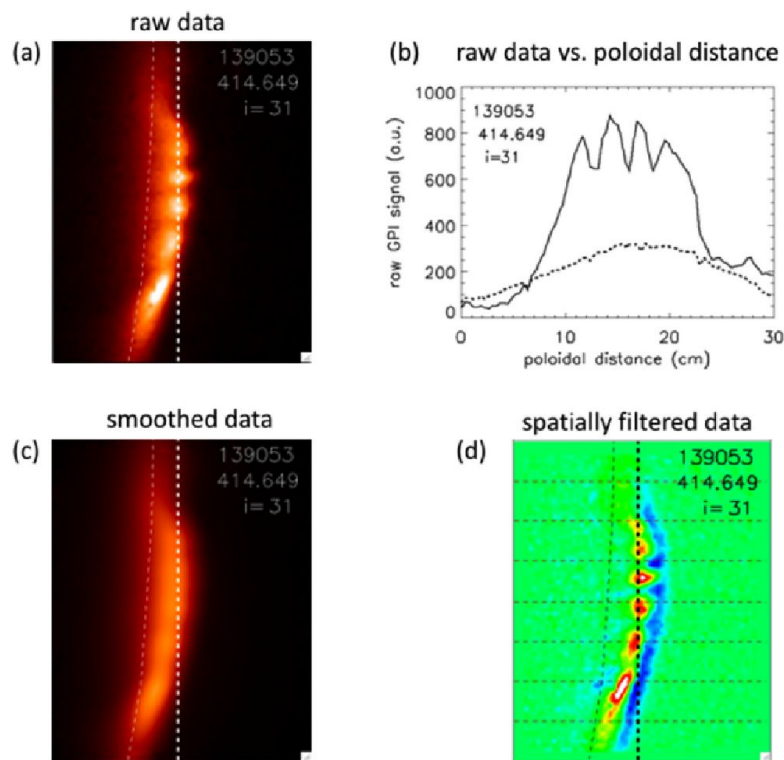


**Figure PED-2:** Spatial high-pass filtering of GPI images. Part (a) is a single frame of raw data from Fig. 2(a) of Ref. [P-1], and (b) is the raw GPI data vs poloidal distance at the column  $i=31$  where the wake modulation is near maximum, along with the time-averaged data in this column over 1 ms (dashed line). Part (c) is the spatially smoothed frame, after boxcar averaging in both directions over 7 pixels (2.6 cm). Part (d) is the raw data frame minus the smoothed frame, now drawn using a color scale with red/white as maxima and blue/black as minima. The wake maxima are shown as red/white regions. The separatrix is shown as a thin dashed line, and horizontal grids are shown for reference with a vertical (i.e., poloidal) spacing of 5 cm.

**References**

- [PED-1] R. Lunsford, et al., 2018 *Nucl. Fusion* **58** 036007.
- [PED-2] A. Bortolon, et al., 2016 *Nucl. Fusion* **56** 056008.
- [PED-3] R. Lunsford, et al., 2018 *Nucl. Fusion* **58** 126021.
- [PED-4] S. J. Zweben, et al., *Phys. Plasmas* 26, 072502 (2019).

**Divertor and Scrape-Off-Layer**

*Divertor Disconnection Of Blob Filaments And Blob Velocity Scaling*

The disconnection of midplane filaments from the divertor target plate is expected from theoretical models to have an effect on their radial velocity, thus possibly affecting the radial heat flux width. In the 2018 NSTX-U end of the year report, experimental observations of turbulence disconnection were compared to an electrostatic two-region blob model [DSOL-1]. Blob disconnection from the divertor target was observed transitioning from the Cs regime (sheath connected) to the Ci (connected ideal-interchange) and RX (resistive X-point) regimes, confirming the role of X-point geometry for the disconnection of midplane filaments from the divertor target. The radial region showing turbulence disconnection also coincided with the minimum in the turbulence radial velocity.

Experimental measurements of blob radial velocity (estimated from time-delayed cross correlations) are compared here with the expected scaling from the electrostatic two-region model. Blob disconnection from the divertor is expected to modify the blob radial velocity, due to changes in effective resistivity of the blob circuit. As discussed in Ref. [DSOL-2], the X-point geometry promotes short circuiting of the polarization charge that drives the blob radial velocity. The stretching of the flux tubes in the proximity of the X-point, at constant collisionality, decreases the effective resistivity of the filament current loop, increases its inertia and reduces the filament  $v_{rad}$ .

The dimensionless blob size  $\hat{\delta}$  is obtained through

normalizing the experimental blob size  $\delta_b$  by the characteristic blob scale  $\delta_* = \rho_s \left( \frac{L_{||}^2}{\rho_s R} \right)^{1/5}$ , where  $L_{||}$  is the midplane to target connection length,  $\rho_s$  is the sound Larmor radius, and R is the

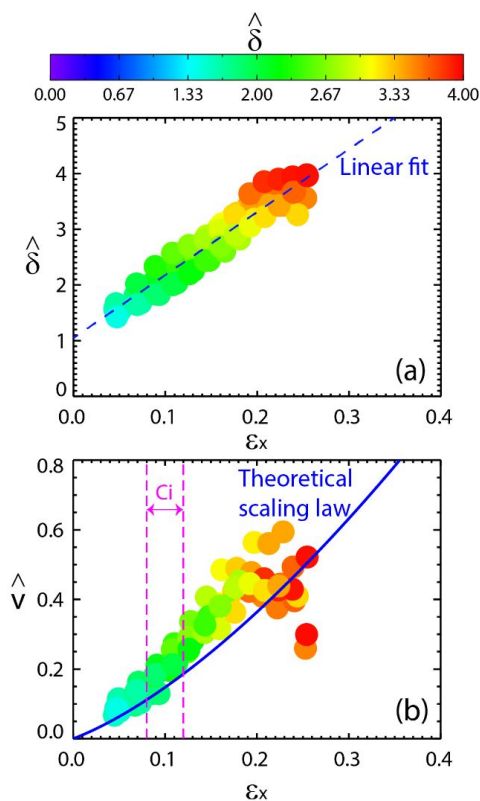


**Figure DSOL-1:** (a) Experimental values of normalized blob size as a function of  $\epsilon x$ ; (b) experimental values of normalized blob velocity as a function of  $\epsilon x$ .

major radius. A proxy for the X-point magnetic fanning parameter  $\varepsilon_x$  [myra\_pop\_2006] is used, obtained by evaluating the ratio of  $\frac{B_T}{RB_p}$  at midplane and at the divertor.  $\varepsilon_x$  increases approximately linearly with the distance from the separatrix (and is thus a proxy for a radial coordinate). In Fig. DSOL-1a, it is shown that the experimental values of  $\hat{\delta}$  have a linear dependence on  $\varepsilon_x$ . In Fig. DSOL-1b, the experimental values of normalized radial blob velocity  $\hat{v} = v_{rad}/v_*$  (where  $v_* = c_s(\delta_*/R)^{1/2}$  and  $c_s$  is the sound speed) are shown as a function of  $\varepsilon_x$ . Overlaid in blue is the theoretical scaling law for the Ci regime from the two region model  $\hat{v} = \varepsilon_x \hat{\delta}^{1/2}$ , obtained using the linear fit for  $\hat{\delta}(\varepsilon_x)$  from Fig. DSOL-4a. The experimental blob  $v_{rad}$  follows the theoretical scaling, with the lower  $v_{rad}$  near the separatrix expected from the two-region model.

The Ci regime for this dataset strictly applies only over the small range  $0.08 < \varepsilon_x < 0.12$  (shown in magenta) derived from the lower boundary with the RX regime ( $\varepsilon_x \hat{\delta}^{5/2} = \Lambda$ ,  $\Lambda = 0.4$ ) and the upper boundary with the Cs regime ( $\varepsilon_x \hat{\delta}^{5/2} = 1$ ). Most of the data for  $\varepsilon_x < 0.2$  seems, however, to follow the Ci scaling (the Ci boundaries have uncertainties due to data mapping to  $\varepsilon_x$  and due to plasma parameters used in the normalizations).

The data for  $\varepsilon_x > 0.2$  shows a distinct break from the Ci scaling, consistent with a transition from Ci scaling to Cs scaling ( $\hat{v} = 1/\hat{\delta}^2$ ) for sufficiently large  $\delta$ .

## References

- [DSOL-1] J. Myra, et al., Phys. Plasmas 13, 112502 (2006).  
 [DSOL-2] D. D'Ippolito, et al., Phys. Plasmas 18, 060501 (2011).

## Materials and PFCs

Studies on the use of impurity powder injection for wall conditioning and pedestal control were conducted on international devices. While these studies were supported by NSTX-U at a modest level, the techniques and science will be applied to NSTX-U, and many of the staff conducting experiments will also work on boundary physics on NSTX-U. Thus, for completeness, highlights from the international studies on EAST, KSTAR and ASDEX-Upgrade are included here.

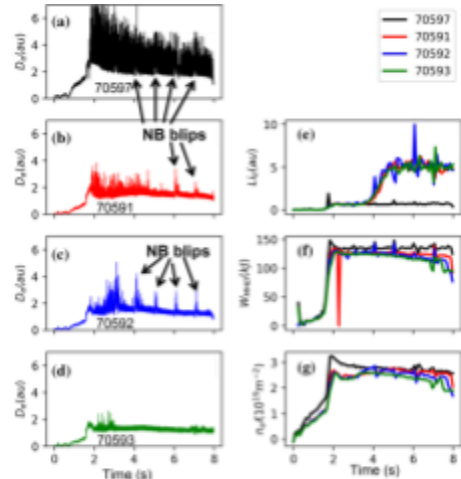
### Impurity Powder Injection

Impurity powder droppers (IPD) have been deployed on EAST, KSTAR and ASDEX-Upgrade, as well as DIII-D and LHD. NSTX-U will also have a similar IPD unit. Results from international devices are documented below.

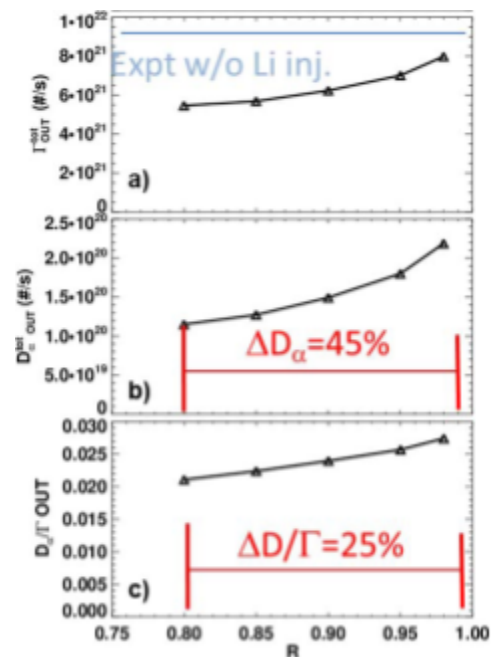
**EAST:** Lithium powder was injected via a conventional powder dropper based on a design originally used in NSTX [PFC-1]. Since the first ELM suppression results in EAST that used carbon PFCs [PFC-2], the upper divertor in EAST had been replaced with an ITER-style tungsten mono-block. Results from AUG with metallic PFCs using Li pellet injection had not shown neither performance enhancement nor ELM modification [PFC-3]; this raised the possibility that Li stability and confinement benefits may occur only in devices with low-Z PFCs. New experiments were therefore conducted with injection of solid Li micro-spheres using the new W upper divertor in EAST. These new experiments were successful: ELMs were eliminated in discharges with Li powder injection using the upper tungsten divertor [PFC-4]; Li powder injection and conditioning also contributed to the achievement of record 100 s pulse lengths in EAST [PFC-5]. The likely cause of the edge stability improvement that resulted in ELM stabilization is pedestal-localized turbulence and/or recycling reduction that resulted in a density and pressure profile change, mirroring results with Li evaporation in NSTX [PFC-6] and Li injection in DIII-D [PFC-8].

Fig. PFC-1 above compares four discharges in EAST: three in a sequence with constant Li injection rate, followed a few discharges later by an ELMy H-mode reference with no Li powder [PFC-4]. In addition to progressively easier ELM suppression in the discharge sequence, the baseline  $D_{\alpha}$  was continuously reduced, indicating a progressive conditioning effect, as also observed in NSTX with pre-discharge Li evaporation [PFC-6]. Note that the stored energy was decreased by up to 10% in the final discharge; we hypothesize that because recycling continues to be reduced even at a constant Li injection rate, a reduced Li powder injection rate could have been used with increasing shot number, to maintain ELM suppression with the minimal effect on density and stored energy.

Analysis of the recycling reduction aimed to quantify the change in divertor recycling coefficient with Li powder injection in EAST [PFC-7]. A variation of the divertor recycling coefficient was used to generate plasma states in SOLPS, with two values of the upstream separatrix density



**Fig. PFC-1:** Upper divertor  $D_{\alpha}$  emission from (a) reference #70597, (b) first discharge with dropper #70591, (c) second discharge with dropper #70592, (d) third discharge with dropper #70593. Also shown in panel (e) is the Li-II line emission (f) the plasma stored energy,  $W_{MHOD}$ , and (g) the line density from the POINT diagnostic.



**Fig. PFC-2:** results of SOLPS analysis of discharges with ELM suppression by Li powder injection. A net reduction of the recycling coefficient by  $\sim 25\%$  is the best match to the data.

since the separatrix location has substantial uncertainty. The analysis showed that the experimental value of the outer divertor baseline particle flux could be reproduced at near-unity recycling before Li powder injection, and that powder injection dropped the recycling coefficient by about 25% (Fig. PFC-2, [PFC-7]). The uncertainties in this analysis are unfortunately relatively large, due to lack of heat flux data from IR thermography.

**AUG and KSTAR:** Whereas the use of Li injection has limited (but growing) interest in the worldwide community, due to safety and tritium retention issues, B is a more common choice for wall conditioning. A new Impurity Powder Dropper (IPD) was designed by staff at the PPPL to inject a wider range of impurity species than the original dropper, include boron compounds [PFC-8]. This IPD is now deployed on the ASDEX-Upgrade, DIII-D, EAST and KSTAR devices, and one will soon be installed on LHD. The new design is based on an original design that dropped spherical, non-sticky impurities through an aperture on a vibrating piezoelectric disk driven at resonant frequencies; the injected impurities accelerated via gravity into a drop tube and into the boundary plasma [PFC-1]. The IPD uses piezoelectric crystals for a horizontal drive off the edge of a surface into a drop tube, and it is compatible with a wide range of impurity species and particle sizes, including boron-based compounds [PFC-8]. The IPD consists of four reservoirs that can each hold a separate material. Powders fall from the reservoirs onto troughs that, when vibrated by piezoelectric actuators, drop the powder into a common drop tube and into the plasma (Fig. PFC-3). The orientation and mechanical resonant frequency of each of the four sub-systems is set to minimize incidental dropping of powders in separate reservoirs. The dropped powders pass through an optical flow meter in order to monitor the flow rate, and a photodiode mounted at the top points down the length of the drop tube to watch for light emission from the plasma when powders reach the plasma periphery. An example of the calibrated flow rate for two difference materials is shown in Fig. PFC-3c. The powders fall a total distance of several meters, depending on the specific implementation at each site.

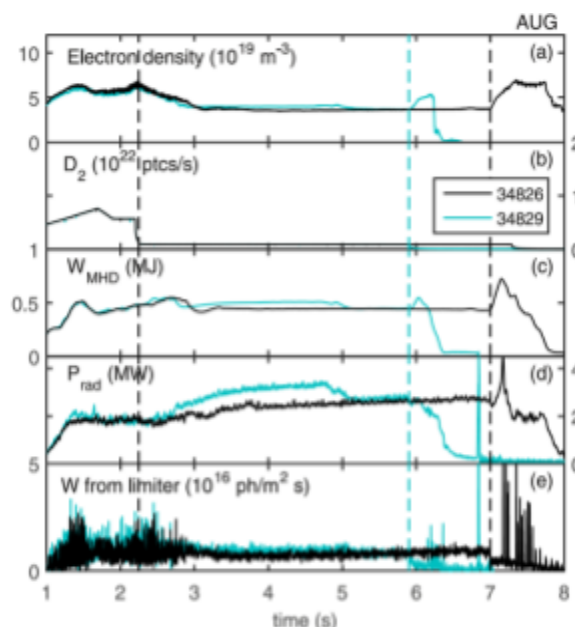


*Fig. PFC-3: comparison of two discharges with ELM suppression by magnetic perturbations, following a sequence of B conditioning discharges. No B was injected in these discharges.*

Experiments carried out in the ASDEX-Upgrade (AUG) and KSTAR tokamaks explored the utility of real-time boron coating generation via injection of B and B enriched powders during tokamak operation. These results complement the DIII-D results with B conditioning described in the previous section. Wall conditioning improvement similar to boronization was observed in AUG (tungsten PFCs) following injection of pure B and boron nitride (BN) powder into H-mode

plasmas designed to condition the wall [PFC-9,10]. These discharges were taken 18 days and 104 discharges after a conventional gaseous diborane boronization, at which point the conventional boronization conditioning effect had worn off. Fig. PFC-4 compares the time evolution of two such discharges in AUG: both had low gas puffing for low density/collisionality, and magnetic perturbations for ELM suppression. While there were modest differences between these identically programmed discharges, there was no evidence of a degradation of wall conditions between them. Thus it can be concluded that the conditioning effect from one or two high B injection rate conditioning discharges lasts for at least 4 subsequent discharges, at least 30 shot seconds, and a cumulative 200 MJ of input energy. Finding the conditioning lifetime requires additional experiments, which will be the subject of future experiments. Other measured improvements due to the B conditioning at high injection rates included reduction of O and W influx from limiters. For completeness, we note that boron injection into ELMy H-Mode KSTAR discharges was tried and showed reduced recycling similar to DIII-D and AUG, but also mitigation of ELMs. This ELM mitigation effect in KSTAR was even more pronounced with BN injection, as discussed in the next paragraph.

Conceptually, BN injection is of interest because of the potential effects of N to enhance radiated power, combined with the positive effects of B for wall conditioning. BN injection into AUG increased both the radiated power (by > 100%) and energy confinement (by 10-20%) (Fig. PFC-4), similar to N<sub>2</sub> gas injection. Moreover, the generation of ammonia was reduced by more than 90% with solid BN injection as compared to gaseous N<sub>2</sub> injection [PFC-10,11]. In comparison, the first BN injection in KSTAR H-mode discharges resulted in substantial changes in ELM stability: 5 sec long ELM-quiescent phases were observed (graphite PFCs), along with clear changes in edge turbulence relative to the ELMy H-mode with ~ 100 Hz ELMs [PFC-10]. Fig. PFC-5 shows that the effect in KSTAR depends on the injection rate: short bursts at a high injection rate is more effective at ELM suppression than long bursts at low rates. Note that due to time delays in the drop tube, the injection starts about one second after the orange time markers in the figure, and it lasts for at least one sec longer than the programmed duration, obviating causality assessment via time correlation.

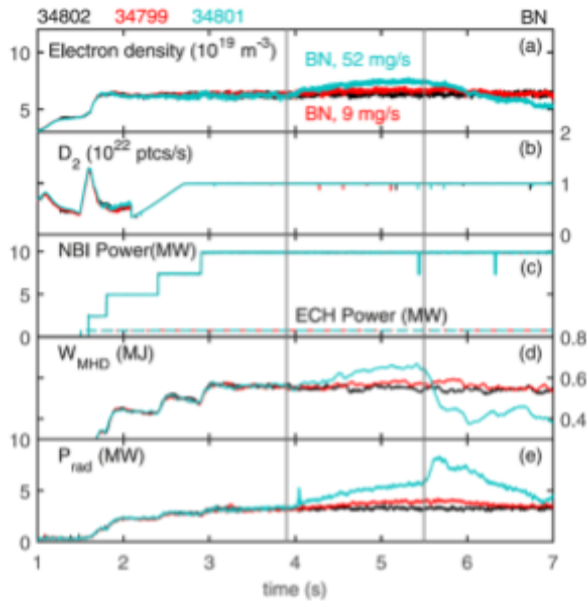


**Fig. PFC-4:** Temporal evolution of plasma discharge quantities for a reference discharge (black), with 9 mg/s of BN injection (red) and 52 mg/s of BN injection (blue). Stored energy and confinement improved with BN injection at high rates, similar to N2 gas injection. The blue discharge encountered the core  $\beta_N$  limit of 2.7 at 5.5 sec. This could easily be avoided with  $\beta_N$  feedback on input power.

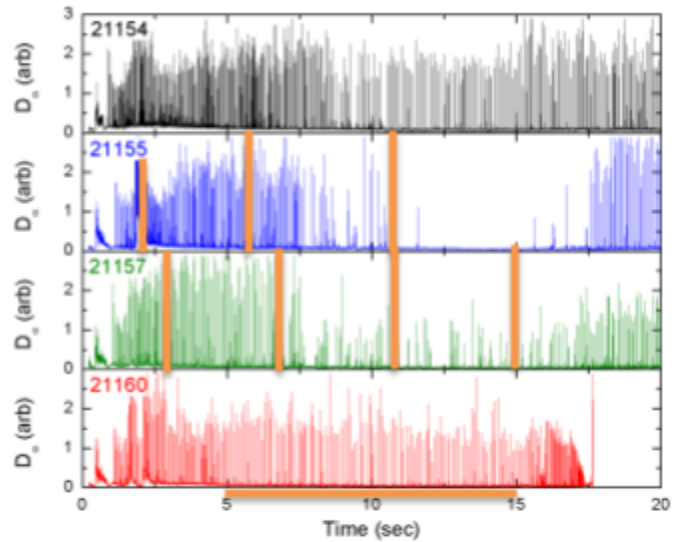


**Fig. PFC-5:** comparison of BN injection in KSTAR with a reference ELMy H-mode. The injection rates and times are indicated in the captions; note there is a substantial delay trigger  $> 1$  sec. Courtesy of E.P. Gilson, presented at the 2019 KSTAR conference, Feb. 20-22, 2019.

Flowing Liquid Metal PFCs In EAST

Due to its strong chemical reactivity with vacuum impurity gases, maintaining a clean Li plasma-facing surface for hydrogen pumping requires continuous flow for long pulse discharges, a key purpose of the flowing liquid Li (FLiLi) limiter program in EAST [PFC-12,13,14], and an important future emphasis in NSTX-U. Three generations of limiters have now been exposed to EAST H-mode plasmas. Table PFC-1 compares their design characteristics and the types of plasmas exposed to them.

**Table PFC-1:** Comparison Of Three Generations Of The FLiLi Limiter

Generation	Heat Sink	SS thickness (mm)	JxB pumps	Max. $P_{aux}$ (MW)	Max. $q_{exh}$ (MW/m <sup>2</sup> )	Max. $W_{MHD}$ (kJ)
1	Cu + SS	0.1	1	1.9	3.5	120
2	Cu + SS	0.5	2	4.5	4	170
3	Mo (TZM)	NA	2	8.3	TBD	280

A second generation flowing liquid Li limiter was designed with several upgrades [PFC-15] to prevent the damage observed in the first generation system. First, a thicker stainless-steel protective layer (0.5mm vs. 0.1 mm) was used to prevent PMI from exposing the Cu heat sink to the liquid Li. Next an additional j x B magnetic pump was added for a more uniform supply of Li to the distributor on the top of the limiter. In addition, surface texturing was implemented in the second generation, which improved the wetting uniformity of the liquid Li flowing on the front face. Also, an improved method for manufacturing the top Li distributor from two pieces was developed; this new design avoided the crack that developed during deployment of the first generation distributor.

The second generation limiter was inserted into plasma discharges on two separate dates [PFC-16], demonstrating an ability to restart Li flow after it has been stopped for more than a week. Camera images after the first exposure showed a relatively pristine limiter surface, but photographs after the second exposure showed streaks on the plasma-facing surface, indicating the formation of surface-contaminating compounds that may have hindered free flow in the second exposure. The limiter plate condition after plasma exposure for the second generation showed no visible damage, whereas the first generation limiter showed visible damage on the right-hand side of the limiter face [PFC-14,15]. In addition, the fractional surface area that was un-wetted by the Li was < 20% in Gen 1, vs. ~70% in Gen. 2.

The upper divertor  $D_\alpha$  emission and ELM size were continuously reduced in otherwise constant discharge conditions into which the second generation limiter was inserted [PFC-16]: plasma current  $I_p = 0.45$  MA, toroidal field  $B_T = -2.5$  T,  $P_{aux} = 2.9$  MW, in an upper single-null configuration with ion grad-B drift toward the lower divertor. These results showing progressive conditioning and ELM mitigation are qualitatively similar to Li powder injection on EAST [PFC-4], as well as with pre-discharge Li evaporation in NSTX [PFC-6]. Finally, short-lived *true* ELM-free phases (and also ohmic H-modes) were observed for the first time in EAST with increasing  $\tau_E$  and transient  $H_{H98y2} \leq 2$  when the second generation limiter was inserted. We refer to these as *true* ELM-free H-modes because of the density accumulation observed, which is not seen in the ELM suppressed cases observed with e.g. real-time Li powder injection.

Due to the continuing success of the FLiLi limiter program, a third generation limiter constructed entirely of TZM, an alloy with > 99% Mo, was fabricated by conventional manufacturing techniques [PFC-17]. Mo was chosen due to its higher sputtering resistance as compared to stainless steel, and its good compatibility with conventional manufacturing as compared to tungsten. The front face of the limiter was polished to a mirror-like finish to facilitate flow. The third generation FLiLi was inserted into the edge of EAST H-mode plasmas in an upper single-null configuration with ion grad-B drift toward the upper divertor. Fig. PFC-8 compares reference discharge (black) with one in which the FLiLi limiter was inserted to within 3 cm of the separatrix (red) with  $I_p = 0.55$  MA,  $B_t = 2.5$  T,  $P_{aux} = 7.9-8.3$  MW, EM pump current = 100 A. The neutral Li line emission is higher with the limiter inserted, as expected, while the  $D_\alpha$  emission from the upper divertor is substantially lower. The stored energy is slightly higher with the limiter inserted, though this is partly due to modestly higher heating power. The line-average density is

comparable. Overall the limiter performed well for this set of discharges. Upon removal, however, damage to the electron drift side of the limiter plate was evident, as was damage to the right-hand side of the collector. The reasons for the damage are under investigation. These studies will be used to inform the design of future flowing liquid Li components for NSTX-U.

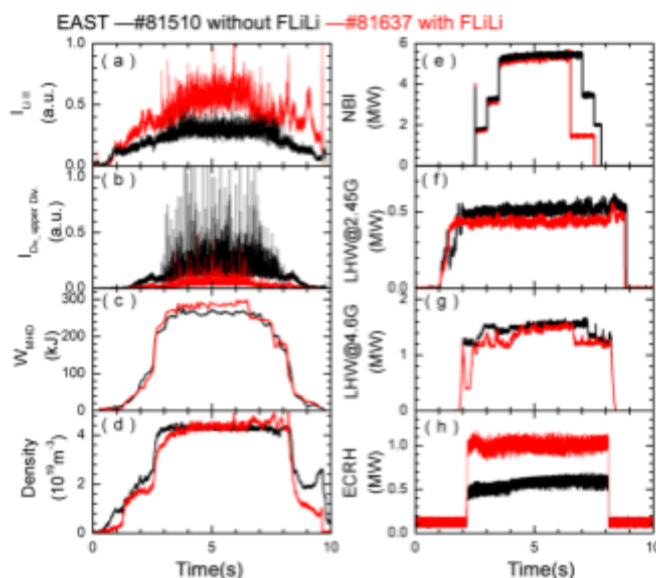


**Fig. PFC-8:** Comparison of plasma with (red - #81637) and without (black-#81510) the 3<sup>rd</sup> generation FLiLi limiter inserted: (a) Li-II emission, (b) Upper divertor  $D_{\alpha}$  emission, and (c) Plasma stored energy, (d) line-average density, (e) neutral beam injected power, (f) low frequency lower hybrid power, (g) high frequency lower hybrid power, and (h) electron cyclotron resonant heating power. The auxiliary heating power with FLiLi was 6% higher, partly resulting in higher stored energy.

## References:

- [PFC-1] D. K. Mansfield, et al., 2010 *Fusion Eng. Des.* **85** 890.
- [PFC-2] J. S. Hu, et al., 2015 *Phys. Rev. Lett.* **114** 055001.
- [PFC-3] P. T. Lang, et al., 2017 *Nucl. Fusion* **57** 016030.
- [PFC-4] R. Maingi, et al., 2018 *Nucl. Fusion* **58** 024003.
- [PFC-5] Z. Sun, et al., 2019 *Nucl. Mater. Energy* **19** 124.
- [PFC-6] R. Maingi, et al., 2012 *Nucl. Fusion* **52** 083001.
- [PFC-7] J. M. Canik, et al., 2018 *IEEE Trans. Plasma Sci.* **46** 1081.
- [PFC-8] A. Nagy, et al., 2018 *Rev. Sci. Instrum.* **89** 10K121.
- [PFC-9] A. Bortolon, et al., 2019 *Nucl. Mater. Energy* **19** 384.
- [PFC-10] R. Lunsford, et al., 2018 *Proc. 27th International Conf. on Fusion Energy, Ahmedabad, India, 18-22 Oct. 2018* Paper FIP/2\_3; *Nucl. Fusion* (2019) in preparation.

- [PFC-11] A. Drenik, 2019 *invited talk to be presented at the 2019 Euro. Conf. on Plasma Phys. and Control. Fusion, Milan, Italy, 8-12 July 2019.*
- [PFC-12] J. S. Hu, et al., 2016 *Nucl. Fusion* **56** 046011.
- [PFC-13] G. Z. Zuo, et al., 2017 *Nucl. Fusion* **57** 046017.
- [PFC-14] J. S. Hu, et al., 2019 *Nucl. Mater. Energy* **18** 99.
- [PFC-15] G. Z. Zuo, et al., 2017 *Rev. Sci. Instrum.* **88** 123506.
- [PFC-16] G. Z. Zuo, et al., 2019 *Nucl. Fusion* **59** 016009.
- [PFC-17] R. Maingi, et al., 2018 *Proc. 2018 International Conf. on Fusion Energy, Ahmedabad, India, 22-27 Oct. 2018* Paper FIP\_3\_5\_Ra.

## Core Science

### Transport and Turbulence Physics Research

NSTX transport and turbulence studies in FY2019, in the absence of operation, have focused on analyzing existing data, performing experiment-theory comparisons, and carrying out collaboration activities

Understanding plasma transport in phases with significant MHD activities in tokamak plasmas is crucial for predicting and thus controlling plasma behavior for future fusion devices, e.g., ITER. Since high-k turbulence could be an important candidate in driving anomalous electron thermal transport, the interactions between MHD modes and high-k turbulence may play an important role in determining anomalous electron thermal transport. Here we present a detailed study of the effect of an MHD mode in the core region on high-k turbulence ( *at  $r/a \sim 0.6 - 0.68$ , and with  $3.5 \leq k_{\perp} \rho_s \leq 14.3$*  ) in the plasma current flat-top phase of a NSTX H mode plasma discharge. We emphasize that both the high-k turbulence and the MHD mode were measured simultaneously [see Fig. TT-1a] by the high-k scattering system in the scattering mode and in the interferometric mode, separately. This provides a prerequisite to further study their possible nonlinear coupling in experiment.

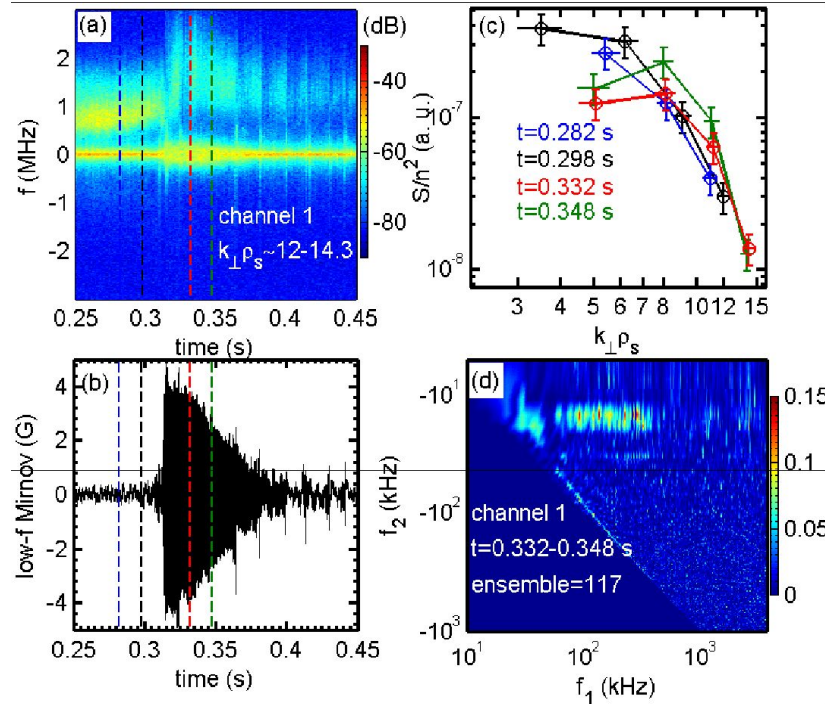


**Figure TT-1:** (a) The spectrogram of channel 1 high- $k$  scattering signals; (b) time evolution of low frequency MHD mode amplitude; (c) the high- $k_{\perp}$  spectrum at four Thomson scattering time points. Note that both  $t=0.282$  s and  $t=0.298$  s are before the occurrence of MHD mode, and both  $t=0.332$  s and  $t=0.348$  s are in phase with MHD mode; (d) squared auto-bicoherence  $b^2(f_1, f_2)$  of channel 1 high- $k$  scattering signals from  $t=0.332$  s to  $t=0.348$  s with 117 ensembles (i.e., noise level =  $1/117=0.0085$ ). Note that the vertical dash lines in both (a) and (b) denote four Thomson scattering time points.

Toroidal mode number ( $n$ ) of the MHD mode has been identified to be  $n = 1$  from Mirnov arrays. Plasma toroidal rotation velocity  $V_t$  shows a rapid damping (not shown) around the region of  $q = 2$  ( $q$  profile from Irdfit09) with the occurrence of the MHD mode, so MHD mode's poloidal mode number should be  $m = 2$ . Following the occurrence of the 2/1 MHD mode [see Fig. TT-1b], high- $k$  turbulence frequency shows an obvious jump, and turbulence spectral width appears to be larger [see Fig. TT-1a]. This high- $k$  scattering system also can provide the wavenumber spectrum [see Fig. TT-1c] covering both the MHD-free phase (e.g.,  $t = 0.282$  s and  $t = 0.298$  s) and MHD phase (e.g.,  $t = 0.332$  s and  $t = 0.348$  s). The high- $k$  turbulence power is found to be quasi-stationary before the occurrence of the MHD mode. But in phase with the 2/1 MHD mode, obvious turbulence suppression has been observed at lower- $k$  (i.e.,  $k_{\perp} \rho_s \leq 8$ ); meanwhile, a slight increase of turbulence power also has been observed at higher- $k$  (i.e.,  $k_{\perp} \rho_s \geq 8$ ). These results clearly imply that high- $k$  turbulence is temporally correlated to the 2/1 MHD events. Having shown the turbulence-MHD temporal correlation, we will show their spectral correlation through using the bi-spectral analysis method. The bispectral analysis is carried out for the time period of  $t = 0.332 - 0.348$  s with ensemble number  $N = 117$  (i.e., noise level =  $1/N = 0.0085$ ) and  $\Delta f = 3.6$  kHz, i.e., time window  $\Delta t = 1/3.6$  kHz), which means the spectral analysis is time-averaged over several fundamental MHD periods (fundamental

frequency of 2/1 MHD mode is  $f \approx 16 \text{ kHz}$ ). The squared auto-bicoherence  $b^2_{\tilde{n}_e, \tilde{n}_e, \tilde{n}_e}(f_1, f_2)$  of channel 1 high-k signal as a function of  $f_1$  and  $f_2$  is plotted in Fig. TT-1d. When  $f_2$  is around  $-16 \text{ kHz}$  (i.e., the fundamental frequency of the MHD mode), many bright parts (the value is more than the noise level) can be found at the frequency range of  $54 < f < 400 \text{ kHz}$ ,  $1055 < f < 1421 \text{ kHz}$  and  $1930 < f < 3062 \text{ kHz}$ . These results prove that the fundamental 2/1 MHD mode can nonlinear couple with the high-k turbulence in a broad frequency range.

First, nonlinear, global GTS simulations of NSTX-U plasma were successfully carried out to access low-k turbulence and associated transport in an L-mode discharge (shot #204551A08 at  $t=0.9-1.2 \text{ sec}$ ). The simulations identified significant low-k fluctuations due to ITG and DTEM in the outer core region (normalized minor radius  $\rho > 0.65$ ) with a relatively weak equilibrium ExB shear, consistent with BES measurements in the region that show increasing amplitude of ion scale fluctuations. More specifically, linear spectrum clearly shows the excitation of very low-k modes separated from the typical ITG range at the region around  $\rho=0.73$ , which is a signal of DTEM (see Fig. TT-2 right panel). In the further outer core region, only ITG is observed. The simulated low-k turbulence is shown to produce large energy transport for ions, but not for electrons in the outer core region (see Fig. TT-2 left panel).

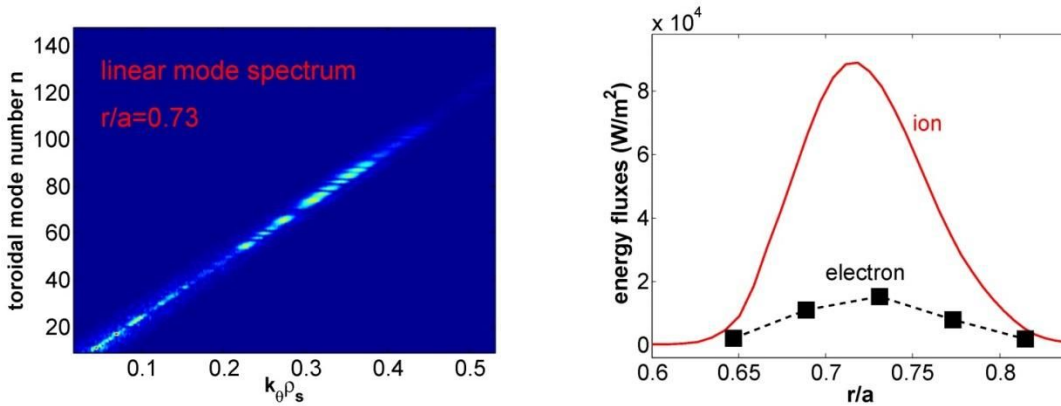


**Figure TT-2:** Left panel: linear mode spectrum shows both ITG ( $k_\theta \rho_s \sim 0.2 - 0.4$ ) and DTEM ( $k_\theta \rho_s < 0.2$ ) are unstable near  $r/a=0.73$  in this L-mode discharge (left); Right panel: simulated ion and electron energy flux produced the ITG and DTEM turbulence.

In a project jointly supported by NSTX-U and other funds, a new orbit-modulated *reduced* transport formulation is developed to extend our first principles understanding of the edge radial electric field. Careful construction of the model demonstrates that, in steady state, ion orbit excursions (including orbit losses) can only indirectly affect the radial electric field by modulating the effects of transport and sources. Further, the formulation allows for truly self-consistent calculations of the effects of the ion orbit excursions, including their interactions with turbulence, collisions, impurities, and neutrals. The formulation will be applied to NSTX and NSTX-U data, in order to investigate the dominant processes determining the edge radial electric field at low aspect ratio.

### Diagnostic And Related Developments

Velocimetric algorithms and codes are being developed, which are applicable for gas-puff-imaging (GPI) and beam-emission spectroscopy (BES) data from NSTX-U. The algorithms infer velocities by comparing adjacent frames of GPI or BES movies and inverting a continuity equation. The original routines enforced a divergence-free 2D velocity in the perpendicular plane. They have been error-checked and are being documented in two upcoming publications before being made publicly available for use in the community. A new algorithm has been developed and implemented in which 2D flow divergence is allowed but penalized. The new algorithm has advantages in dealing with incompatible data and alternate boundary conditions. As an example, Fig. TT-3 shows a velocity field obtained with the new optical-flow velocimetry algorithm using GPI diagnostic data.

### Collaboration Activities

Calculations have been carried out to determine scattering location, volume length (along the laser beam), and wavenumbers for a coherent CO<sub>2</sub> scattering diagnostic system on HL-2A located at Southwestern Institute of Physics in Chengdu, China. The coherent CO<sub>2</sub> scattering diagnostic system on HL-2A uses a tangential scattering scheme where the probe beam is launched in the mid-plane with a tangential radius of 155 cm and two reference beams are also launched in the mid-plane at an angle of  $2.9 \times 10^{-3}$  and  $6.1 \times 10^{-3}$  radians, respectively, with respect to the probe beam (these angles also set scattering angles). Two detectors mixing the reference beam and scattered light provide scattering measurements. Drift wave turbulence anisotropy with respect to local magnetic field was taken into account in calculations

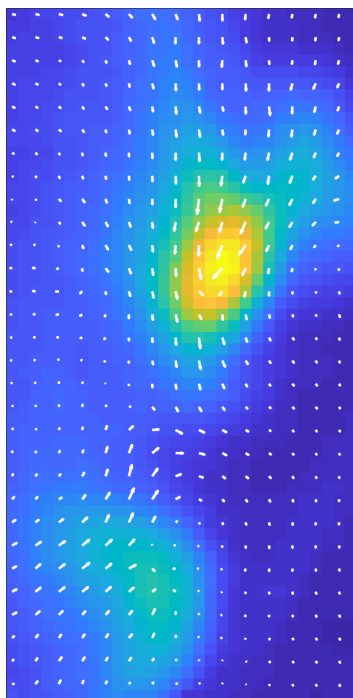


**Figure TT-3:** Results of new optical-flow velocimetry algorithm, using a soft penalty for velocity divergence. GPI emission, roughly proportional to electron density, is indicated in a false-color scheme (yellow is high density, blue is low density). White arrows indicate the magnitude and direction of the inferred velocity. The GPI frame straddles the separatrix at the outboard midplane. It is oriented almost perpendicular to the field, with the  $x$ -axis approximately radial and the  $y$ -axis approximately binormal, meaning perpendicular to the magnetic field but within the flux surface.

of scattering location, volume, and wavenumbers with magnetic geometry from equilibrium reconstruction of HL-2A plasmas. Calculations show that the scattering locations for both reference beams are at the tangential radius, i.e., scattering happening on the high-field side of the plasma. The scattering channel with the  $2.9 \times 10^{-3}$  radian scattering angle (i.e. channel 1) has a  $k_r$  of  $15 \text{ cm}^{-1}$  and a  $k_\theta$  of  $7 \text{ cm}^{-1}$  with an effective scattering volume length of 3.5 cm, and the scattering channel with the  $6.1 \times 10^{-3}$  radian scattering angle (i.e. channel 2) has a  $k_r$  of  $32 \text{ cm}^{-1}$  and a  $k_\theta$  of  $14.6 \text{ cm}^{-1}$  with an effective scattering volume length of 1.6 cm. These calculations show that the tangential scattering scheme of the coherent  $\text{CO}_2$  scattering diagnostic system on HL-2A leads to excellent, radially localized scattering measurements of the wavenumber spectrum of drift-wave density fluctuations.

## Energetic Particles

Energetic particle research on NSTX-U has focused in FY-19 on two main areas: namely (i) understanding the physics of instabilities near the ion-cyclotron range of frequency, and (ii) develop and validate reduced models for fast ion transport by several classes of instabilities. In addition to work on Alfvénic instabilities (AEs), the latter topic has been extended in FY-19 to

include the effects on fast ion transport of low-frequency instabilities such as sawteeth, fishbones and neoclassical tearing modes (NTMs); see separate summary of Milestone R19-4 activities. Collaborative work has progressed with colleagues from DIII-D and MAST-U.

### Study Of High-frequency Instabilities In The Ion-cyclotron Frequency Range

Magnetic fluctuations in the ion-cyclotron frequency range are commonly observed in NSTX and NSTX-U plasmas. In many respects, the fluctuations appear similar to the ion cyclotron emission (ICE) seen in conventional tokamaks, in which ICE appears as a sequence of narrow frequency peaks at harmonics of the edge ion cyclotron frequency of super-thermal ions. However, a complete theoretical understanding of ICE is still lacking. Improved theoretical understanding is necessary to use ICE as a diagnostic of confined fast ions. Measurements of ICE on spherical tokamaks, with lower magnetic field and similar beam energies to those on higher field tokamaks, provide data from a new parameter regime to test theoretical models for ICE.

A significant difference between previous observations of ICE and the ICE on NSTX is that the frequency of ICE in NSTX and NSTX-U corresponds to the ion cyclotron frequency deeper in the plasma, near the location of an internal transport barrier. (See Fig. EP-1 [EP-1]). Measurements of the emission with a toroidal array of fast probes show that the emission is a long wavelength, with a spatially coherent mode. The emission frequency does not follow an Alfvénic scaling with density as seen for compressional AEs, but does show a linear scaling with local magnetic field strength. The measured emission shows a compressional polarization consistent with a compressional Alfvén wave. No correlation between the neutron rate and the ICE amplitude is seen. Future dedicated experiments and diagnostic improvements will provide further clarification of ICE characteristics, as required to develop a comprehensive theoretical understanding of ICE for its use as a fast ion diagnostic tool in fusion reactors.

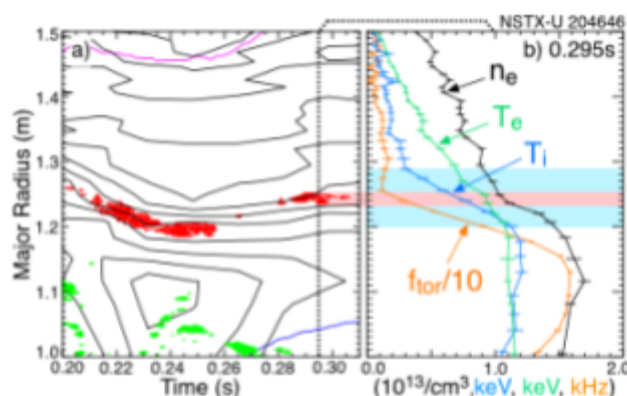


**Fig. EP-1:** (a) ICE spectrogram mapped to the major radius (red) overlaid on density contours (black), (b) magnetic fluctuation spectrum mapped to the major radius (red), electron density (black), and ion temperature (blue) profiles at 0.298 s. (From [EP-1]).

At sub- $f_{ci}$  frequencies, Compressional and Global Alfvénic modes have been correlated with decreased plasma heating efficiency, supposedly due to enhanced thermal electron transport [EP-2]. A remarkable result from the NSTX-U experimental campaign in FY2016 is that those instabilities can be completely suppressed by additional NBI from the second, more tangential NBI lines [EP-3], thus potentially enabling improved performance for future NSTX-U operations.

Work has continued in FY2019 to understand the mechanisms for CAE/GAE suppression. Three-dimensional nonlinear simulations through the HYM code show a robust physical stabilizing mechanism, via modest off-axis beam injection, in excellent agreement with experimental observations cf. Fig. EP-2 [EP-4]. HYM simulations of NSTX-U discharges have been performed to study the excitation and stabilization of GAEs in the NSTX-U right before and shortly after the additional off-axis NB injection. Before the additional beam injection, the simulations show unstable counter-rotating GAEs with toroidal mode numbers and frequencies that closely match the experimentally observed modes. Additional off-axis beam injection has been modelled by adding beam ions with pitch  $\sim 1$ , and by varying the NB ion density. The complete stabilization occurs at less than 7% of the total beam ion inventory. A new analytic theory of GAE stability [EP-5] has also been derived, suggesting a different interpretation for GAE stabilization mechanism compared to previous publications [EP-6].

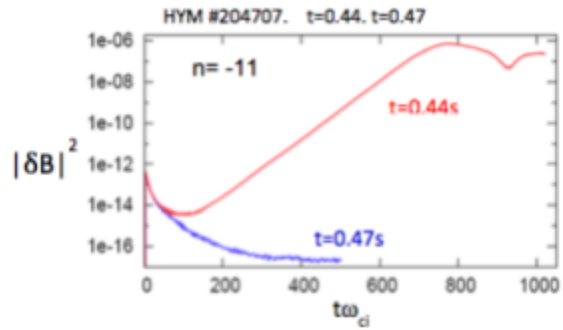


**Fig. EP-2:** Time evolution of  $n=-11$  GAE magnetic energy from linear phase to saturation for  $t=0.44$ s NSTX parameters (red), and decay of initial perturbation for stable case corresponding to  $t=0.47$ s with additional off-axis beam injection (blue). (From [EP-4]).

#### Development, Verification, And Validation of Reduced Models For Energetic Particle Transport

One of the main ongoing activities of the NSTX-U EP Topical Science Group is to develop and validate reduced models for fast ion transport by different types of instabilities. As in past years, the approach is to combine results and insight from experimental analysis with code development, verification, and validation, thus leveraging the close collaboration with the Theory Group at PPPL. Transport models are targeting different types of instabilities that, according to experiments on NSTX/NSTX-U and other devices, are mostly responsible for enhanced fast ion transport in constant of motion space: (i) Alfvénic modes in the TAE range of frequency associated with energy and radial transport, and (ii) lower-frequency modes such as sawteeth, fishbones and NTMs primarily resulting in radial fast ion transport.

The estimate of reliable bounds for the nonlinear instability and saturation amplitude of Alfvénic waves in the TAE frequency range is an outstanding issue for reliable projections of the performance of fusion devices. An analytical expression for nonlinear wave evolution in the presence of scattering has been derived [EP-7], which provides a rapid means for prediction and interpretation of experimental data and for the verification of numerical codes. Neglecting resonance overlap, the nonlinear dynamics of a wave near marginal stability follows from a time-delayed, integro-differential cubic equation that includes diffusive processes, e.g.,

associated with scattering from classical collisions as well as from background turbulence [EP-8]. Scattering is the dominant effect due to collisions assumed to be much larger than the nonlinear bounce frequency near the resonance. An asymptotic expression for the AE amplitude was found. The solution can recover trends observed in magnetic fluctuation data from NSTX, such as for the saturation amplitude and characteristic evolution time scales of TAE/RSAE modes.

Besides the time-averaged saturation amplitude, complex behavior of Alfvénic modes is often observed in tokamak discharges. Rapid frequency changes, referred to as *chirps*, occur at fast time scales much shorter than the typical time for changes in the equilibrium (milliseconds vs tens of milliseconds for typical NSTX/NSTX-U plasmas). Aside from being an interesting test of the capability of numerical simulation, the existence of chirping can significantly modify high energy particle distributions and be a signature of non-linear regimes possibly culminating in large “avalanches,” which cause enhanced fast ion redistribution and loss of a large fraction of the confined fast ions. Chirping of Alfvénic modes has been reproduced with the guiding center code ORBIT [EP-9]. The shape of the frequency sidebands from the simulations agrees with theory [EP-9] and with experimental observations. From this study, it appears that there must be strong mode damping along with significant drive for mode chirping to occur. Results suggest that chirping is caused when small changes in the equilibrium bring a saturated Alfvén mode in contact with the Alfvén continuum and suddenly experience strong damping. From parameter scans in the simulations, collisions inhibit chirping by destroying the coherence of the particle distribution around the dominant wave-particle resonances. The required collision rates to inhibit chirping agrees with earlier analytical theory [EP-10].

Building on the improved understanding of AE dynamics with strong fast ion drive for realistic experimental conditions, work is also in progress to develop a heuristic Predator-Prey model to interpret the dynamics of *multiple* Alfvén eigenmodes instabilities excited simultaneously by energetic beam ions [EP-11]. In the model, two systems, each consisting of a predator (AEs) and a prey (resonant NB ions), are coupled together. The first system works as a source of particles for the second system, which in its turn plays the role of a sink for those particles. The model is expected to help understanding the interplay of three time scales as observed in the Resonance Broadened Quasi-linear (RBQ) code simulations. (See Fig. EP-3.)

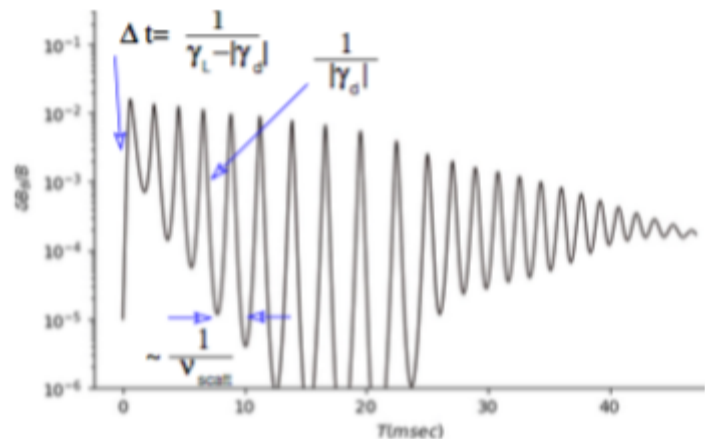


**Fig. EP-3:** Intermittent amplitude of a single  $n=5$  RSAE showing interplay between drive, damping rate and pitch angle scattering. (From [EP-11]).

In collaboration with MAST-U and York University, a different approach has also been explored in FY-18 and FY-19 to interpret experimental NSTX/NSTX-U data and inform on the parameter space where instabilities are expected to exist [EP-12], with possible applications for real-time AE control, mitigation, and suppression. A machine learning algorithm is used to speed up the process of characterizing the behavior of magnetic perturbations from corresponding frequency spectrograms, which is typically performed by humans. The analysis reveals a rich set of correlations between different mode characters (such as quiescent, fixed-frequency, chirping, avalanching instabilities) and weighted averages of plasma parameters obtained from TRANSP (such as  $v_{inj}/v_{Alfvén}$ , q-profile,  $\beta_{inj}/\beta_{Alfvén}$ ). These results yield similar correlations to previous work (see [EP-13]), detailing correlation between parameters of a specific NSTX discharge and mode character.

#### Development Of Reduced Models For Energetic Particle Transport In Integrated Simulations

The improved physics understanding achieved through ongoing theoretical and numerical work is used to advance the Quasi-Linear RBQ model for fast ion transport by instabilities. The RBQ-1D model has undergone thorough verification against known analytical solutions for fast ion transport [EP-14]. Over the last year, the model was improved to allow the simultaneous evolution of AE amplitudes with overlapping resonances to the level that self-consistent amplitudes are computed. This capability allowed to make predictive simulations for future devices.

Several analytic, theory-based verification exercises confirmed the validity of results from the RBQ model based on DIII-D test scenarios. They include the amplitude dependence on the scattering rate, nonlinear EP dynamics near the resonance island, and the nonlinear amplitude saturation. A major arbitrariness in earlier formulations of resonance broadening quasilinear theory [EP-15] is regarding what should be the shape of the resonance functions (i.e., the form of the diffusion coefficient envelope that surrounds the resonances). A first-principle method has been recently developed [EP-16] to analytically determine the collisional resonance broadening function in quasilinear theory where discrete resonances are excited without any mode overlap. The proposed methodology allows for realism and self-consistency in the modeling and is currently being implemented into the RBQ code. It has been demonstrated that a quasilinear system that employs the calculated broadening functions systematically recovers the nonlinear growth rate and mode saturation levels for near - threshold plasmas previously calculated from nonlinear kinetic theory.

A second approach for reduced modeling of fast ion transport in TRANSP, the so-called “kick model,” has also benefited from the improved physics understanding of Alfvénic instabilities. In general, interpretive simulations of NSTX/NSTX-U and DIII-D scenarios can recover experimental data from a variety of fast ion and fluctuation diagnostics [EP-17]. However, as for RBQ-1D, the next step is to enable and validate quantitative *predictive* simulations to guide future experiments and optimize scenarios. To this end, the additional physics elements that emerge from detailed theoretical and numerical studies guide further improvements to the

model, e.g., to include a self-consistent, time dependent computation of the mode amplitude evolution in the TRANSP simulations.

To enable rapid tests of new approaches for reduced fast ion transport models and their integration with TRANSP, a procedure has been developed to use the stand-alone version of the NUBEAM module. The set of scripts allows to test the evolution of the energetic particle population, based on the comprehensive physics already contained in NUBEAM, and by adding a closed loop with new models that mimic a time-dependent evolution of instabilities.

The improved numerical tools for integrated simulations, including the effects of instabilities on the fast ion evolution, have been extensively used for collaborative work with DIII-D colleagues over FY19. Activities included analysis of the onset of chirping AE activity in DIII-D plasmas and interpretive/predictive simulations of the effects of the new off-axis NB system recently developed on DIII-D. More details can be found in the FY19 Report from the ITER & Tokamaks department.

#### Extension Of Fast Ion Transport Models To Low-Frequency MHD

Besides the work on understanding and modeling the interaction of Alfvénic instabilities on energetic particles, significant progress has been made in FY19 in collaboration with DIII-D and MAST-U to extend modeling tools to lower-frequency instabilities such as NTMs, sawteeth, kink and fishbones. A short description of the main achievements is given below. A more extensive report can be found in the summary of the R19-4 Milestone activities.

In collaboration with DIII-D, interaction of NTMs with NB ions was extensively studied in FY19 [EP-18], building on initial promising results for interpretive analysis to assess the effects of NTMs on fast ion transport [EP-19]. The analysis has been performed through the kick model in TRANSP, with input provided by the ORBIT code based on either ad-hoc or analytical expressions for the NTM-induced perturbation [EP-18]. Overall, simulations can recover experimental results in terms of neutron rate deficit (Fig. EP-4) and main features of the perturbed fast ion distribution, thus suggesting that the reduced model approach is a viable path for future predictive simulations through integrated modeling with TRANSP. Work has begun to extend the analysis of fast ions

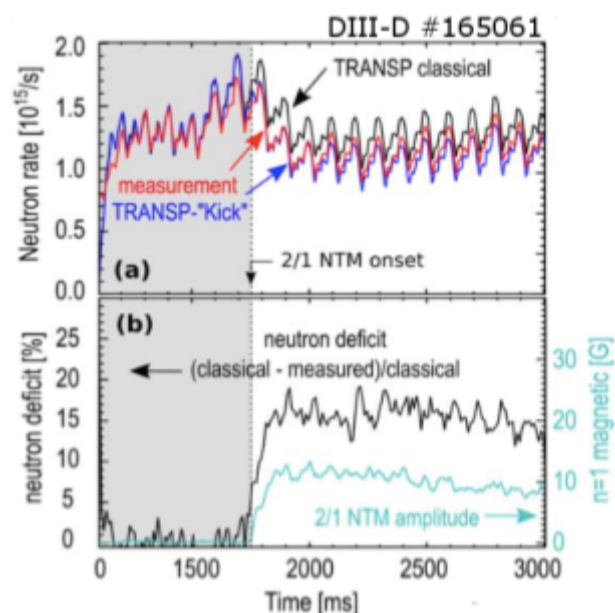


**Fig. EP-4:** (Top) Neutron rate from classical TRANSP simulations compared to experimental measurements and TRANSP + kick model simulations including redistribution of fast ions by NTM. (Bottom) Neutron deficit and NTM amplitude. (From [EP-18]).

by NTMs to NSTX/NSTX-U scenarios, with the overall goal of improving NTM stability predictions and NTM effects on plasma transport in TRANSP simulations [EP-20].

In parallel with NTM studies, the kick model approach has also been tested for kink, fishbone and sawtooth instabilities [EP-21, EP-22, EP-23]. In all cases, an analytical 1/1 perturbation is assumed to be the dominant cause of enhanced fast ion transport. So far, NSTX/NSTX-U scenarios have been used for the model validation work [EP-17]. Work has started in collaboration with MAST-U colleagues and collaborators to extend the analysis to MAST scenarios [EP-24]. Initial results will be presented at the 2019 IAEA Technical Meeting on Energetic Particles [EP-25]. The overall goal is to develop a general framework to handle the effects of low-frequency MHD perturbations in integrated simulations, possibly complemented by approaches such as RBQ to handle Alfvénic instabilities in an efficient way for long-time-scale simulation.

### CAE/GAE Stability

A new analytic theory has been developed to investigate the stability properties of CAEs and GAEs driven by realistic neutral beam distributions [EP-26]. Consequently, a new instability regime is discovered that was not considered by previous authors who implicitly assumed  $v_{||,res} \ll v_0$ , whereas this condition is not usually satisfied in experiments. The new instability regime was found to be responsible for the excitation and stabilization of GAEs in early NSTX-U experiments, which could not be fully described by previous theories [EP-4]. In contrast to previous work, our theory demonstrates that it is possible to destabilize modes with any value of  $k_{\perp} \rho_b$ , not just those restricted to a certain range. When the beam distribution is sufficiently wide in velocity space, such as present in NSTX(-U) experiments, approximate marginal stability conditions have been derived which have an excellent agreement with the numerically integrated expressions for fast ion drive/damping. Qualitatively, these conditions demonstrate that counter-propagating modes are preferentially driven by perpendicularly injected beams (small  $v_{||}/v_0$ ) and damped by tangential injection. The opposite is true for co-propagating modes (typically CAEs in experiments): they are driven by more tangential injection and damped by perpendicular beams. With these insights, the analytic theory can make quantitative predictions for CAE/GAE excitation and stabilization with different beam mixes. Cross-comparison of the derived analytic stability boundaries, hybrid simulation results, and NSTX observations across many discharges shows better than 80% agreement with theory

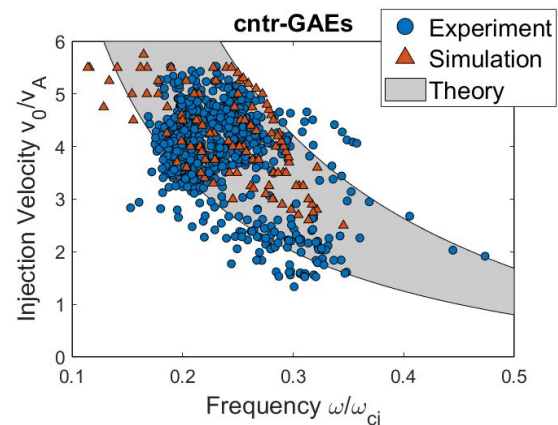


**Fig. EP-5:** Comparison of cntr-GAE instabilities between analytic theory, HYM simulations (red triangles), and NSTX experiments (blue circles). Analytic theory predicts net fast ion drive in the shaded region between the two curves (From [EP-26]).

for counter-CAEs and co-GAEs (Fig. EP-5, above). Lastly, the effect of coupling between the compressional (CAE) and shear (GAE) modes due to two-fluid effects has been considered. For counter-CAEs, the coupling leads to the largest growth rate occurring with  $k_{\parallel}/k_{\perp} \sim 1$ , instead of  $k_{\perp} = 0$  in the zero coupling limit, suggesting that a two-fluid description of the thermal plasma may be important in order to accurately model counter-CAEs.

## References:

- [EP-1] E. D. Fredrickson, et al., Phys. Plasmas **26** (2019) 032111.
- [EP-2] D. Stutman, et al., Phys. Rev. Lett. **112** (2009) 115002.
- [EP-3] E. D. Fredrickson, et al., Phys. Rev. Lett. **118** (2017) 265001.
- [EP-4] E. Belova, et al., Phys. Plasmas (submitted, 2019).
- [EP-5] J. Lestz, et al., Phys. Plasmas (submitted, 2019).
- [EP-6] E. D. Fredrickson, et al., Nucl. Fusion **58** (2018) 082022.
- [EP-7] V. N. Duarte and N. N. Gorelenkov, Nucl. Fusion **59** (2019) 044003.
- [EP-8] V. N. Duarte, et al., Nucl. Fusion **57** (2017) 054001.
- [EP-9] R. B. White, et al., Phys. Plasmas (submitted, 2019).
- [EP-10] H. L. Berk, et al., Phys. Rev. Lett. **76** (1996) 1256.
- [EP-11] N. N. Gorelenkov, et al., “*Predator-prey paradigm for Alfvén instability dynamics in realistic RBQ simulations*,” to be presented at the 16th IAEA-TCM on Energetic Particles in Magnetic Confinement Systems, Shizuoka City - Japan (September 3-6, 2019).
- [EP-12] B. J. Q. Woods, et al., “*Machine-learning driven correlation studies between Alfvénic and sub-Alfvénic chirping and fast ion loss at NSTX*”, IEEE Transactions on Plasma Science (submitted, 2019).
- [EP-13] E. D. Fredrickson, et al., Nucl. Fusion **54** (2014) 093007.
- [EP-14] N. N. Gorelenkov, et al., Phys. Plasmas **26** (2019) 072507.
- [EP-15] H. L. Berk, et al., Nucl. Fusion **35** (1995) 1661.
- [EP-16] V. N. Duarte, et al., Phys. Rev. Letters, preprint arXiv:1906.01780 (submitted, 2019).
- [EP-17] M. Podestà, et al., Nucl. Fusion (in press, 2019).  
<https://doi.org/10.1088/1741-4326/ab3112>
- [EP-18] L. Bardoczi, et al., Plasma Phys. Control. Fusion **61** (2019) 055012.
- [EP-19] W. W. Heidbrink, et al., Nucl. Fusion **58** (2018) 082027.
- [EP-20] J.-H. Yang, et al., “*Characterization Of Tearing Modes On NSTX*”, to be presented at the 61<sup>st</sup> APS-DPP Meeting, Fort Lauderdale FL (October 21-25, 2019).
- [EP-21] D. Liu, et al., Nucl. Fusion **58** (2018) 082028.
- [EP-22] D. Kim, et al., Nucl. Fusion **58** (2018) 082029.
- [EP-23] D. Kim, et al., Nucl. Fusion **59** (2019) 086007.
- [EP-24] M. Cecconello, et al., Plasma Phys. Control. Fusion **57** (2015) 014006.
- [EP-25] M. Cecconello, et al., “*Analysis of TAEs and FBs induced fast ion redistribution and losses in MAST using a reduced fast ion transport model*,” to be presented at the 16th IAEA-TCM on Energetic Particles in Magnetic Confinement Systems, Shizuoka City - Japan (September 3-6, 2019).

[EP-26] J. Lestz, et al., "Analytic stability boundaries for compressional and global Alfvén eigenmodes driven by fast ions. I. Interaction via ordinary and anomalous cyclotron resonances" and "Analytic stability boundaries for compressional and global Alfvén eigenmodes driven by fast ions. II. Interaction via Landau resonance." Both to be submitted to Phys. Plasmas (2019).

## Macrostability

### Assessment Of Error Field Effects Due To Coil Misalignments In NSTX-U: Physics Requirements On Error Field Corrections and Monte-Carlo Analyses

A small misalignment of primary magnets can induce significant degradations and thus should be either mechanically adjusted or compensated by additional error field correction (EFC) coils. The efforts to predict resonant and non-resonant error field effects have been continued jointly between the NSTX-U research and recovery teams to assess physics requirements (PRs) of coils and EFC capabilities in NSTX-U. The predictions of resonant & non-resonant EF effects have been performed with IPEC and M3D-C1 simulations, with the following PRs updated and finalized from 2018;

(PR1) Full IPEC  $\delta B_{21}$  EF should be reduced to  $<0.95G$  in L-mode.

(PR2) Full IPEC  $\delta B_{21}$  EF should be  $<3G$  in H-mode.

(PR3) TF EF NTV should be reduced to  $<1.2Nm$

(PR4) The resonant M3D-C1  $\delta B_{21}$  fields should be correctable with  $\sim 0.6kA$  EFC coil currents.

As described in the annual NSTX-U 2018 report, PR1-2 are based on the parametric scaling of EF tolerance against locked modes which is still an active area of research as will be briefly introduced by the next section, and PR3 is based on the estimated torque by NSTX-U NBIs.

The Monte-Carlo analyses were then performed over the PF4U, PF4L, PF5U, PF5L shifts in pancakes and coils and also tilts relative to inner-TF coils, ignoring other PF misalignments which produce an order-of-magnitude less EF effect. IPEC and M3D-C1 codes were used first to estimate the resonant and non-resonant EF effects from the individual unit shift and tilt (mm and mrad, respectively) and then linearly or non-linearly combined through the Monte-Carlo analyses. A set of PF4/5/TF coil tolerances have been successfully determined then, with the shifts  $<8mm$  and the tilts  $<1.1mrad$  depending on the individual shift or tilt. Fig. MS-1 shows the examples of the Monte-Carlo analysis for (a) IPEC-NTV to test non-resonant EF effects against PR3 and (b) M3D-C1 to test resonant EF effects against PR4, on

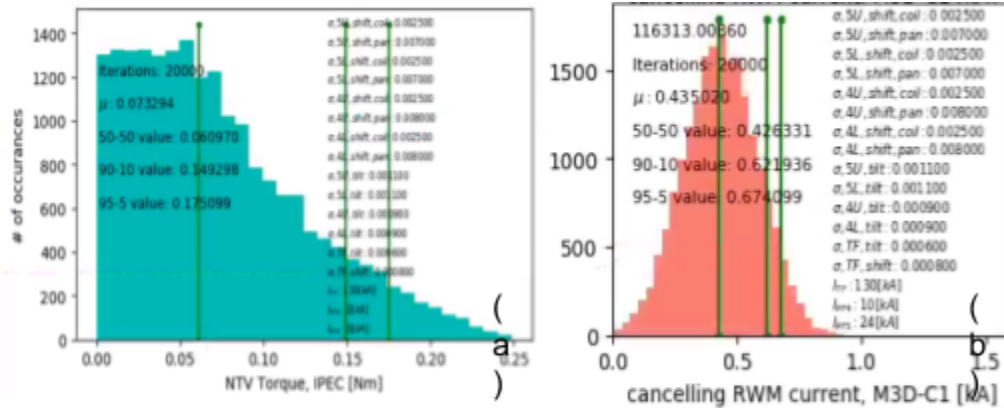


**Fig MS-1:** Monte-Carlo analyses over the combinations of PF4/5/TF coil shifts and tilts, for (a) non-resonant EF effects and (b) resonant EF effects. Three vertical (green) lines indicate (a) IPEC- NTV and (b) M3D-C1 dB21 values with 50%, 90%, 95% probabilities.

NSTX-U target plasmas with full performance with 2MA and 1T. One can see that (a) NTV  $\ll$  1.2Nm and (b) dB21  $\sim$  0.6kA, by 95% over the possible combinations of PF4/5/TF shifts and tilts under the coil tolerances, meeting PR3-4 and also other PRs and other engineering requirements. The full details on the methods of the calculations and assessments for each requirement can be found in [MS-1].

Study Of Multi-Mode Characteristics Of Error fields using M3D-C1

During the 2016 NSTX-U experimental campaign, locked modes in the plasma edge presented clear evidence of the presence of error fields. Extensive metrology and plasma response modeling with IPEC and M3D-C1 have been conducted to understand the various sources of error fields in NSTX-U as built in 2016, and to determine which of these sources have the greatest effect on the plasma. In particular, modeling finds that the error field from misalignment of the toroidal field (TF) coils may have a significant effect on the plasma. The response to the TF error field was shown to depend on the presence of a  $q = 1$  surface, in qualitative agreement with experimental observations. It was found that certain characteristics of the TF error field present new challenges for error field correction. Specifically, the error field spectrum differs significantly from that of coils on the low-field side (such as the NSTX-U error field correction coils), and does not resonate strongly with the dominant kink mode, thus potentially requiring a multi-mode correction. Furthermore, to mitigate heat fluxes using poloidal flux expansion, the pitch angle at the divertor plates must be small ( $\sim 1^\circ$ ). Using perturbed equilibrium calculations together with analysis from TRIP3D, the potentially significant local perturbation to the pitch angle from uncorrected error fields was quantified as shown in Fig. MS-2. Estimates for coil alignment tolerances in NSTX-U were derived based on consideration of both heat flux and core resonant fields independently. These estimates have been used to inform the allowable tolerances in the NSTX-U recovery project [MS-2, below].

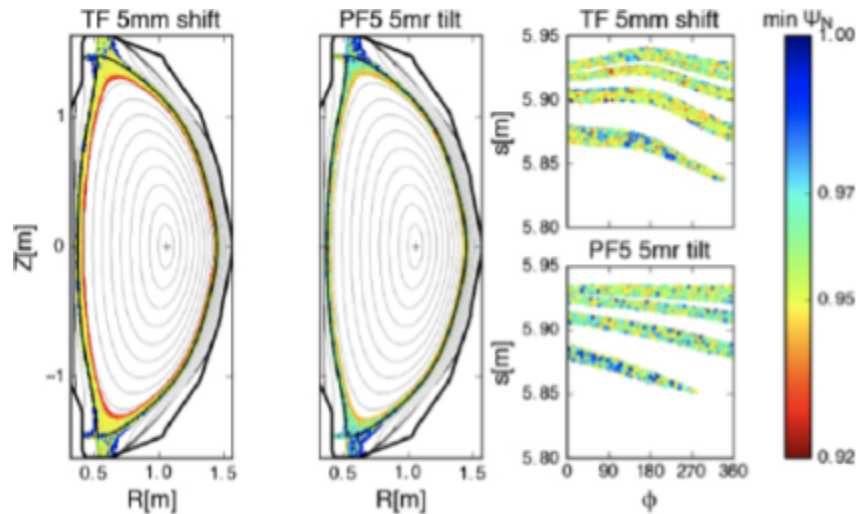


**Fig. MS-2:** Poincaré plots (left) and lower horizontal divertor footprints (right) of the magnetic field lines that hit the wall due to a 5 mm shift of the TF center rod and a 5 mrad tilt of the PF5L coil. The colours represent the minimum normalized poloidal flux reached by each field line, which serves as a proxy for the field line temperature.

Machine Learning Approaches To Predict The Ideal MHD Stability Properties

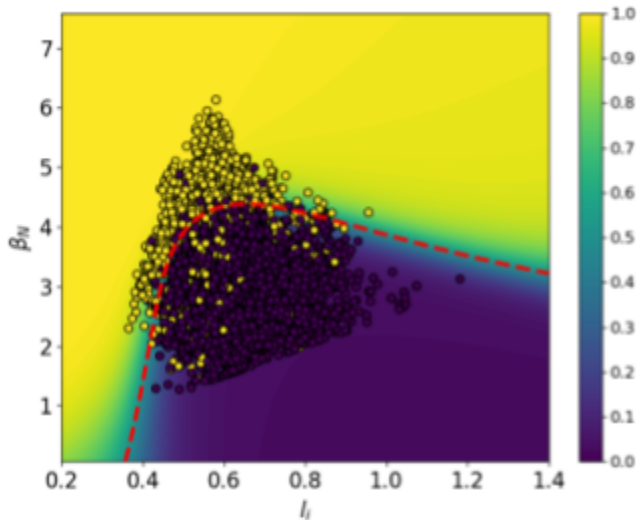


**Fig. MS-3:**  $\beta_N$  vs.  $I_i$  decision boundary. Yellow points indicate ideal unstable DCON calculated NSTX equilibria, while purple are stable. The contour colors indicate the probability distribution predicted by the neural network, with the red dashed line indicating the decision boundary (output probability = 0.5).

One of the biggest challenges in achieving the goal of producing fusion energy in tokamak devices is avoidance or mitigation of plasma current disruptions due to instabilities. In order to analyze these disruptions, the Disruption Event Characterization and Forecasting (DECAF) framework has been developed, integrating physics models of several causal events that can lead to a disruption. Two different machine learning approaches have been proposed to improve the ideal magnetohydrodynamic (MHD) no-wall limit component of the full kinetic stability model included in DECAF. First, a multilayer perceptron neural network has been trained on sets of calculations with the DCON code, to obtain a closed form equation of the no-wall limit as a function of relevant plasma parameters, assuming each one having the same

impact on the ideal stability. This approach led to an increase in classification performance (for example, see Fig. MS-3, above), but at the cost of a lower predictive capability when trying to reproduce the DCON computed change in plasma potential energy without wall effects,  $\delta W^{n=1}_{no-wall}$ . Therefore, a second, less interpretable yet more powerful algorithm, the Random Forest Regressor, was adopted to predict the actual value of  $\delta W^{n=1}_{no-wall}$ . When trained on a large database of equilibria from the National Spherical Torus Experiment (NSTX), the Random Forest can significantly improve the prediction performance as well as the classification of stable/unstable points. Furthermore, this tree-based method provides an analysis of the contribution of each input feature, showing that the plasma parameters that most affect the estimated value of  $\delta W^{n=1}_{no-wall}$  are the ones expected by the underlying physics, namely  $\beta_N$ , internal inductance, and pressure peaking.

Applications Of Resistive DCON To Compact Toroidal Device In General Fusion

Many novel fusion concepts are in the Magnetized Target Fusion (MTF) regime and propose to use compact toroid plasma targets, in some cases heating the plasma to fusion conditions via compression. Compression is attractive for heating because of the high power that can be delivered and because compression can be achieved through a liquid metal blanket, as in the General Fusion concept [MS-3].

In order to assess the stability issues, CORSICA has been used to generate equilibria inside each geometry under the assumptions of adiabatic compression and a constant q profile. For each equilibrium, the linear ideal and resistive MHD stability is evaluated with Resistive DCON (RDCON). Fig. MS-4 is a map that shows multiple possible compressions in parameter space

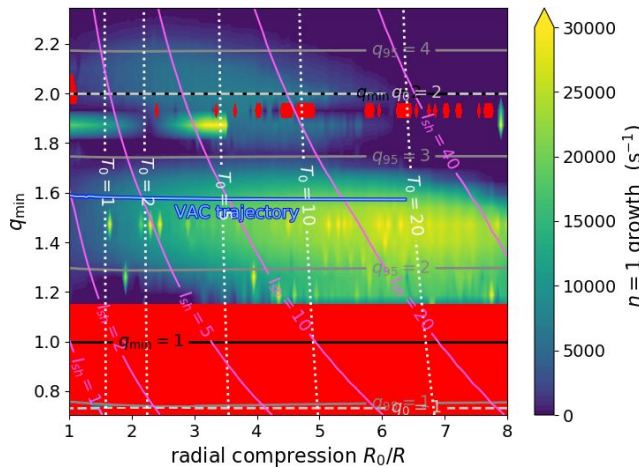


**Fig. MS-4:** Tearing stability map for compact toroid device in General Fusion predicted by resistive DCON.

as horizontal curves. An example compression trajectory from the MHD code VAC is overlaid in blue. Ideal unstable regions are shown in red, while teal/yellow regions indicate the degree of resistive MHD stability. Points on the safety factor profile:  $q_0$ ,  $q_{min}$ , and  $q_{95}$ , are shown as horizontal lines. The current in MA running poloidally through the central shaft is shown as magenta contours. Electron temperature recorded in keV at the magnetic axis is shown as nearly vertical dotted lines. Many of the regions in parameter space which are ideal MHD stable exhibit resistive instability before maximum compression is reached. However, some narrow pathways remain that permit a stable plasma to be fully compressed.

---

### Progress With The Electromagnetic Particle Injector (EPI)

The shattered pellet injector now being considered for ITER uses the MGI valve to propel the frozen pellet. This will limit its velocity to only about 200-300 m/s, and because it will be located many meters away from the plasma, its response time is further slowed. The penetration depth of the shattered fragments into ITER grade plasmas is unknown. The Electromagnetic Particle Injector (EPI), on the other hand, has the potential for delivering the radiative payload inside ITER's  $q = 2$  surface on a  $<6$  ms time scale, which is much faster and deeper than what can be achieved using present methods. To address this important issue, a novel system based on the rail-gun concept was designed, and an initial test system fully assembled and tested.

The EPI system accelerates a sabot containing the radiative payload. The sabot is a metallic capsule that can be accelerated to high velocity by an electromagnetic impeller. At the end of its acceleration, within 2 ms, the sabot will release a radiative payload of a known velocity and distribution. This sabot design offers a flexibility of carrying a variety of payload which for example can be granules of low-Z material, or tungsten dust, or shell pellet containing smaller pellets or noble gas. In the EPI method, a radiative payload consisting of microspheres of Be, BN or B, or other acceptable low-Z materials or high-Z impurities such as W would be injected to the plasma center for thermal and runaway electron mitigation. The radiative payload would be accelerated to the required velocities ( $\sim 500$  m/s for present tokamaks - 1 km/s or higher for ITER) by the EPI system.

Experimental tests on a prototype system have been able to verify the primary advantages of the EPI concept. These are the rapid response time and the capability to attain the required high projected speeds on this fast time scale. Initial experimental tests from a prototype system (EPI-1) have demonstrated the acceleration of a 3.2 g sabot to over 150 m/s within 1.5 ms, consistent with the calculations, giving confidence that larger ITER-scale injector can be developed [MS-4], as highlighted by the Nuclear Fusion journal.

Following these successful experiments, a new upgraded system (EPI-2) has been designed for 3 T external field augmentation to improve overall system efficiency. Recent results from the operation of this system at 1.3 T (limited by power supply) has extended the attainable velocities to 300 m/s during the same 1.5 ms acceleration phase using a power supply that is 60% of the size used in the earlier EPI-1 experiments that attained 150 m/s. In addition, the basic aspects of radiative payload separation from the sabot, and sabot capture has been tested at a velocity of 160 m/s (limited by present power supplies). In addition, the concept can be extended to over 2 km/s. M3D-C1 simulations to assess the payload velocity and size requirements to achieve an inside to out controlled thermal quench in NSTX-U are in progress.

#### **References:**

[MS-1] S. Gerhardt, et al., "Physics Calculations Supporting Alignment Requirements for the PF-4, PF-5, and TF Coils", PPPL Report NSTXU\_11232\_CALC\_100 (2017).  
<https://drive.google.com/open?id=1vt9mdIYEDILTGzrEyeBKSII7v0GNQTdz>

[MS-2] N. Ferraro, et al., Nucl. Fusion 59, 086021 (2019).

[MS-3] M. Laberge, et al., IEEE 25<sup>th</sup> Symposium on Fusion Engineering (SOFE), pp.1-7 (2013).

[MS-4] Raman, et al., Nucl. Fusion **59**, 016021(2019).

<http://iopscience.iop.org/article/10.1088/1741-4326/aaf192/pdf>

## Integrated Scenarios

### Solenoid-Free Startup and Ramp-Up

#### Coaxial Helicity Injection (CHI)

In support of CHI development for NSTX-U and future STs, employment of non-inductive plasma start-up techniques would considerably simplify the design of a spherical tokamak fusion reactor. Transient coaxial helicity injection (CHI) is a promising method, expected to scale favorably to next-step reactors. The implications, however, of reactor-relevant parameters on the initial breakdown phase for CHI have not yet been considered. During the past year, we evaluated CHI breakdown in reactor-like configurations using an extension of the Townsend avalanche theory. We found that a CHI electrode concept in which the outer vessel wall is biased to achieve breakdown, while previously successful on NSTX and HIT-II, may exhibit a severe weakness when scaled up to a reactor. On the other hand, concepts which employ localized biasing electrodes such as those used in QUEST and URANIA would avoid this issue. Assuming that breakdown can be successfully attained, we then applied scaling relationships to predict plasma parameters attainable in the transient CHI discharge. Assuming the use of 1Wb of injector flux, we found that plasma currents of 1 MA should be achievable. Furthermore, these plasmas are expected to ohmically self-heat with more than 1MW of power as they decay, facilitating efficient hand-off to steady-state heating sources. These optimistic scalings are supported by Tokamak Simulation Code (TSC) simulations. Results from TSC simulations are shown in Figure SF-1, which shows that the generated closed flux plasma current increases in proportion to the injected current as indicated by simple scaling relations and that at high levels of injected flux the CHI plasma can significantly self-heat to very high temperatures [SF-1].

In support of full non-inductive start-up and ramp-up studies, we have designed a double biased electrode configuration with optimized injector coil locations for a high-field test on the URANIA ST, at the University of Wisconsin. This is awaiting the completion of high toroidal field design for URANIA, after which the CHI design will be finalized. In support of power supplies for the CHI studies on URANIA, we have finished experimental testing of an electrolytic capacitor-based power supply module with SCR switching at the full 2 kV planned for the first studies on URANIA. Assembly of the full power supply is now in progress.

---

*Three-Dimensional Plasmoid-Mediated Reconnection And The Effect Of Toroidal Guide Field In Simulations Of Coaxial Helicity Injection*

The research team investigated the physics of three-dimensional plasmoid-mediated magnetic reconnection during transient Coaxial Helicity Injection (CHI) plasma start-up using nonlinear MHD simulations in a spherical tokamak [SF-2]. We numerically i) examined the role of three-dimensional magnetic reconnection arising from current-sheet instabilities on the formation of plasmoid-mediated closed flux surfaces, and ii) examined the effect of toroidal guide field on the MHD stability during transient CHI. Consistent with NSTX experiments, we found that even in the presence of non-axisymmetric edge magnetic fluctuations, current-carrying axisymmetric ( $n=0$ ) plasmoids are rapidly formed while twisted open field lines are being injected, and are merged to form a large current-carrying magnetic bubble for plasma startup in a tokamak.

As shown in Fig. SF-2, two types of current sheets are formed during helicity injection. A primary inner current sheet in the injection region, which is responsible for global 2-D plasmoid reconnection and formation of closed flux region. As the poloidal field vanishes in the injection region (reconnection site), this primary inner current sheet can become unstable to 2-D  $n=0$  plasmoid instability and break into magnetic islands (plasmoids) as shown in Fig. SF-2b. A secondary outer current sheet due to accumulation of flux in the edge region can also form as flux expands. This outer current sheet, however, can be unstable to 3-D current-sheet instabilities, i.e. the non-axisymmetric ( $n \neq 0$ ) reconnecting current-driven instability.

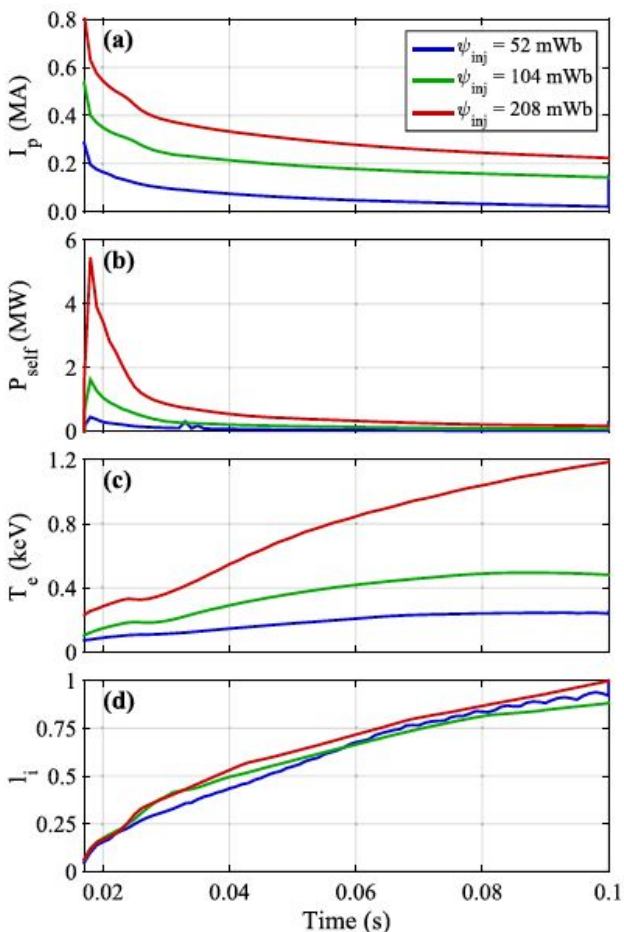


**Figure SF-1:** Time traces of the CHI generated plasma current, the self-heating power, the intrinsic CHI plasma electron temperature and the normalized internal plasma inductance as the CHI injector flux is increased from 52 mWb (NSTX best case) to four times this value (208 mWb). At high injector flux, the self-heating power due to Ohmic decay rapidly increases to more than 4 MW, and the electron temperature increases to over 1 keV. The normalized plasma internal inductance is less than 0.6 during the initial plasma start-up phase. Reactors would inject on the order of 1 to 2 Wb of flux and would employ additional heating and current drive sources to maintain the normalized internal inductance in the range of 0.4 to 0.7, while ramping the current up to the levels required for sustained operation.

A large volume of closed flux surfaces is formed during the decay phase (Fig. SF-2c). The enclosed current density during the decay phase at  $t = 9.37$  ms is shown in Fig. SF-2c. Poloidal flux within the last closed flux surface is 45 mWb, which is about 65-70% of the injector flux. It is therefore found that even in the presence of 3-D fluctuations during the injection phase, in transient CHI a large volume of closed flux surfaces still is feasible as the fluctuations also decay in the decay phase. The poloidal cut of current density showing a closed current supported by an X-point formation remains at an equilibrium state during the decay phase (Fig. SF-2c).

We also find that the 3-D physics response is drastically different for simulations at higher toroidal field and complete stabilization of non-axisymmetric fluctuations were achieved at higher toroidal flux. As next-step ST devices will operate at both higher toroidal flux and injector poloidal flux, three-dimensional MHD simulations are critical and essential for prediction and accessibility to these regimes of maximum start-up in larger STs, such as ST-FNSF (Fusion Nuclear Science Facility). Our 3-D simulations presented here show the promising results that transient CHI, a leading technique for non-inductive startup current-drive technique in spherical tokamaks, could be scalable to higher poloidal injector flux as well as toroidal flux.

In summary, in transient CHI, it is shown that 3-D perturbations arising from neighboring outer edge  $n \neq 0$  current-sheet instabilities, if present, could contribute to an enhancement of global magnetic reconnection for formation of current-carrying axisymmetric ( $n=0$ ) plasmoids and to ultimate merging to a large current-carrying magnetic bubble for plasma startup in a tokamak.

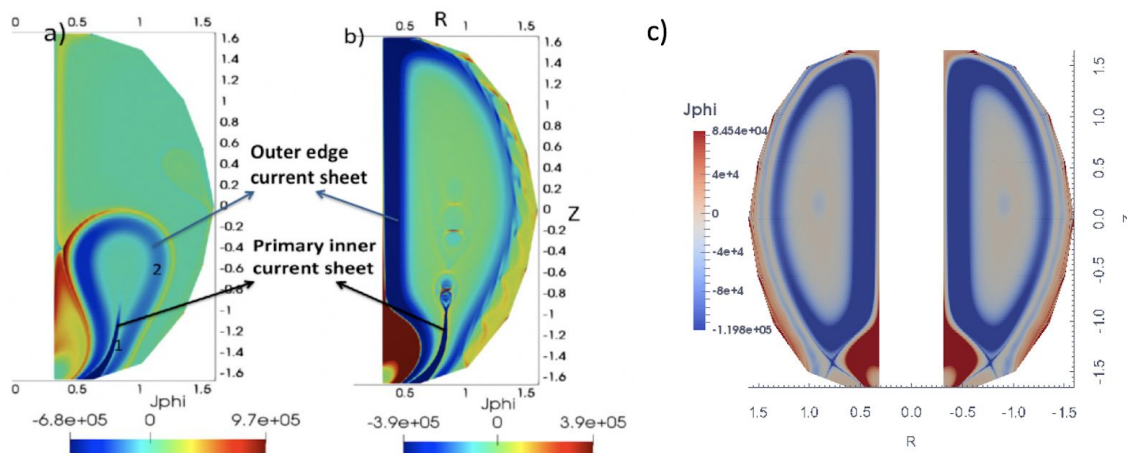


**Figure SF-2:** 3-D simulations: Time-evolving current sheets during flux expansion 1) primary inner current sheet, where reconnecting  $n=0$  plasmoids form 2) outer edge current sheet, where non-axisymmetric edge magnetic fluctuations could excite. Poloidal  $R$ - $Z$  cut of total toroidal current density,  $J[A/m^2]$  a) during early expansion at  $t=6.6ms$  b) at  $t=8.7ms$ , c) during the decay at  $t=9.37ms$ .

### QUEST-NSTX-U Collaboration

The QUEST Device in Kyushu University, Japan is the largest ST facility in Japan. It aims to explore solenoid-free start-up and fully non-inductive steady-state operations at relatively high plasma beta.

An area in which the implementation of CHI on QUEST is different from that on NSTX is that the Poloidal Field (PF) coils that are needed for equilibrium control are much farther away from the CHI electrodes, and the power supplies that operate these coils have slower current slew rates than the ones on NSTX. In addition, the toroidal field capability of QUEST (0.25 T) is much lower than that on NSTX. Both these factors have made it more difficult to properly shape the injector flux into a narrow flux foot print condition that is necessary for forcing reconnection to occur in the injector region.

During 2019, experiments were conducted in two different configurations aimed at elongating and moving the plasma column towards the Center Stack. In both configurations, toroidal current persistence was seen after the injector current was reduced to zero, but the CHI discharge appeared to be not yet fully detached from the electrode plate. Results from these

studies were used to improve the Power Supply-PF coil combinations for an experiment that aimed at biasing the high voltage electrode plate with respect to the inboard Center Stack. This new configuration could further reduce the injector flux footprint width leading to an easier detachment of the CHI plasma from the electrode plate. In addition, this configuration utilizes higher toroidal field region for CHI which could result in a higher current amplification factor and possibly higher toroidal current. Initial experiments in this inboard configuration were able to successfully generate CHI discharges using only the gas used for ECH and without any additional gas injection from the CHI system. An addition of simple flat insulating plates considerably reduced absorber arcing, allowing the discharge to grow and fill the vessel. For the first time, much smaller injector currents in the range of 7kA were able to grow the plasma (similar to that in NSTX) resulting in three times higher current multiplication. Some additional improvements to the insulator configuration for further suppressing absorber arcs are being considered. The generation of 45 kA of toroidal current from the operation of a new reactor-relevant transient CHI electrode configuration that should be easier for implementation in reactor configurations is described in [SF-3].

#### References:

- [SF-1] K.C. Hammond, R. Raman, and S.C. Jardin, *Physics of Plasmas* **26**, 032501 (2019).  
<https://doi.org/10.1063/1.5087259>
- [SF-2] F. Ebrahimi, Accepted for publication in *Physics of Plasmas* (2019).
- [SF-3] K. Kuroda, R. Raman, et al., *Plasma Physics and Controlled Fusion* **60** (2018) 115001.

## Wave Heating and Current Drive

### Modeling Of High Harmonic Fast Wave Scenarios For NSTX Upgrade [WCD-1]

The NSTX-Upgrade will operate with toroidal magnetic fields ( $B_T$ ) up to 1 T, nearly twice the value used in the experiments on NSTX, and the available neutral beam injection (NBI) power will be doubled. The doubling of  $B_T$  while retaining the 30 MHz RF source frequency has moved the heating regime from the high harmonic fast wave (HHFW) regime used in NSTX to the mid harmonic fast wave regime. By making use of the full wave code AORSA (assuming a Maxwellian plasma) [WCD-2], we have explored different HHFW scenarios for two possible antenna frequencies (30 and 60 MHz) and with and without NBI. Both frequencies have large electron absorption for a large wave toroidal number particularly without NBI (see Figure WCD-1a). With the presence of NBI, the fast ions absorption can be dominant in some scenarios (see Figure WCD-1b). Therefore, a competition between electron and fast ion absorption is clearly apparent, partially explaining why in previous NSTX HHFW experiments, a

less efficient electron heating was observed. Moreover, at the toroidal field of 1 T, a direct thermal ion damping might be possible under the condition when the ion temperature is larger than electron temperature. In general, the electron and ion absorption are found very sensitive to the ratio of electron and ion temperature. The impact of the hydrogen species is also studied, showing that for hydrogen concentration below 2%, the hydrogen absorption is not significant (see Figure WCD-2). However, a larger hydrogen concentration could open up new HHFW heating scenarios in NSTX-U particularly without NBI (see Figure WCD-2b). Launching at a high toroidal wave number appears to be one way to significantly reduce the ion damping and in turn to obtain large electron damping in the core, which can play an important role in the transport studies for NSTX-U. Finally, a higher magnetic field could also play a role in increasing the electron temperature and consequently the electron absorption.

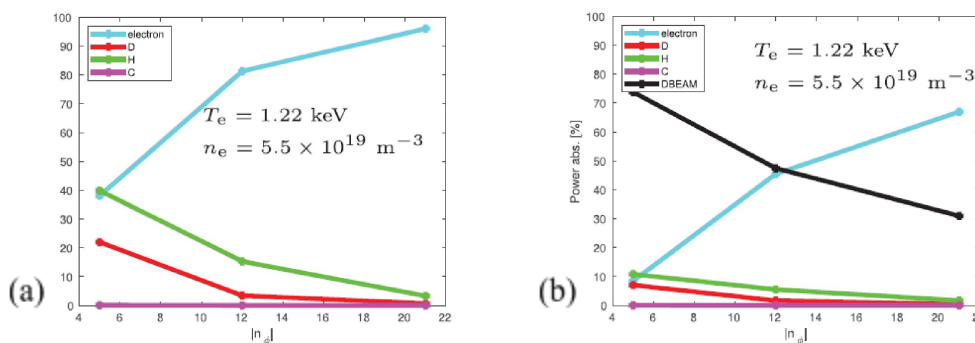


**Figure WCD-1:** Absorption of electrons, thermal deuterium (D), thermal hydrogen (H), thermal carbon (C), and fast ions (Dbeam) as a function of the toroidal mode number  $|n_\phi|$  assuming 2% H concentration for NSTX-U plasma. The left figure does not include a fast ions population whereas the right figure fast ions are present. Black curves represent fast ion absorption, green curves represent H absorption, red curves represent thermal D absorption, and magenta curves represent C absorption. The temperature and the density values are shown in each panel.

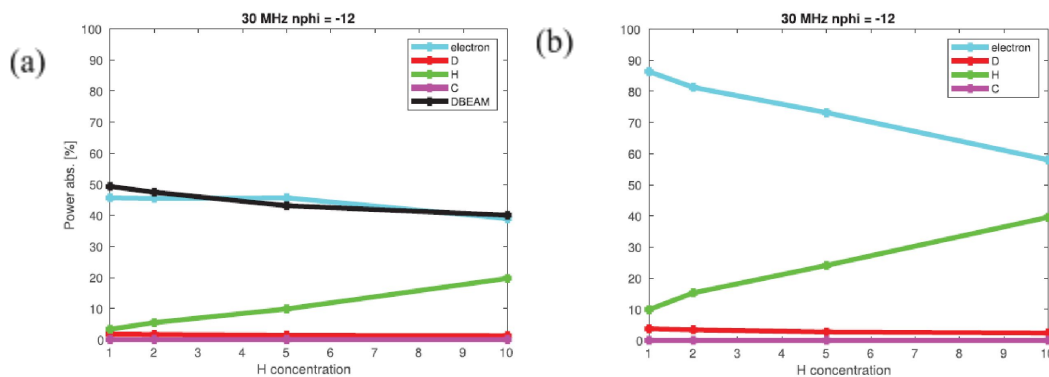


**Figure WCD-2:** Absorption of electrons, thermal deuterium (D), thermal hydrogen (H), thermal carbon (C), and fast ions ( $D_{beam}$ ) as a function of the H concentration (1, 2, 5, and 10%) for NSTX-U plasma assuming  $f = 30$  MHz and  $n_\phi = -12$ . Left figure includes a fast ions population whereas in the right figure fast ions are not present. Black curves represent fast ion absorption, green curves represent H absorption, red curves represent thermal D absorption, and magenta curves represent C absorption (which is basically negligible).

## Effect Of Wall Boundary On The Scrape-Off Layer Losses Of High Harmonic Fast Wave In NSTX And NSTX-U [WCD-3]

We have performed numerical simulations of high harmonic fast waves (HHFWs) in the scrape-off-layer (SOL) of the National Spherical Torus Experiment (NSTX)/NSTX-U using a recently developed 2D full wave code [WCD-4, WCD-5]. We have shown that a realistic NSTX SOL boundary can significantly affect HHFW propagation and power losses in the SOL (see Figure WCD-3a). In NSTX SOL boundaries, HHFW is easily localized near the antenna and propagates less to the SOL, and thus, less power is lost to the SOL (see Figure WCD-3b). We have also showed that the lower SOL power losses occur when the SOL volume is smaller and the distance between the last closed flux surface and the antenna is shorter. We have investigated the effect of electron density in front of the antenna and the ambient magnetic field strengths on the SOL power losses as well. Showing consistency with the experiments [WCD-6], SOL losses are minimized when the SOL density is near the critical density where the fast wave cutoff is open, and the plasma is strongly magnetized.

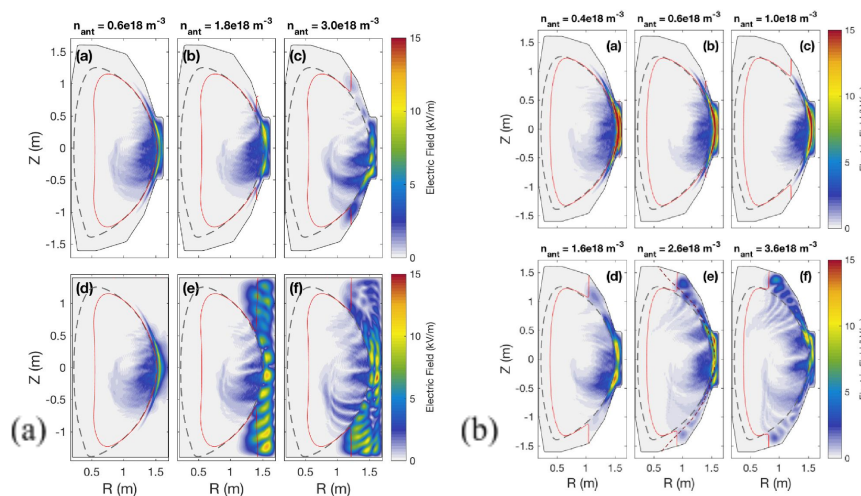


**Figure WCD-3:** (a) Total electric field amplitude by adopting (a)–(c) NSTX boundary and (d)–(f) rectangular boundaries for  $n_{\text{phi}} = -21$ . (b) Total electric field amplitude by For  $n_{\text{phi}} = -12$  in the NSTX boundaries.

## 3D Full Wave Fast Wave Modeling With Realistic Antenna Geometry And SOL Plasma For NSTX-U [WCD-7]

In a fusion device powered significantly by RF, the loss of RF power in the SOL can be a real PMI issue for possible RF sheaths and plasma facing component damage. Indeed, many experiments in different fast wave (FW) heating regimes such as hydrogen minority heating and HHFW have found strong interactions between RF waves and the SOL region. A significant interaction between FW and energetic ions generated by NBI also plays an important role in the current experiments. Commonly, RF simulations in the plasma core are neglecting the SOL plasma and they compute the RF field in a 2D domain assuming one single toroidal wave

number. State-of-the-art RF SOL/antenna simulation is yet limited to a relatively small volume in front of the antenna, and it involves significant physics simplification such as stratifying antenna strap structure and/or treating the antenna front volume as vacuum. The PPPL team (in collaboration with the RF SciDAC team) examined the full 3D device geometry, including realistic antenna geometry. This was in order to capture the 3D effects and the antenna-plasma interaction in the SOL plasma and, at the same time, the core wave propagation. We used an open source, Petra-M code [WCD-8], and performed 3D full wave simulations in the HHFW regime in NSTX-U. A scan of the antenna phasing shows a strong interaction between FWs and the SOL plasma for lower antenna phasing, which is consistent with previous NSTX HHFW observations (see Figure WCD-4). Furthermore, the first attempt to evaluate the effect of the 3D wave field on the fast ion population from NBI beams in NSTX-U was done by using the 3D field obtained from the Petra-M simulations in the SPIRAL full-orbit following particle code [WCD-9].

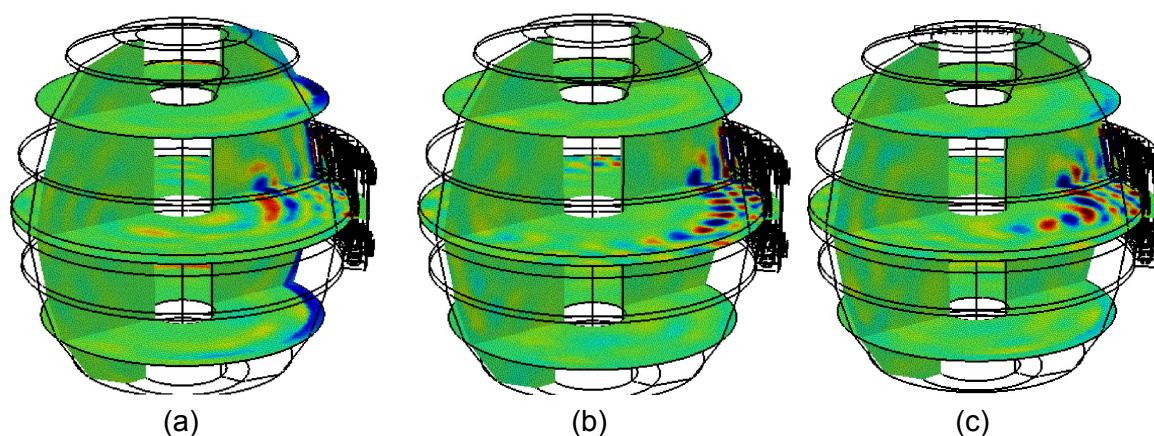


**Figure WCD-4:**  $E_z$  component of the wave electric field evaluated by Petra-M for the full 3D NSTX-U torus including the HHFW antenna and three different antenna phasing:  $30^\circ$  (a),  $90^\circ$  (b),  $150^\circ$  (c).

## Modeling Of 2nd Harmonic Electron Cyclotron Heating And Current Drive Solenoid-free Start-up Experiment In QUEST [WCD-10, WCD-11]

The QUEST ECH solenoid-free start-up experiment utilizing the 28 GHz gyrotron at 2<sup>nd</sup> harmonic frequency has demonstrated remarkable efficiency and achieved record start-up current values [WCD-12] (see Figure WCD-5). The experiment provides rich opportunities to understand and optimize ECH-based tokamak/ST current start-up and ramp-up concept. Another potentially noteworthy aspect of the QUEST 28 GHz experiment is its very high frequency to toroidal magnetic field ratio, which is 28 GHz/0.25T or 112 GHz/1T. The higher frequency enables higher density limit and for reactors with several Tesla toroidal field, this start-up scenario can largely avoid the usual density limit often encountered by ECCD.

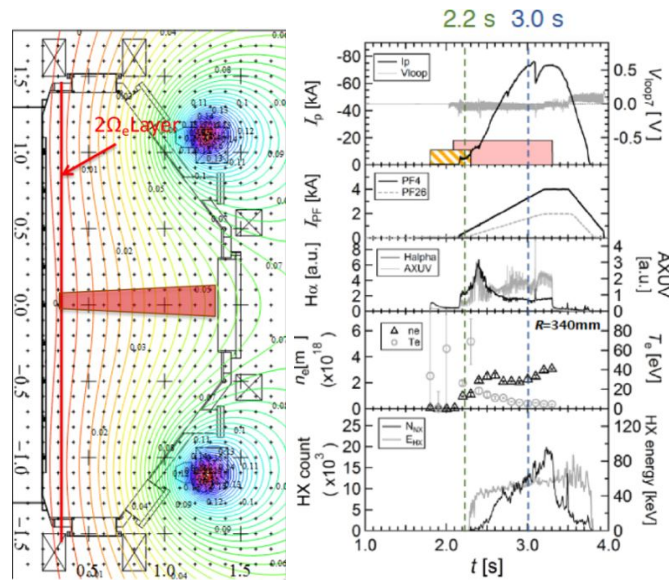


**Figure WCD-5:** The QUEST 2nd Harmonic ECH solenoid-free start-up. (a) Experimental set up. (b) Time evolution of various parameters as labeled.

Conversely, this higher harmonic scenario would enable utilization of ECH at lower magnetic field as in the case of many ST experiments. This scenario may also be attractive for the ECH assisted start up for the initial phase of ITER, where the toroidal magnetic field maybe relatively low  $\sim 2$  T. To better understand the QUEST experimental results, we initiated a modeling effort at PPPL. Improved modeling should also help develop better predictive capability for future ST and tokamak-based reactors. An ST/tokamak start-up modeling is a highly coupled non-linear problem as the magnetic field topology evolves dramatically from an open vacuum field configuration to a closed configuration. The plasma temperature evolves from a very cold collisional regime to a very hot collisionless regime. For this task, we developed a grid-based start-up code where plasma parameters, generated plasma currents, and resulting poloidal magnetic fields are evolved from the vacuum fields [WCD-10, WCD-11]. Initially, 2nd harmonic electron cyclotron heating takes place with multi-pass ECH absorption as the single-pass absorption is relatively small at low temperature. The current generated in this stage is purely pressure-driven since the launched wave phase and polarization information is likely lost quickly. The grad-B drift driven current together with the precessional currents can then create a closed flux surface configuration and then the bootstrap current in a closed configuration can further enhance the plasma current. The ECH heating efficiency increases with plasma current since the confinement is increased, and the resulting electron temperature rise would further increase the ECH absorption and plasma currents. Once the plasma temperature becomes sufficiently high ( $\sim 1$  keV), a single-pass absorption can rise sufficiently to transition to the ECCD phase. The entire start-up process is, therefore, a self-amplifying non-linear problem where a very rapid spontaneous plasma current rise (e.g., “current jump”) can be expected. See Figure WCD-6 for the entire start-up process.

An important point to note is that two-component distribution (hot minority and colder bulk) is highly advantageous for hot electrons to be generated for efficient ECCD, as observed in the QUEST start-up experiment. The analysis showed that the QUEST experiment was able to generate energetic electrons by heating small hot component  $\sim 3\%$  to minimize the collisional drag. Once heated to  $\sim 10$  keV, the hot component could be sustained even with the subsequent density rise to  $3\text{-}4 \times 10^{12}\text{cm}^{-3}$ .

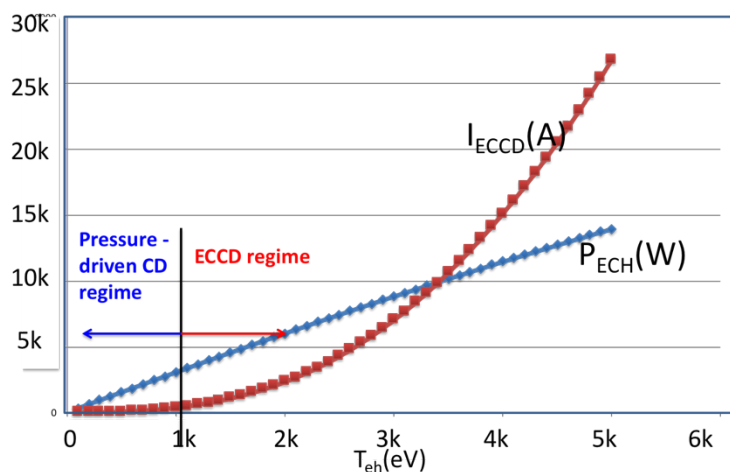


**Fig. WCD-6:** 2<sup>nd</sup> Harmonic ECH and ECCD as a function of hot electron temperature.

#### References:

- [WCD-1] N. Bertelli, et al., 2019 *Nucl. Fusion* **59** 086006.
- [WCD-2] E.F. Jaeger, et al., 2001 *Phys. Plasmas* **8** 1573.
- [WCD-3] E.-H. Kim, et al., 2019 *Phys. Plasmas* **26** 062501.
- [WCD-4] E.-H. Kim, et al., 2015 *Geophys. Res. Lett.* **42** 5147.
- [WCD-5] E.-H. Kim and J. R. Johnson 2016 *Geophys. Res. Lett.* **43** 13.
- [WCD-6] J. C. Hosea, et al. 2008 *Phys. Plasmas* **15** 056104.
- [WCD-7] N. Bertelli, invited talk at the 23rd Topical Conference on Radiofrequency Power in Plasmas (Hefei, China, May 14-17, 2019). Proceeding submitted to AIP Conf. Proc. (2019).
- [WCD-8] S. Shiraiwa, et al., 2017 *EPJ Web of Conferences* **157** 03048.
- [WCD-9] G. J. Kramer, et al., 2013 *Plasma Phys. Control. Fusion* **55** 025013.
- [WCD-10] M. Ono, et al., 2018 60th APS-DPP (Portland, OR)  
<http://meetings.aps.org/link/BAPS.2018.DPP.TP11.93>
- [WCD-11] M. Ono, et al., submitted to AIP Conf. Proc. (2019).
- [WCD-12] H. Idei, T. Onchi, T. Kariya, et al., EX/P3-21, IAEA 2018.

## Advanced Scenarios and Control

### Reduced Model For Direct Induction Startup Scenario Development On MAST-U And NSTX-U

A reduced semi-empirical model using a time-dependent axisymmetric vacuum field solver was used in FY19 to develop the prefill and feed-forward coil current targets required for reliable direct induction (DI) startup on MAST-U and NSTX-U [ASC-1]. The calculations are constrained by operational limits unique to each device, such as the geometry of the conductive elements and active coils, power supply specifications, and coil heating and stress limits. The calculations are also constrained by semi-empirical models for sufficient breakdown, current drive, equilibrium and stability of the plasma developed from a shared database.

A large database of DI startup on NSTX and NSTX-U is leveraged to quantify the requirements for achieving a reliable breakdown ( $I_p \sim 20$  kA). It is observed that without pre-ionization, STs access the large E/P regime at modest loop voltage ( $V_{loop}$ ), where the electrons in the weakly ionized plasma are continually accelerating along the open field lines. This ensures a rapid (order millisecond) breakdown of the neutral gas even without pre-ionization or high-quality field nulls. Figure ASC-1 illustrates the good agreement between the observed and simulated timing of the breakdown using a unique discharge on NSTX where the breakdown occurs nine milliseconds after the application of loop voltage. The vertical magnetic field ( $B_z$ ) measured on the inboard of NSTX is shown in Figure ASC-1a. The applied external  $B_z$  is decreasing while the plasma generates positive  $B_z$ . The vertical line corresponds to the approximate  $B_z$  generated by 3 kA of plasma current. The bottom two panels show calculations of the electron density (panel b) and  $I_p$  (panel c) using different model assumptions. The discharge did not have any ECH pre-ionization (PI), thus the red traces represent the most applicable predictive model. The timing of  $I_p = 3$  kA (horizontal dotted line on panel c) in the model is in good agreement with the inferred timing from panel a. The development of a reduced model for the timing of the plasma breakdown contributes to a time-dependent simulation framework for optimizing the startup scenario on MAST-U and NSTX-U (see R19-2 milestone).

The reduced model also reproduces the timescale of the initial increase in  $I_p$  on NSTX. This is shown in figure ASC-2, where the dependence of the shortest time period required to increase the plasma current from 3 to 20 kA ( $t_{br}$ ) on prefill pressure (point color) and average applied electric field (x-axis) is reproduced by the semi-empirical model (solid lines).

Most discharges that fail in the startup phase in tokamaks are due to an inconsistency in the evolution of the plasma current ( $I_p$ ) and equilibrium field or loss of vertical stability during the burn-through phase. The requirements for the self-consistent evolution of the fields following breakdown ( $I_p > 20$  kA) are derived from demonstrated DI startup on NSTX, NSTX-U, and MAST (see figure R19-2-1 in R19-2 milestone). Predictive calculations for breakdown and the

start of  $I_p$  ramp-up completed for MAST-U and NSTX-U illustrate that the maximum  $I_p$  ramp rate ( $dI_p/dt$ ) in the early startup phase is limited by the voltage limits on the poloidal field coils on MAST-U and passive vertical stability on NSTX-U [ASC-1].

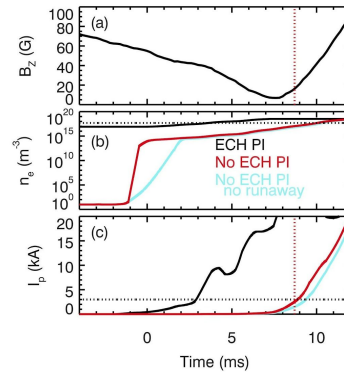


**Fig ASC-1:** (a) Measured  $B_z$  signal on NSTX. Simulated line-averaged plasma density (b) and plasma current (c) using different model assumptions. Red traces correspond to experimental conditions.

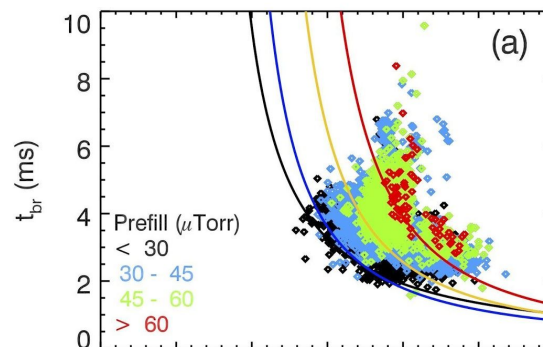


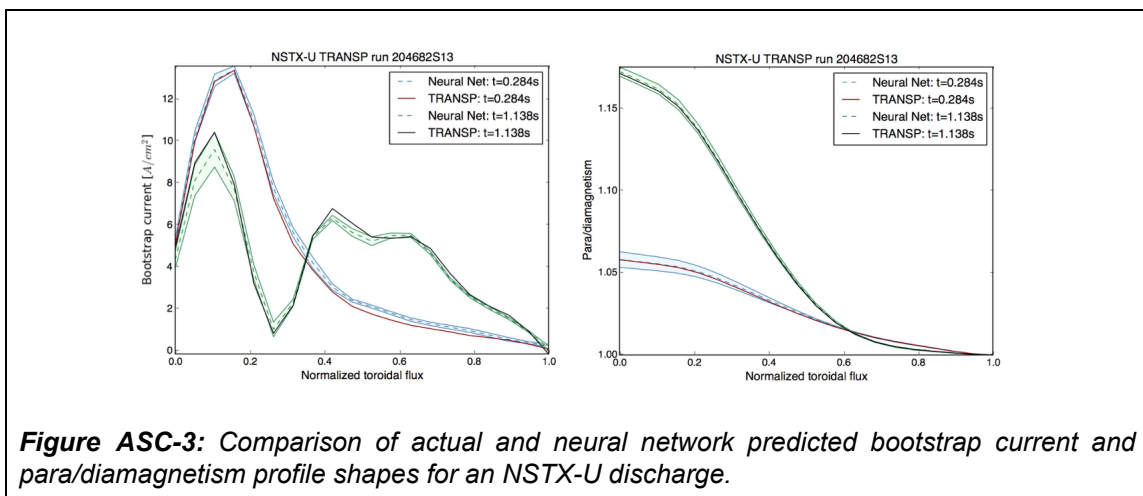
**Fig ASC-2:** Database of startup on NSTX. The time required to increase  $I_p$  from 3 to 20 kA ( $t_{br}$ ) versus the average applied electric field. Colored points indicate range of prefill pressure. Solid lines are a reduced model for the fastest time scale of the  $I_p$  increase for different prefill values: black (10), blue (30), orange (45) and red (60).

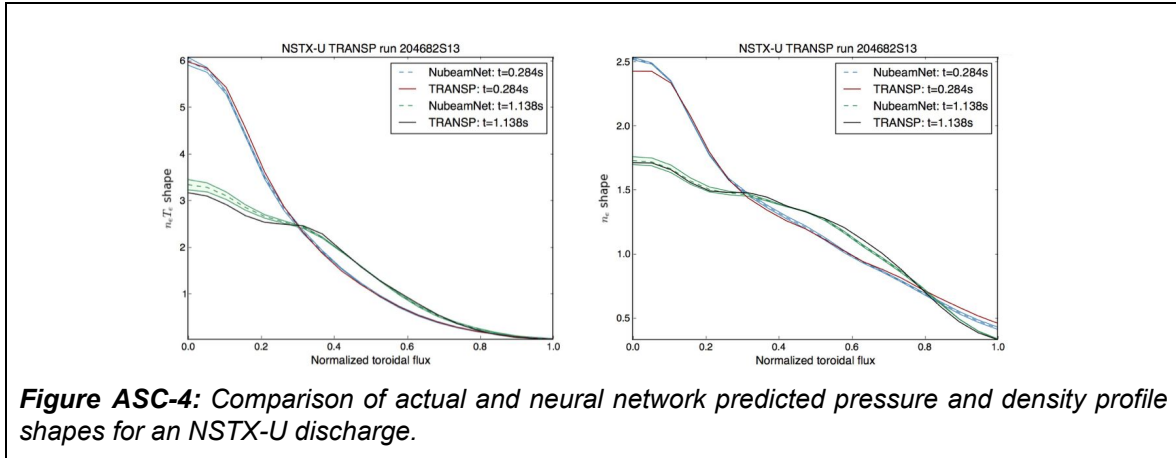
## Reduced Model For Current Profile, Density, Temperature, And Fast Ion Pressure On NSTX-U

A control-oriented modeling approach for magnetic and kinetic profiles in NSTX-U was developed. The approach includes a fast solver for the magnetic diffusion equation, and it makes use of neural network models for geometric parameters, plasma resistivity, bootstrap current, and current drive. The neural network models build on the successful development of an accelerated neutral beam calculation based on a neural network trained on a database of NUBEAM calculations [ASC-2]. The models make use of an ensemble of neural networks, and profile quantities are projected onto empirically derived basis functions to reduce the dimensionality of the data. The neural networks were trained on a database of between-shots

TRANSP runs for the initial NSTX-U run period. Example predictions are compared with expected profiles in Figure ASC-3, showing agreement well-suited for real-time control. While the database is limited, the approach shows promise and can be extended as additional experimental data become available. The use of neural networks improves upon the control-oriented models used in previous efforts [ASC-3, 4], in which geometric quantities were assumed fixed and the resistivity and bootstrap current were assumed to have fixed profile shapes.

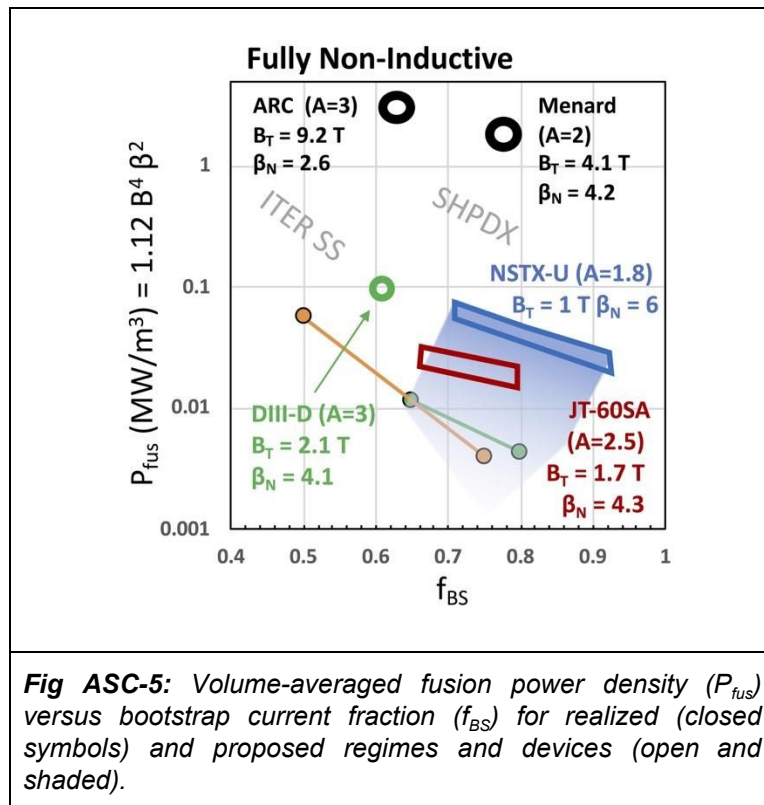
The modeling approach has also been extended to include a reduced model for density and temperature evolution. Since physics-based reduced models do not yet accurately predict the electron temperature and density profiles in NSTX-U, a semi-empirical approach has been taken. A neural network has been trained to predict the profile shapes, while the magnitudes are constrained based on a prescribed Greenwald fraction, a zero-dimensional power balance, assumptions on  $Z_{\text{eff}}$ , impurity species, and the ratio of  $T_e/T_i$ . Example profile shape predictions are shown in Figure ASC-4, and show good agreement with expected values. The combined set of models enables prediction of many of the important quantities needed for scenario development: current profile, ion/electron densities and temperatures, current drive and heating from neutral beams, fast ion pressure, and bootstrap current. The models presently take plasma boundary shaping parameters as input, but the approach will be coupled to the equilibrium response models developed in previous years to enable prediction of equilibrium and profile evolution from beam powers and coil voltages. The profile prediction model presently running in Matlab/Simulink takes only a few seconds to simulate one second of plasma evolution. It is expected that development of a C/C++ version and implementing parallelization will enable faster-than-real-time predictions.





Non-Inductive Scenario Database

Design studies have identified novel, high-field compact fusion pilot plant concepts that operate at large fusion power density ( $P_{fus}$ ) and large bootstrap current fraction ( $f_{BS}$ ). Figure ASC-5 shows the parameters of two such devices with aspect ratio between 2 to 3 (open black circles). A database of non-inductive operating regimes on tokamaks was formed via literature search and input from international experts. Representative non-inductive regimes demonstrated on JT-60U (closed orange circles) and DIII-D (closed green circles) are shown in figure ASC-5. The open symbols show proposed regimes for DIII-D (green), JT-60SA (red) and NSTX-U (blue). The shaded blue region is the approximate operational space that can be explored on NSTX-U. This work motivates the advanced tokamak research program on DIII-D and NSTX-U as an essential part of enabling compact pilot plant systems. This work was completed in preparation for the APS-DPP Community Planning Process.



Use Of TOKSYS In Developing A Shorted-Turn-Protection Algorithm

NSTX-U operated in 2016 with a Digital Coil Protection System designed to prevent operation beyond coil current limits or mechanical stress limits. This system effectively constrains operation to a safe envelope; however, it does not actively detect or respond to electrical faults in coils, leads, and rectifiers. While such events cannot be detected until they are likely terminal for the component involved, it is desirable to have the ability to de-energize the system if such an event is detected to avoid propagating damage to other components through arcing or water leaks. A shorted turn detection algorithm was implemented for the 2016 campaign based on predicted coil current changes in response to voltage commands; however, the algorithm did not account for coupling between coils, the vessel, or the plasma. This necessitated the use of large fault detection thresholds. To improve upon the design, a new algorithm was proposed that makes use of the TOKSYS model of NSTX-U developed by the ASC group to make improved current evolution predictions. A prototype of the fault detection algorithm was implemented in Simulink. Code generation tools were used to generate C++ code from the model, which was then tested for timing and determinism on the NSTX-U real-time computer.

### TRANSP Developments

In addition to the uncertainties in the predictive turbulence models for thermal transport and their assessed limits when applied to low aspect ratio tokamaks, a major limitation for prediction of kinetic profiles during the ramp-up phase is the need for constraining density profile and pedestal parameters. It is therefore concluded that activities in support of ASC modeling should focus on two areas: first, the development of a semi-empirical model for the pedestal height and width based on the existing NSTX and NSTX-U database; second, make the core-edge coupling and the implementation of a two-dimensional model for neutrals a priority for TRANSP development. This is where activities will focus during FY20, with the support of a graduate student from Princeton University.

### **References:**

- [ASC-1] Battaglia, et al., 2019 *Nucl. Fusion* <https://doi.org/10.1088/1741-4326/ab3bd5>
- [ASC-2] M.D. Boyer, et al., 2019 *Nucl. Fusion* **59** 056008.
- [ASC-3] Z. Ilhan, et al., 2019 *Fus. Eng. and Des.* *in press*.
- [ASC-4] M.D. Boyer. et al., 2013 *Plasma Phys. Control. Fusion* **55** 105007.

---

## NSTX-U Publications

### Papers Published by NSTX-U Researchers (Oct. 2018 - Sept. 2019)

1. HASKEY S, Grierson B, Chrystal C, et al.,  
Main Ion And Impurity Edge Profile Evolution Across The L- to H-mode Transition On DIII-D  
PLASMA PHYSICS AND CONTROLLED FUSION **60** 105001 (October 2018).
2. MUNARETTO S, Strait EJ, Wang Z  
Conceptual Design Of Extended Magnetic Probe Set To Improve 3D Field Detection In NSTX-U  
REV. SCI. INST. **89** 10J108 (October 2018).
3. NAZIKIAN R, Petty C, Bortolon A, et al.,  
Grassy-ELM Regime With Edge Resonant Magnetic Perturbations In Fullynoninductive Plasmas In The DIII-D Tokamak  
NUCLEAR FUSION **58**, 106010 (October 2018).
4. REYMOND L, Diallo A , Vekselman V,  
Using Laser-induced Rydberg Spectroscopy Diagnostic For Direct Measurements Of The Local Electric Field In The Edge Region Of NSTX/NSTX-U: Modeling  
REVIEW OF SCI INST **89**, 10C106 (October 2018).
5. DELGADO-APARICIO L, Wallace J, Yamazaki H, et al.,  
Simulation, Design, And First Test Of A Multi-energy Soft X-Ray (SXR) Pinhole Camera In The Madison Symmetric Torus (MST)  
REVIEW OF SCI INST **89**, 10C116 (October 2018).
6. SUN Z, Baldwin J, Xu W, et al.,  
Initial Results And Designs Of Dual-filter And Plenoptic Imaging For High-temperature Plasmas  
REVIEW OF SCI INST **89**, 10E112 (October 2018).
7. YONEDA R, Hanada K, Eiserafy H, et al.,  
High-field-side Rf Injection For Excitation Of Electron Bernstein Waves  
PLASMA AND FUSION RESEARCH **13**, 3402115 (October 2018).
8. BARCHFELD R, Domier CW, Ren Y, et al.,  
The High-K Poloidal Scattering System For NSTX-U  
REVIEW OF SCI INST **89** 10C114 (October 2018).
9. KURODA K, Raman R, Hanada K, et al.,  
Initial Results From Solenoid-Free Plasma Start-Up Using Transient CHI on QUEST  
PLASMA PHYSICS AND CONTROLLED FUSION **60** 115001 (November 2018).
10. LUNSFORD, R, Hsu JS, Sun Z, et al.,  
ELM Frequency Enhancement And Discharge Modification Through Lithium Granule Injection Into EAST H-Modes

- 
- NUCLEAR FUSION **58** 126021 (December 2018).
11. SCOTTI F, Zweben S, Soukhanovskii V, et al.,  
Divertor Leg Filaments In NSTX-U  
NUCLEAR FUSION **58** 126028 (December 2018).
12. DIALLO A, Dominski J, Barada K, et al.,  
Direct Observation Of Nonlinear Coupling Between Pedestal Modes Leading To The  
Onset Of Edge Localized Modes  
PHYS. REV. LETT. **121** 235001 (December 2018).
13. LOPEZ N and Ram AK  
Mode-conversion Of The Extraordinary Wave At The Upper Hybrid Resonance In The  
Presence Of Small-amplitude Density Fluctuations  
PLASMA PHYSICS AND CONTROLLED FUSION **60** 125012 (December 2018).
14. RAMAN R, Lay W-S, Jarboe TR, et al.,  
Electromagnetic Particle Injector For Fast Time Response Disruption Mitigation In  
Tokamaks  
NUCLEAR FUSION **59** 016021 (January 2019).
15. SOUKHANOVSII VA, Blanchard WR, Dong JK, et al.,  
Supersonic Gas Injector For Plasma Fueling In The National Spherical Torus Experiment  
FUSION SCIENCE AND TECHNOLOGY **75** 1 (January 2019).
16. SKINNER CH, Chrobak CP, Jaworski MA, et al.,  
Elemental And Topographical Imaging Of Microscopic Variations In Deposition On  
NSTX-U And DIII-D Samples  
NUCLEAR MATERIALS AND ENERGY **18** 35 (January 2019).
17. CHANG CS, Ku S, Churchill RM  
X-Point Ion Orbit Physics In Scrape-off Layer And Generation Of A Localized  
Electrostatic Potential Perturbation Around X-point  
PHYS. PLASMAS **26** 014504 (January 2019).
18. KAYE SM, Battaglia DJ, Baver D, et al.,  
NSTX/NSTX-U Theory, Modeling and Analysis Results  
Published online in NUCLEAR FUSION (January 2019).
19. MENARD JE,  
Compact Steady-state Tokamak Performance Dependence On Magnet And Core  
Physics Limits  
PHIL. TRANS. R. SOC. A **377** 20170440 (January 2019).
20. WANG ZR, Logan NC, Munaretto S, et al.,  
Identification Of Multiple Eigenmode Growth Rates In DIII-D And EAST Tokamak  
Plasmas  
NUCLEAR FUSION **59** 024001 (February 2019).
21. WANG ZR, Logan NC, Munaretto S, et al.,  
Identification Of Multiple Eigenmode Growth Rates In DIII-D And EAST Tokamak  
Plasmas  
NUCLEAR FUSION **59** 024011 (February 2019).
22. VAIL PJ, Boyer MD, Welander AW, et al.,
-

- 
- Design And Simulation Of The Snowflake Divertor Control For NSTX-U  
PLASMA PHYSICS CONTROLLED FUSION **61** 035005 (March 2019).
23. FREDRICKSON ED, Gorelenkov NN, Bell RE, et al.,  
Emission In The Ion Cyclotron Range Of Frequencies (ICE) On NSTX And NSTX-U  
PHYS. PLASMAS **26** 032111 (March 2019).
24. HAMMOND KC, Raman R, Jardin SC  
Application Of Transient CHI Startup To Future ST And AT Devices  
PHYS. PLASMAS **29** 032501 (March 2019).
25. ILHAN ZO, Boyer MD, Schuster E,  
TRANSP-based Closed-Loop Simulations Of Current Profile Optimal Regulation In  
NSTX-Upgrade  
Published online in FUSION ENGINEERING and DESIGN (March 2019).
26. FISHER AE, Hvasta MG, Kolemen E.,  
Study Of Liquid Metal Surface Wave Damping In The Presence Of Magnetic ElDs And  
Electrical Currents  
NUCLEAR MATERIALS AND ENERGY **19** 101 (March 2019).
27. WEHNER WP, Schuster E, Boyer MD, et al.,  
TRANSP-Based Optimization Towards Tokamak Scenario Development  
Published online in FUSION ENGINEERING and DESIGN (April 2019).
28. LAU C, Berry LA, Jaeger EF and Bertelli N  
Cold-plasma finite element wave model for helicon waves  
PLASMA PHYSICS CONTROLLED FUSION **61** 045008 (April 2019).
29. PERKINS RJ, Hosea JC, Taylor G, et al.,  
Resolving Interactions Between ICRF Heating And The SOL Plasma In EAST Using  
Divertor Probes  
PLASMA PHYSICS AND CONTROLLED FUSION **61** 045011 (April 2019).
30. DUARTE VN and Gorelenkov NN  
Analytic Nonlinear Collisional Dynamics Of Near-threshold Eigenmodes  
NUCLEAR FUSION **59** 044033 (April 2019).
31. LAGGNER FM, Diallo A, LeBlanc BP, et al.,  
A Scalable Real-time Framework For Thomson Scattering Analysis: Application To  
NSTX-U  
REV. SCI. INST. **90** 043501 (April 2019).
32. RINDT P, Morgan TW, van Eden GG, et al.  
Power Handling And Vapor Shielding Of Pre-filled Lithium Divertor Targets In  
Magnum-PSI  
NUCLEAR FUSION **59** 056003 (May 2019).
33. BOYER MD, Kaye S, Erickson K.  
Real-time Capable Modeling Of Neutral Beam Injection On NSTX-U Using Neural  
Networks  
NUCLEAR FUSION **59** 056008 (May 2019).
34. GUTTENFELDER W, Kaye SM, Kriete DM, et al.,  
NSTX-U L-Mode Plasma In Support Of Transport And Turbulence Validation
-

- 
- NUCLEAR FUSION **59** 056027 (May 2019).
35. NICHOLS JH, Jaworski MA, Skinner CH, et al.,  
Global Modeling Of Wall Material Migration Following Boronization In NSTX-U  
NUCL. MATER. ENERGY **19** 445 (May 2019).
35. BARDÓCZI L, Podestà M, Heidbrink WW and Van Zeeland MA,  
Quantitative Modeling Of Neoclassical Tearing Mode Driven Fast Ion Transport In  
Integrated TRANSP Simulations  
PLASMA PHYS. CONTROL. FUSION **61** 055012 (May 2019).
36. VAIL PJ, Izacard O and Kolemen E  
Optimization Of The Snowflake Divertor For Power And Particle Exhaust On NSTX-U  
NUCL. MATER. ENERGY **19** 516 (May 2019).
37. KAYE SM, Battaglia DJ, Baver D, et al.,  
NSTX/NSTX-U Theory, Modeling And Analysis Results  
NUCLEAR FUSION **59** 112007 (June 2019).
38. KIM E-H, Bertelli N, Ono M, et al.,  
Effect Of Wall Boundary On Scrape-off Layer Losses Of High-harmonic Fast Wave In  
NSTX and NSTX-U  
PHYS. PLASMAS **26** 062501 (June 2019).
39. BOYER MD, Erickson KG, Grierson BA et al.,  
Feedback Control Of Stored Energy And Rotation With Variable Beam Energy And  
Perveance On DIII-D  
NUCLEAR FUSION **59** 076004 (July 2019).
40. ZWEBEN SJ, Myra JR, Diallo A, et al.,  
Blob Wakes In NSTX  
PHYS. PLASMAS **26** 072502 (July 2019).
41. BERTELLI N, Ono M, Jaeger EF  
Modeling Of High Harmonic Fast Wave Scenarios For NSTX Upgrade  
NUCLEAR FUSION **59** 086006 (August 2019).
42. FERRARO NM, Park J-K, Myers CE, et al.,  
Error Field Impact On Mode Locking And Divertor Heat Flux In NSTX-U  
NUCLEAR FUSION **59** 086021 (August 2019).
41. REN Y, Smith DR, Zweben SJ, et al.,  
Experimental Observation Of Electron-scale Turbulence Evolution Across L-H Transition  
In National Spherical Torus Experiment  
NUCLEAR FUSION **59** 096045 (September 2019).
42. LUNSFORD R, Raman R, Brooks A, et al.,  
Modeling Of Ablatant Deposition From Electromagnetically Driven Radiative Pellets For  
Disruption Mitigation Studies  
Published on line in FUS. SCI. TECH. (2019)
43. BATTAGLIA DJ, Gerhardt SP, Kirk A, et al.,  
Reduced-Model Framework Supporting Direct Induction Startup Scenario Development  
For MAST-U And NSTX-U  
Published on line in NUCLEAR FUSION (2019).
-

44. EBRAHIMI F,  
Three-Dimensional Plasmoid-Mediated Reconnection And The Effect Of Toroidal Guide Field Simulations Of Coaxial Helicity Injection  
Accepted for publication in PHYS. PLASMAS (2019).
45. ROZENBLAT R, Kolemen E, Laggner FM, et al.,  
Development Of Real-time Software For Thomson Scattering Analysis At NSTX-U  
Accepted For Publication In FUS. SCI. TECH. (2019).
46. RUIZ-RUIZ J, Guttenfelder W, White A, et al.,  
Validation Of Gyrokinetic Simulations Of An NSTX H-Mode Plasma And Comparisons With A High-K Scattering Synthetic Diagnostic  
Accepted for publication in PLASMA PHYS. CONT. FUSION (2019).
47. EBRAHIMI F,  
Three-Dimensional Plasmoid-Mediated Reconnection And The Effect Of Toroidal Guide Field Simulations Of Coaxial Helicity Injection  
Accepted for publication in PHYS. PLASMAS (2019).
48. ROZENBLAT R, Kolemen E, Laggner FM, et al.,  
Development Of Real-Time Software For Thomson Scattering Analysis At NSTX-U  
Accepted For Publication In FUS. SCI. TECH. (2019).
49. RUIZ RUIZ J, Guttenfelder White AE, et al.,  
Validation Of Gyrokinetic Simulations Of An NSTX H-Mode Plasma And Comparisons With A High-k Scattering Synthetic Diagnostic  
Accepted for publication in PLASMA PHYS. CONT. FUSION (2019).
50. WHITE RB, Duarte VN, Gorelenkov NN, et al.,  
Modeling Of Chirping Toroidal Alfvén Eigenmodes In NSTX  
Accepted for publication in PHYS. PLASMAS (2019).

## **NSTX-U Presentations**

### **Invited / Oral Talks at Scientific Conferences (Oct. 2018 - Sept. 2019)**

1. S. Sabbagh (Columbia University) “MDC-21: Global Mode Stabilization Physics And Control – Status And Progress,” 32nd ITPA Topical Group Meeting on MHD, Disruptions, and Control in Naples, Italy, Oct. 2018.
2. S. Sabbagh (Columbia University) “Progress On Disruption Event Characterization And Forecasting (DECAF) in Tokamaks,” 32nd ITPA Topical Group Meeting on MHD, Disruptions, and Control in Naples, Italy, Oct. 2018.
3. J. Menard (PPPL), “Overview Of Recent Progress in Understanding NSTX And NSTX-U Plasmas,” and “Overview Of New MAST Physics In Anticipation Of First Results From

- 
- MAST Upgrade,” (rapporteured overview presentation by S. Kaye and J. Harrison), 27th Annual IAEA Fusion Energy Conference, Ahmedabad, India, Oct. 2018.
4. M. Podesta (PPPL), “Reduced Energetic Particle Transport Models Enable Comprehensive Time-Dependent Tokamak Simulations,” 27th Annual IAEA Fusion Energy Conference, Ahmedabad, India, Oct. 2018.
  5. S.-H. Ku (PPPL), “A Gyrokinetic Discovery Of Fast L-H Bifurcation Physics In A Realistic, Diverted Tokamak Edge Geometry,” 27th Annual IAEA Fusion Energy Conference, Ahmedabad, India, Oct. 2018.
  6. R. Lunsford (PPPL), “Active Conditioning Of ASDEX-Upgrade Tungsten PFCs Through Boron Particulate Injection,” 27th Annual IAEA Fusion Energy Conference, Ahmedabad, India, Oct. 2018.
  7. R.J. Goldston (PPPL), “Development Of A Lithium Vapor Box Divertor for Controlled Plasma Detachment,” 27th Annual IAEA Fusion Energy Conference, Ahmedabad, India, Oct. 2018.
  8. T. Rafiq (Lehigh University), “Effects Of Microtearing Modes On The Evolution Of Electron Temperature Profiles In High Collisionality NSTX Discharges,” 27th Annual IAEA Fusion Energy Conference, Ahmedabad, India, Oct. 2018.
  9. N. Gorelenkov (PPPL), “Quasi-linear Resonance Broadened Model For Fast Ion Relaxation In the Presence Of Alfvénic Instabilities (Invited),” 60th Annual Meeting of the APS Division of Plasma Physics, Nov. 5–9 in Portland, Oregon.
  10. K. Hammond (IPP Garching), “Application Of Transient CHI Plasma Start-Up To Future ST And AT Devices (Invited),” 60th Annual Meeting Of the APS Division Of Plasma Physics, Nov. 5–9 in Portland, Oregon.
  11. S.A. Sabbagh (Columbia Univ.), “Disruption Event Characterization And Forecasting In Tokamaks (Invited),” 60th Annual Meeting Of The APS Division Of Plasma Physics, Nov. 5–9 in Portland, Oregon.
  12. J.E. Menard, “Status And Plans For The NSTX-U Recovery Project,” 60th Annual Meeting of the APS Division of Plasma Physics, Nov. 5–9 in Portland, Oregon.
  13. D. Battaglia, “Enhanced Pedestal H-mode Regime On NSTX,” 60th Annual Meeting of the APS Division of Plasma Physics, Nov. 5–9 in Portland, Oregon.
  14. J. Ruiz-Ruiz (MIT), “Validation Of Novel Hybrid Scale ETG Simulations In NSTX Via Comparisons Of Simulated Turbulence With A New, High-K Scattering Synthetic Diagnostic,” 60th Annual Meeting of the APS Division of Plasma Physics, Nov. 5–9 in Portland, Oregon.
-

- 
15. S. Munaretto (General Atomics), "Assessment Of Equilibrium Field Coil Misalignments On The Divertor Footprints In NSTX-U," 60th Annual Meeting of the APS Division of Plasma Physics, Nov. 5–9 in Portland, Oregon.
  16. J.-K. Park (PPPL), "New Aspects Of Error Fields From High Field Side In Tokamaks," 60th Annual Meeting of the APS Division of Plasma Physics, Nov. 5–9 in Portland, Oregon.
  17. R. Maingi (PPPL), "Summary of the FESAC Transformative Enabling Capabilities Panel Report (Invited)," American Nuclear Society Winter Meeting and Expo/TOFE Conference, Nov. 11-15, Orlando, Florida.
  18. S. Kaye (PPPL), "A Strategic Plan for U.S. Burning Plasma Research: Update on Panel Activities and Progress (Plenary)," American Nuclear Society Winter Meeting and Expo/TOFE Conference, Nov. 11-15, Orlando, Florida.
  19. Y. Ren (PPPL), "Experimental Observation Of High-K Turbulence Evolution Across L-H Transition In NSTX (Invited)," 2nd AAPPs-DPP meeting, Nov. 10-16, Kanazawa, Japan.
  20. A. Diallo (PPPL), "Energy Exchange Dynamics Across L-H Transitions In NSTX (Invited)," 2nd AAPPs-DPP meeting, Nov. 10-16, Kanazawa, Japan.
  21. M. Ono (PPPL), "NSTX-U/PPPL Liquid-Lithium PFC/Divertor Research Activities And Plans (Invited)," National Institute For Fusion Science Research Meeting on "Theories And Applications Of Divertor," Nov. 30, Gifu, Japan.
  22. M. Ono (PPPL), "Liquid-Lithium Divertor/PFC Experiments And R&D At NSTX-U/PPPL (Invited)," 35th Annual Meeting of the Japan Society of Plasma Science and Nuclear Fusion Research, Dec. 3-6, Osaka, Japan.
  23. A. Diallo (PPPL), "Introduction To H-Mode Plasmas: L-H Transition, Pedestal, ELMs And Stationary And Transient Power Fluxes," 10th ITER International School, Jan. 21, Daejeon, South Korea.
  24. N. Bertelli (PPPL), "Initial Benchmark Of Ray-Tracing Codes For QUEST Plasmas and Fokker-Planck Simulations In TST-2 Plasma for SXR Diagnostic," Workshop on QUEST and Related Spherical Tokamak Radio-Frequency Startup and Sustainment Plasma Research, Jan. 31-Feb. 1, Kyushu, Japan.
  25. L. Delgado-Aparicio (PPPL), "Multi-Energy X-Ray Diagnostics For LH And EC Current Drive Studies At TST-2 and QUEST," Workshop on QUEST and Related Spherical Tokamak Radio-Frequency Startup and Sustainment Plasma Research, Jan. 31-Feb. 1, Kyushu, Japan.
  26. M. Ono (PPPL), "NSTX-U Start-Up Research Program And Modeling Of 2nd Harmonic ECH And ECCD Solenoid-Free Start-up Experiment In QUEST," Workshop on QUEST
-

---

and Related Spherical Tokamak Radio-Frequency Startup and Sustainment Plasma Research, Jan. 31-Feb. 1, Kyushu, Japan.

27. N. Bertelli (PPPL), "Initial Benchmark Of Ray-tracing Codes And Fokker-planck Simulations In TST-2 Plasma For SXR Diagnostic," 7th RIAM Workshop Kyushu University, Kasuga, Japan, 1-2 February 2019 N. Bertelli (PPPL).
28. F. Poli (PPPL), "Recent Progress In Integrated Modeling And Issues Relevant To Preparing For ITER First Operation," 2019 KSTAR Conference, Feb. 20-22, Daejon, South Korea.
29. D. Boyer (PPPL), "Advanced Plasma Control Using Neural Net Algorithms For Faster Than Real-Time Simulation," 019 KSTAR Conference, Feb. 20-22, Daejon, South Korea.
30. S. Sabbagh (Columbia Univ.), "Expanded Study Of The Generalized Neoclassical Toroidal Viscosity Offset Rotation Profile In KSTAR," 2019 KSTAR Conference, Feb. 20-22, Daejon, South Korea.
31. S. Sabbagh (Columbia Univ.), "Progress On Disruption Prediction Capability Including Transport And Stability Analysis Of High-Performance KSTAR Plasmas," 019 KSTAR Conference, Feb. 20-22, Daejon, South Korea.
32. M. Ono (PPPL), "NSTX-U Spherical Tokamak Program And Possible Synergistic Collaboration Areas for the KSTAR Program (Invited)," 2019 KSTAR Conference, Feb. 20-22, Daejon, South Korea.
33. R. Maingi (PPPL), "Similarities Between Flowing Liquid Lithium And Lithium Powder Injection Experiments On EAST, And Lithium Evaporation Experiments on NSTX," US-Japan and International Workshop on Power and Particle Control in DEMO Fusion Reactor by Liquid Metal Plasma-Facing Components, March 11-13, Princeton, NJ.
34. R. Maingi (PPPL), "The Nearly Continuous Improvement Of Discharge Characteristics And Edge Stability With Increasing Lithium Coatings In NSTX," US-Japan and International Workshop on Power and Particle Control in DEMO Fusion Reactor by Liquid Metal Plasma-Facing Components, March 11-13, Princeton, NJ.
35. R. Goldston (PPPL), "Advances Towards A Simplified Lithium Vapor Box Divertor," US-Japan and International Workshop on Power and Particle Control in DEMO Fusion Reactor by Liquid Metal Plasma-Facing Components, March 11-13, Princeton, NJ.
36. M. Ono (PPPL), "Comments On Liquid Lithium Loop System To Solve Challenging Technology Issues For Fusion Power Plants," US-Japan and International Workshop on Power and Particle Control in DEMO Fusion Reactor by Liquid Metal Plasma-Facing Components, March 11-13, Princeton, NJ.

37. T. Brown (PPPL), "Design Status In The Development Of Liquid Metal Divertor And First-wall Concepts Within A PPPL Toroidal Confinement Facility Study," US-Japan and International Workshop on Power and Particle Control in DEMO Fusion Reactor by Liquid Metal Plasma-Facing Components, March 11-13, Princeton, NJ.
38. J. Menard (PPPL), "Systems Studies For A Tokamak-based Divertor Test Facility," US-Japan and International Workshop on Power and Particle Control in DEMO Fusion Reactor by Liquid Metal Plasma-Facing Components, March 11-13, Princeton, NJ.
39. V. Duarte (PPPL), "Verifying Reduced Quasilinear Models For Fast Ion Relaxation (Invited)," U.S. Transport Task Force Meeting, March 18-21, Austin, TX
40. S. Kaye (PPPL), "ITPA Global H-Mode Database Update," Transport and Confinement ITPA meeting, March 25-27, Austin, Texas.
41. W. Guttenfelder (PPPL), "Predictions Of Electron Scale Pedestal Turbulence In DIII-D ELMy H-Modes (Invited)," Sherwood Fusion Theory Conference, April 15-17, Princeton, NJ.
42. N. Ferraro, "Simulations Of Fast Thermal Quenches Using A Two-temperature Model (Invited)," Sherwood Fusion Theory Conference, April 15-17, Princeton, NJ.
43. T. Rafiq, "Microtearing Modes In Low Collisionality NSTX Plasmas," Sherwood Fusion Theory Conference, April 15-17, Princeton, NJ.
44. S. Kaye (PPPL), "A Strategic Plan For U.S. Burning Plasma Research," Sherwood Fusion Theory Conference, April 15-17, Princeton, NJ.
45. R. Raman, "Electromagnetic Particle Injector (EPI) As A Fast Time Response Disruption Mitigation Concept," Stewart Prager Symposium, April 4-5, Princeton, NJ.
46. N Bertelli (PPPL), "3D Full Wave Fast Wave Modeling With Realistic Antenna Geometry And SOL Plasma (Invited)," 23rd Topical Conference on RadioFrequency Power in Plasmas, May 14-17, Hefei, China.
47. M. Boyer, "Accelerated Predictive Transport Models Using Machine Learning For Scenario Optimization And Control Of Tokamaks (Invited)," 2nd International Conference on Data Driven Plasma Science, May 13-17, Marseilles, France.
48. M. Boyer, "Real-Time Control And Estimation In Tokamaks With Machine Learning Accelerated Predictive Models," 3rd IAEA Technical Meeting of Fusion Data Processing, Validation and Analysis", May 28-31, Vienna, Austria.

- 
49. N. Ferraro, "Magnetohydrodynamic Simulations Of Fusion Plasmas With M3D-C1 (Invited)," 11th International Conference on Computational Physics, June 2019, Hangzhou, China.
  50. R. Raman, "Electromagnetic Particle Injector (EPI) As A Fast Time Response Disruption Mitigation Concept," 28th IEEE SOFE Meeting, June 2019, Jacksonville, FL.
  51. D. Battaglia, "The NSTX-U Facility In The 2020s: Advancing The Physics Basis For Configuration Optimization Toward A Compact Fusion Pilot Plant," APS-DPP Community Planning Workshop, July 2019, Madison, WI.
  52. R. Goldston, "Development Of A Liquid Lithium Divertor For A Compact Fusion Power Plant," APS-DPP Community Planning Workshop, July 2019, Madison, WI.
  53. M. Ono, "Integrated Rf Program To Develop Fusion Reactor Relevant Actuators," APS-DPP Community Planning Workshop, July 2019, Madison, WI.
  54. J. Menard, "Development Of Mission Need and Preliminary Design Of A Sustained High Power Density Tokamak Facility," APS-DPP Community Planning Workshop, July 2019, Madison, WI.
  55. R. Raman, "Demonstration Of Solenoid-free Start-up Of Low Inductance Plasma For Advanced St Or Tokamak Scenarios Using Transient Coaxial Helicity Injection," APS-DPP Community Planning Workshop, July 2019, Madison, WI.
  56. Y. Ren, "Experimental Observation Of Electron-scale Turbulence Evolution Across The L-h Transition In NSTX," 9th East-Asia School and Workshop on Laboratory, Space and Astrophysical Plasmas, July 29- August 2 2019, Nagoya, Japan.
  57. R. Raman, "The Electromagnetic Particle Injector For Disruption Mitigation In Tokamaks," Theory and Simulation of Disruptions Workshop, August 5-7, Princeton NJ.
  58. J. Ruiz-Ruiz, "Validation Of Ion And Electron-scale Gyrokinetic Simulations In An NSTX H-Mode And Comparisons With A Synthetic Diagnostic For High-K Scattering," August 2019, Oxford University, UK.
  59. Y. Ren, "Scattering Diagnostics In High Temperature Plasmas (Remote)," 2019 Summer School on Plasma Physics Experiments and Diagnostics, August 16-23 2019, Hangzhou, China. (The lecture was given from a remote location.)
  60. M. Podesta, "Energetic Particle Transport In NSTX/NSTX-U Multi-mode Scenarios Through Integrated Simulations," 16th IAEA Technical Committee Meeting on Energetic
-

Particles in Magnetic Confinement Systems - Theory of Plasma Instabilities, Sept. 3-6, Shizuoka City, Japan.

61. N. Bertelli, "3D HHFW Full Wave Simulations With Realistic Antenna Geometry And SOL Plasma In NSTX-U," U.S.-Japan Workshop on Heating and Current Drive RF Physics, Sept. 4-6, 2019, Princeton, NJ.
62. N. Bertelli, "From A Reflectrometry Code To A 'Standard' EC Code To Investigate The Impact Of Edge Density Fluctuations On The EC Wave Propagation," U.S.-Japan Workshop on Heating and Current Drive RF Physics, Sept. 4-6, 2019, Princeton, NJ.
63. F. Scotti, "Transport And Turbulence In The Scrape-off Layer And Divertor Of The National Spherical Torus Experiment," International Symposium of Advanced Energy Science, September 2019, Kyoto University, Japan.

## **Seminars and Colloquia by NSTX-U Researchers**

1. R. Maingi "Real-Time Impurity Injection For Wall Conditioning, ELM And H-Mode Pedestal Control, And Divertor Exhaust Enhancement," October 2018, Univ. of Wisconsin - Madison.
2. W. Guttenfelder, "Intro to Magnetized Plasma Turbulence," October 2018, University of Tennessee - Knoxville.
3. F. Ebrahimi, "Three-dimensional Coherent Plasmoids In Current-Carrying Plasmas," October 2019, Fifth Annual Dalton Schnack Memorial Seminar, University of Wisconsin, Madison, WI.
4. W. Guttenfelder, "Containing A Star On Earth: The Promise Of Fusion Energy," (APS Outreach), November 2019, Portland State University, Portland, OR.
5. W. Guttenfelder, "Containing A Star On Earth; My Path From Electrical Engineering To Fusion Energy Research," November 2019, Washington Twp Library High School Seminar Series, NJ.
6. F. Ebrahimi, "Three-Dimensional Magnetic Reconnection And Relaxation In Current-carrying Plasmas," November 2018, PPPL Advisory Board, Princeton, NJ.
7. T. Stoltzfus-Dueck, "Intrinsic Rotation Mechanisms In Tokamaks Validated By Experiments," November 2018, PPPL Advisory Board, Princeton, NJ.
8. R. Maingi, "The Use Of Impurity Injection For Wall Conditioning, Power Exhaust, And ELM Stability. Recent Results From ASDEX-Upgrade, DIII-D, EAST, and KSTAR," January 2019, CEA Cadarache, France.

9. R. Maingi "Real-Time Impurity Injection For Wall Conditioning, ELM And H-mode Pedestal Control, And Divertor Exhaust Enhancement," January 2019, Southwest Institute of Physics in Chengdu, China.
10. R. Maingi, "The Nearly Continuous Improvement Of Discharge Characteristics and Edge Stability with Increasing Lithium Coatings in NSTX," January 2019, Southwest Institute of Physics in Chengdu, China.
11. A. Diallo "Energy Exchange Dynamics Across The LH Transition In NSTX," January 2019, National Fusion Research Institute (NFRI), South Korea.
12. N. Ferraro, "Modeling Edge Localized Modes," PPPL/UMD Theory/Stellarator Mini-Meeting, January 2019, Princeton, NJ.
13. N. Bertelli, "Initial Benchmark Of Ray-tracing Codes For Quest Plasmas And Fokker-planck Simulations In TST-2 Plasma For SXR Diagnostic," January/February 2019, Workshop on QUEST and Related Spherical Tokamak Radio-Frequency Startup and Sustainment Plasma Research.
14. L. Delgado-Aparicio, "Multi-Energy X-Ray Diagnostics For LH And EC Current Drive Studies At TST-2 And QUEST," January/February 2019, Workshop on QUEST and Related Spherical Tokamak Radio-Frequency Startup and Sustainment Plasma Research.
15. M. Ono, "NSTX-U Start-Up Research Program And Modeling Of 2nd Harmonic ECH And ECCD Solenoid-Free Start-Up Experiment In QUEST," January/February 2019, Workshop on QUEST and Related Spherical Tokamak Radio-Frequency Startup and Sustainment Plasma Research.
16. W. Guttenfelder, "Predictions Of Electron Scale Turbulent Transport In DIII-D ELMy H-Mode Pedestals," February 2019, General Atomics, San Diego, CA.
17. W. Guttenfelder, "Intro To Neutral & Magnetized Plasma Turbulence," PPPL Graduate seminar, February 2019, Princeton, NJ.
18. F. Poli, "Integrated Modeling," PPPL Graduate seminar, February 2019, Princeton, NJ.
19. F. Ebrahimi, "Magnetic Explosions: From Space Plasmas To Fusion Energy," February 2019, Ronald E. Hatcher Science on Saturday Series, Princeton, NJ.
20. F. Poli "Recent Progress In Integrated Modeling And Issues Relevant To Preparing For ITER First Operation," February 2019, KSTAR conference, Seoul, South Korea.
21. M. Boyer, "Advanced Plasma Control Using Neural Net Algorithms For Faster Than Real-time Simulation And Advanced Real-time Architectures," February 2019, KSTAR conference, Seoul, South Korea.

- 
22. F. Poli, "The Challenges Of Integrated Tokamak Modeling And The Path Forward To A Whole Device Model," February 2019, Seoul National University, South Korea.
  23. R. Maingi, "Real-Time Impurity Injection For Wall Conditioning, ELM And H-Mode Pedestal Control, And Divertor Exhaust Enhancement," February 2019, EAST seminar, ASIPP, Hefei, China.
  24. A. Diallo, "Suppression Of Energy Losses In Fusion Devices: Challenges And Opportunities," March 2019, Dept. of Engineering Physics, Univ. of Wisconsin, Madison, WI.
  25. R. Maingi, "Access To Low-Density RMP ELM Suppression Regimes Through Boron Powder Conditioning In AUG," S. Sabbagh, "Fusion Energy: Plasmas, Scientists, And Innovation," April 2019, Career Day at The Center School in Somerset, NJ.
  26. V. Duarte (remote), "Realistic 2D Quasilinear Modeling Of Fast Ion Relaxation," April, 2019, DIII-D Friday Science Meeting, Princeton, NJ.
  27. N. Ferraro, "Tokamak Transients," PPPL Graduate Student seminar, April 2019, Princeton, NJ.
  28. J. Menard, "NSTX-U Recovery And Ideas For Next-Step Low-A Tokamaks," Department of Applied Physics and Mathematics Plasma Physics Colloquium, Columbia University, New York, NY.
  29. F. Poli, "The Challenges And Glories Of Integrated Tokamak Modeling," April 2019, PPPL graduate student seminar, Princeton, NJ.
  30. S. Kaye, "Findings And Recommendations Of The National Academy Of Sciences Panel On Burning Plasmas," April 2019, Town Hall, Sherwood Theory Conference, Princeton, NJ.
  31. M. Ono, "Opportunities And Challenges Of Plasma Waves For Magnetic Fusion," April 2019, UCLA, Los Angeles, CA.
  32. W. Guttenfelder "Testing Predictions Of Electron Scale ETG Pedestal Turbulence In DIII-D ELMy H-modes," May 2019, MIT/PSFC, Cambridge, MA.
  33. F. Laggner, "A Scalable Real-time Framework For Thomson Scattering Analysis At NSTX-U," May 2019, IPP Garching, Germany.
  34. F. Poli, "The ABS's Of Modeling A Tokamak," presentation to SULI students, June 2019, Princeton, NJ.
  35. W. Guttenfelder, "Toroidal Magnetized Plasma Turbulence & Transport," PPPL Graduate Student Summer School Lecture, August 2019, Princeton, NJ.

36. J.-K. Park, "Quasi-symmetric Magnetic Perturbations In A Tokamak," Dept. of Nuclear Engineering, Seoul National University, Seoul, South Korea.

## **NSTX-U Awards and Leadership**

### **Major Awards by NSTX-U Researchers**

1. T. Stoltzfus-Dueck, ECRP "Development And Testing Of Reduced Models Of The Edge Radial Electric Field," FES Early Career Researcher Award.

### **Invention Disclosures and Patents**

1. A. Diallo, "Controlling Powder And Granule Injections In Fusion Devices," 19-3588-1 Initial Technology Memo.

### **Hosted / Organized Meetings and Workshops**

1. F. Poli, TRANSP User's Group Meeting (APS-DPP), Portland, OR, Oct. 2018.
2. J.-K. Park, 23rd Workshop on MHD Stability and Control, Los Angeles, CA, Nov. 2018.
3. M. Ono and R. Maingi Co-Hosted the inaugural US-Japan and International Workshop on Power and Particle Control in DEMO Fusion Reactor by Liquid Metal Plasma-Facing Components, PPPL, March 2019.
4. F. Ebrahimi Local chair and the PPPL host of 2019 Sherwood conference, Princeton, NJ, April 2019.
5. M. Ono, Program Committee, 23rd Topical Conference on RadioFrequency Power in Plasmas, Hefei, China, May 2019.
6. N. Ferraro, First Joint MFE/FM&T Community Planning Workshop, Madison, WI, July 2019
7. M. Ono, Program Committee, 6th International Symposium on Liquid Metal Application for Fusion, Urbana-Champaign, IL, Sept. 2019.
8. M. Ono, U.S.-Japan Workshop on Heating and Current Drive RF Physics, Princeton, NJ, Sept. 2019.
9. N. Bertelli, U.S.-Japan Workshop on Heating and Current Drive RF Physics, Princeton, NJ, Sept. 2019.
10. E. Fredrickson, 16th IAEA Technical Meeting on Energetic Particles in Magnetic Confinement Systems - Theory of Plasma Instabilities Shizuoka City, Japan, Sept. 2019.
11. E. Kolemen, 24th Workshop on MHD Stability and Control, NYC, NY, Oct. 2019.
12. J.-K. Park, 24th Workshop on MHD Stability and Control, NYC, NY, Oct. 2019.

---

## NSTX-U PPPL Employee FY19 Leadership in Venues Outside of PPPL

1. Battaglia, D., Deputy Chair, Integrated Scenarios topical group, U.S. BPO.
2. Bertelli, N., PPPL PI of the RF SciDAC project.
3. Boyer, M., Deputy Leader, USBPO Operations and Control Topical Group.
4. Boyer, M., Panel member, DOE FES/ASCR Advancing Fusion with Machine Learning Workshop.
5. Delgado-Aparicio, L., Deputy Leader, USBPO Diagnostics Topical Group.
6. Diallo, A., Deputy Director of the Innovation Network for Fusion Energy (INFUSE).
7. Ebrahimi, F. Invited subcommittee Co-chair of the 2019 APS-DPP program.
8. Ferraro, N., Treasurer, Sherwood Fusion Theory Conference Executive Committee.
9. Ferraro, N., Deputy Leader, USBPO, MHD and Macroscopic Stability Topical Group.
10. Ferraro, N., Co-Chair, APS-DPP Community Planning Process.
11. Gerhardt, S. Leader, ITPA MDC WG-6.
12. Gorelenkov, N., Leader, USBPO Energetic Particles Topical Group.
13. Gorelenkov, N., Lead Author, The Encyclopaedia of Nuclear Energy.
14. Guttenfelder, W., Deputy Leader, U.S. BPO Transport & Confinement Topical Group.
15. Guttenfelder, W., Co-Leader, Discussion Group 5, Austin MFE Strategies Workshop.
16. Guttenfelder, W., Editor, US BPO eNews.
17. Guttenfelder, W., Leader, USBPO, Transport and Confinement Topical Group.
18. Guttenfelder, W., Leader, APS-DPP Community Planning Process Transport and Confinement Expert Group.
19. Hawryluk, R., Chair, Board of Editors, Nuclear Fusion.
20. Hawryluk, R., Chair, Max Planck Society Fachbeirat of the Institute for Plasma Physics.
21. Kaye, S., Coordinator, International H-mode Database Update Task (ITPA.)
22. Maingi, R. served as a Ph.D. committee member for the final defense of I. Waters (University of Wisconsin-Madison), "Particle Exhaust and Neutral Fueling in Spherical Tokamaks with Resonant Magnetic Perturbation Fields."
23. Maingi, R., Managing Guest Editors for the Proceedings of the 23rd International Conference on Plasma Surface Interactions in Controlled Fusion Devices.
24. Maingi, R., Head, domestic liquid metal plasma-facing component development program for fusion devices.
25. Menard, J., Co-chair, International Advisory Committee for China Fusion Engineering Test Reactor (CFETR).
26. Menard, J., Chair, U.S. DOE FES Fusion Facility Coordinating Committee.
27. Menard, J., Co-chair, U.S. Magnetic Fusion Research Strategic Directions organization/workshops.
28. Ono, M., Visiting Professor, Kyushu University, Japan.
29. Ono, M., Associate Editor, Journal of Fusion Energy.
30. Ono, M., Subgroup Leader, DIII-D Program Advisory Committee.

31. Park, J-K, MDC-19 Leader, ITPA MHD, Disruption and Control Topical Group.
32. Park, J-K, Deputy Leader, MS Topical Science Group, NSTX-U Team.
33. Podesta, M., Deputy Chair, U.S. Transport Task Force Executive Committee.
34. Podesta, M., Lead of EP-8 Joint Experiment of Energetic Particle ITPA Topical Group.
35. Poli, F., Leader, BPO Topical Group on Integrated Scenarios.
36. Poli, F., PI of TRANSP funding grant by DOE.
37. Poli, F., Co-Leader, Discussion Group, Austin MFE Strategies Workshop.
38. Poli, F., PI of ITER Task Agreement on EC modeling and application.
39. Poli, F., ITER Scientist Fellow.
40. Ren, Y., Part-time Professor, Harbin Institute of Technology.
41. Wang, W.X., Institutional PI of SciDAC TDS project.
42. Wang, W.X., Visiting Professor, National Institute for Fusion Science, Japan.
43. Wang, Z.R., Visiting Professor, Dalian University of Technology, China.

---

## NSTX-U PPPL Employee Membership and Participation in Scientific Groups and Meetings Outside of PPPL

1. Battaglia, D., Member, Scenarios Expert Group, APS-DPP Community Planning Process.
2. Delgado-Aparicio, L., Member, APS-DPP Committee on Women in Plasma Physics.
3. Delgado-Aparicio, L., Member, ITPA Diagnostics Topical Group.
4. Diallo, A., Editorial Board Member, Plasma Physics and Controlled Fusion, IOP Publishing.
5. Diallo, A., Expert, ITPA Pedestal and Edge Physics Topical Group.
6. Diallo, A., Panelist, IAEA Headquarter 2018 - Consultancy Meeting on Holistic investigations of the Dynamics of the Tokamak Pedestal.
7. Diallo, A., Panelist, NSF/DoE Review Alexandria.
8. Ebrahimi, F., Member, Sherwood Theory Conference Program Committee.
9. Ferraro, N., Member, APS-DPP Committee on Women in Plasma Physics.
10. Ferraro, N., Deputy Leader, USBPO MHD Topical Group.
11. Ferraro, N., Expert, ITPA Pedestal & Edge Physics Topical Group.
12. Gorelenkov, N., Member, ITPA Energetic Particle Physics Topical Group.
13. Guttenfelder, W., Member, APS-DPP Community Planning Process Program Committee.
14. Guttenfelder, W., Member, ITPA Transport and Confinement Topical Group.
15. Guttenfelder, W., Member, Executive Committee, U.S. Transport Task Force.
16. Guttenfelder, W., Member, Program Committee, APS-DPP Community Planning Process.
17. Hawryluk, R., Participant in Helmholtz Association Energy Review Panel.
18. Hawryluk, R., Participant, UKAEA Review of the Fusion Program.
19. Hawryluk, R., Member, DOE National Laboratory Chief Operating Officer Committee.
20. Kaye, S., Member, CCFE Program Advisory Committee.
21. Kaye, S., Member, MAST-U Enhancements Review Committee.
22. Kaye, S., Member, U.K. Fusion Advisory Board.
23. Maingi, R., Co-chair on the TOFE technical session, "Transformative Enabling Capabilities: Liquid Metal Plasma-Facing Components."
24. Maingi, R., TOFE Panel Participant, "Transformative Enabling Capabilities: Advanced Materials and Manufacturing TOFE" technical session.
25. Maingi, R., Panel Participant, "Technology and Science of Lithium Delivery Systems and Impact on Plasma Performance in EAST," for the Plasma Material Interaction technical session, TOFE.
26. Maingi, R., U.S. representative on the ITPA coordinating committee
27. Maingi, R., Expert, ITPA Diagnostics Topical Group.
28. Maingi, R., Expert, ITPA Divertor and SOL Topical Group.
29. Maingi, R., Expert, ITPA Pedestal and Edge Physics Topical Group.

30. Maingi, R., Member, International Advisory Committee of the PSI 2020 Conference.
31. Maingi, R., Member, ITPA Coordinating Committee.
32. Maingi, R., Member, Proto-MPEX Program Advisory Committee.
33. Maingi, R., Member, Technical Program Committee of the H-mode Workshop.
34. Maingi, R., Member, US DoE Fusion Energy Sciences Advisory Committee.
35. Maingi, R., Member, Executive Committee of the IEA TCP-CTP.
36. Maingi, R., Member, H-mode workshop international advisory committee
37. Maingi, R., Program Committee of the 2019 International Symposium on Liquid Metal Applications in Fusion Devices (ISLA).
38. Ono, M., Member, APS-DPP Program Committee (MCF Experiment).
39. Park, J.-K., Expert, ITPA Macro-stability Topical Group.
40. Petrella, J., Panel Participant, "Electrical Insulation Tape Winding and Inspection System," TOFE.
41. Petrella, J., Panel Participant, "NSTX-U Global Thermal Analysis For Bake-Out And Normal Operation Scenarios," Thermal Hydraulics for Fusion Components technical session, TOFE.
42. Podesta, M., Member, ITPA Energetic Particle Physics Topical Group.
43. Podesta, M., Member of the Editorial Advisory Board of Review of Scientific Instruments.
44. Poli, F., Member, USBPO Research Council.
45. Poli, F., Member, ITPA Integrated Operational Scenarios Topical Group.
46. Poli, F., Member, Executive Committee, U. S. Transport Task Force.
47. Poli, F., Member, APS-DPP Program Committee (MCF Theory).
48. Wang, W.X., Member, Festival de Théorie (Aix-en-Provence, France, held biannually) International Scientific Committee.
49. Wang, W.X., Member, Scientific Program Committee of 12th West Lake International Symposium on Plasma Simulation.
50. Zhai, Y., Panel Participant, "Prototype Coil Evaluation For NSTX-U Replacement Inner Poloidal Field Coils" Magnets technical session, TOFE.

---

## NSTX-U Collaborator Institutions

<b>Number</b>	<b>Institution</b>	<b>Country</b>
1	College of William and Mary	USA
2	Columbia University	USA
3	CompX	USA
4	Florida International University	USA
5	General Atomics	USA
6	Idaho National Laboratory	USA
7	Johns Hopkins University	USA
8	Lawrence Livermore National Laboratory	USA
9	Lehigh University	USA
10	Lodestar Research Corporation	USA
11	Los Alamos National Laboratory	USA
12	Massachusetts Institute of Technology	USA
13	Nova Photonics, Inc	USA
14	Oak Ridge National Laboratory	USA
15	Old Dominion University	USA
16	Princeton University	USA
17	Purdue University	USA
18	Sandia National Laboratory	USA
19	Tech-X Corporation	USA
20	University of California - Davis	USA
21	University of California - Irvine	USA
22	University of California - Los Angeles	USA

23	University of California - San Diego	USA
24	University of California, Space Sciences Laboratory	USA
25	University of Colorado	USA
26	University of Illinois	USA
27	University of Maryland	USA
28	University of Rochester	USA
29	University of Tennessee	USA
30	University of Texas	USA
31	University of Washington	USA
32	University of Wisconsin	USA
33	University of Costa Rica	Costa Rica
34	Institute of Plasma Physics-Czech Republic	Czech Republic
35	Hiroshima University	Japan
36	Japan Atomic Energy Agency	Japan
37	Kyoto University	Japan
38	Kyushu University	Japan
39	NIFS National Institute for Fusion Science	Japan
40	Niigata University	Japan
41	University of Hyogo	Japan
42	University of Tokyo	Japan
43	FOM Institute DIFFER	Netherlands
44	ASIPP - Institute of Plasma Physics - Chinese Academy Of Sciences	P.R. China

---

<b>45</b>	<b>Ioffe Physical-Technical Institute</b>	<b>Russia</b>
<b>46</b>	<b>TRINITI - Troitskii Institute of Innovative &amp; Thermonuclear Research</b>	<b>Russia</b>
<b>47</b>	<b>KAIST - Korea Advanced Institute of Science and Technology</b>	<b>South Korea</b>
<b>48</b>	<b>NFRI - National Fusion Research Institute</b>	<b>South Korea</b>
<b>49</b>	<b>Seoul National University</b>	<b>South Korea</b>
<b>50</b>	<b>Ulsan Science Institute of Science &amp; Technology</b>	<b>South Korea</b>
<b>51</b>	<b>Institute for Nuclear Research-National Academy of Science</b>	<b>Ukraine</b>
<b>52</b>	<b>Culham Centre for Fusion Energy</b>	<b>United Kingdom</b>
<b>53</b>	<b>Tokamak Energy</b>	<b>United Kingdom</b>
<b>54</b>	<b>University of York</b>	<b>United Kingdom</b>